Syntheses of Polymers with Diverse Architectures via Metathesis Polymerization and Investigation of Their Structure-Property Relationships

Thesis by

Yan Xia

In Partial Fulfillment of the Requirements for the

Degree of

Doctor of Philosophy

California Institute of Technology

Pasadena, California

2010

(Defended on April 19, 2010)

For Mom, Dad, and my Wife

Acknowledgements

Many people asked me “what do you like about Caltech best?” After nearly five years, I give my short answer without hesitation: “The People!” It is all the wonderful people at Caltech that make it the world’s best place to explore science and made my time here truly unforgettable.

My advisor, Bob Grubbs, has been giving me the total freedom to pursue my interests on some projects that are quite nontraditional in the Grubbs group, yet providing his complete support whenever it is needed. I have been constantly impressed by his broad interest, deep knowledge, and repetitive enthusiasm. (As he said, when you get older and more forgetful, you can get excited about the same thing many times.) His often brief yet insightful and encouraging advice has taught me to think with the big perspective, and the much longer stories almost always following his scientific advice (often about the history of certain chemistry or about his outdoor adventure) have definitely been the best delightful reliefs when I was stressed with not-going-well projects. Outside the lab, the Grubbs camping trips have allowed me to enjoy more American culture; the Christmas dinners with his family have always made me feel I have a home away from home.

“Thank you, Bob!” for providing all these to shape me into an independent researcher and to give me the confidence to challenge myself in the future.

Julie Kornfield has been my coadvisor, and she has a completely different character from Bob. She is definitely the smartest and the most critical lady I have ever seen. Being both means that she will NEVER let it go if I try not to be meticulous in

research. With her training, I will not be afraid of any scientific criticism in the future. On the other hand, she is also a very caring person, always putting others' personal needs/feelings first. From her, I have learned to consider things from the angles of others.

I have also been blessed by an excellent committee: Dave Tirrell, Mark Davis, and Jim Heath. They are all wonderful scientists as well as mentors, and their knowledge pretty much covers the full range of chemistry and materials science, which is sometimes scary as I talk to them about my prop ideas and my research. I have also used certain equipment from all three labs for free at some point of my graduate research (sometimes it can be as long as over a year) and they never seemed to mind. Many members from these groups have also provided me with generous help on training and discussions about my need.

In the Grubbs group, I have had the privilege to work with AJ Boydston for three years on the tough yet enjoyable journey of making cyclic polymers. Since day one, I have been impressed with his outside-the-box thinking, vast chemistry knowledge, and incredible efficiency in everything, ranging from finishing up a reaction to writing up a proposal to setting up a science party for his lovely kids. I also owed him half a tooth on the basketball court. Being an absolutely outstanding scientist and such a fun person to work with, he has become my best friend and a role model for doing research. I am sure he will have a stellar career at the University of Washington soon.

I also had the fortune to work with many other members in the polymer sub-group: Masao Yanagawa and Ron Walker first taught me how to ROMP, although Ron seemed to be more interested in Louisiana and Chinese culture, and he also helped me buy a nice car with his good knowledge of cars (although I had to get the transmission fixed two

months after I bought it). John Matson, “beef”, has been the most polymer person in the group during my time in the Grubbs group, and our basketball coach for a while. John and Ron have also been fixing the clogged GPC tirelessly during the time I had to work with multimillion molecular weight polymers. I really appreciate the effort from both of you! Paul Clark, a professional fisherman and a chemist, is in my year. He has a truly selfless heart and neat skills for kilogram-scale reactions. I look forward to working with him again in a few months. Erin Guidry was the rotaxane master in the group; Mike Page is the happiest person I have seen; Irina Gorodetskaya introduced the cyclic polymer project to me; Rose Conrad is great sources for synthetic chemistry; Jeremiah Johnson is the most hipster chemist I have met with lots of wild ideas. I am happy that Benjamin Sveinbjornsson is going to carry the torch of brush polymers.

The Grubbs group is never short of talents. I have had interactions with other excellent fellow students Jason Jordan, Soon Hong, Donde Anderson, Matt Whited, Kevin Kuhn, Jean Li, Chris Daeffler, Keith Keitz (Thank you for taking good care of the vulnerable “Flory”!), Matt Van Wingerden, Renee Thomas, and Myles Herbert; as well as fabulous postdocs with diverse backgrounds: Cheol Chung, Georgios Vougioukalakis J. B. Bourg, Koji Endo, Vince Lavallo, Peili Teo, and Guangbin Dong. I would like to thank them for all their friendship and help!

Rafael Verduzco was a senior grad student when I worked in Julie’s lab in my first year. He introduced me to basic polymer physics, especially liquid crystal polymers and rheology, and never hesitated to offer his help to get me started. More importantly, he taught me how to communicate with chemical engineers. I look forward to his future

success. I also had many happy chats with Matt Mattson, Ameri David, Zuli Kurji, and Jeremy Wei in Julie's lab.

Brad Olsen was a joint postdoc in three (!) groups at Caltech, but we got to know each other quite a while before he came to Caltech. He is an excellent scientist, mentor, and coworker. He offered tremendous help on the characterization of the brush copolymers, and taught me about almost all aspects of the physics of block copolymers. Without him, Chapter 5 of this thesis would not be complete. I am sure he will have an outstanding independent career and become a rising star in the field of polymer science.

There are so many more wonderful people that I cannot list all their names with the fear that I will forget some. Thank you all of you!

Outside Caltech, I would like to acknowledge our long-time collaborator, Professor Greg McKenna and his student Miao Hu at Texas Tech University, for all their teaching about rheology and patience to bear with my samples; as well as Professor Hans Spiess and his former student Yefeng Yao at Max-Plank Institute for their generous help on the melt state ^{13}C NMR experiments.

Last but not least, I would like to take this time to memorialize my grandma, who taught me to be a genuine person but did not wait to see me finish my study. May you rest peacefully. No words can really describe my gratitude to my parents and to my wife for always putting me first and always being willing to sacrifice everything.

Abstract

Metathesis polymerization using highly active, functional-group-tolerant catalysts is a powerful and versatile method for polymer synthesis. This thesis focuses on the preparation of a variety of advanced polymer architectures using well-defined ruthenium-based metathesis catalysts and the study of materials properties dictated by those unique macromolecular structures.

Chapter 1 introduces olefin metathesis, metathesis polymerization, and recent developments in living/controlled polymerization and polymer functionalization. The goal is to provide a summary of the current toolbox of polymer chemists. The second part of Chapter 1 describes using these tools to synthesize different macromolecular architectures.

Chapters 2 and 3 describe ring-expansion metathesis polymerization (REMP) using cyclic catalysts. Chapter 2 focuses on catalyst development, while Chapter 3 focuses on the REMP mechanism and cyclic polymer characterization.

Chapters 4 and 5 focus on brush polymers. Chapter 4 describes the syntheses of linear and cyclic brush polymers using ring-opening metathesis polymerization (ROMP) and REMP of macromonomers (MMs), respectively. Chapter 5 describes the efficient synthesis of brush copolymers and the study of their melt state self-assembly into highly ordered nanostructures.

Chapter 6 describes the synthesis and electro-optic response of well-defined liquid crystalline (LC) gels that were made from controlled end-linking of telechelic LC

polymers. These gels possessed very fast, reversible electro-optic switching; the degree of response was closely related to network structure.

Table of Contents

List of Schemes

List of Figures

Chapter 1: Introduction

Chapter 2: Cyclic Ruthenium-Alkylidene Catalysts for Ring-Expansion Metathesis Polymerization

Chapter 3: Ring-Expansion Metathesis Polymerization: Catalyst Dependent Polymerization Profiles

Chapter 6: Well-Defined Liquid Crystal Gels from Telechelic Polymers via Ring-Opening Metathesis Polymerization and "Click" Chemistry

Appendix 1: GPC Characterization of Cyclic Polymers

Appendix 2: Hydrogenation of Polyalkenamers

Chapter 1

Introduction

Olefin Metathesis

Olefin metathesis is a versatile carbon-carbon bond rearrangement reaction, catalyzed by transition metal complexes.[1] First proposed by Chauvin in 1971, the mechanism for olefin metathesis involves olefin coordination to a metal carbene and subsequent cycloaddition to form a metallocyclobutane intermediate. This metallocyclobutane can undergo cleavage either in a productive manner to afford a new olefin and a new metal carbene complex or in a non-productive manner to regenerate starting materials (Figure 1). In general, each step in olefin metathesis is a thermodynamically controlled, reversible equilibrium process and requires a driving force, such as the release of ring strain or the loss of a volatile small molecule, to obtain the desired products.

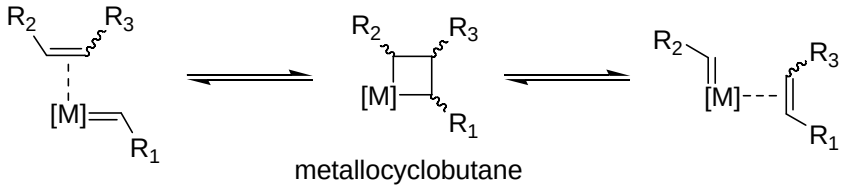

Figure 1. General mechanism of olefin metathesis.

In the first two decades of olefin metathesis (early 1960s to early 1980s), a number of ill-defined multicomponent catalysts were found active to mediate olefin metathesis.[1] The first isolated, well-defined, single-component olefin metathesis catalyst, reported by Gilliom and Grubbs in 1986, was obtained by reacting the Tebbe reagent with norbornene and it was able to catalyze living polymerization of norbornene.[2] Meanwhile, a variety of highly active, well-defined Mo and W based catalysts were developed by the Schrock group.[3] Despite their high reactivity, early transition metal-based catalysts exhibited extreme air and moisture sensitivity, low thermal stability, and

poor tolerance for many functional groups, such as alcohols and aldehydes, due to the electrophilic nature of these metals.

To improve the catalyst stability and functional group tolerance, a new class of Ru-based catalysts was developed by the Grubbs group in the early 1990s.[4] Among them, the Ru(II) benzylidene complex **1** with tricyclohexylphosphine ligands (PCy_3) showed high activity as well as tolerance of air, moisture and a wide range of functional groups,[4] and is now often recognized as the first-generation Grubbs catalyst. Later in 1999, a significant improvement of catalyst activity was achieved by replacing one of the PCy_3 ligands with a strongly sigma-donating donating N-heterocyclic carbene (NHC) ligand.[5] Ru complex **2** not only maintained superb tolerance for air, moisture and organic functionalities, but also rivaled the activity of the highly active molybdenum catalysts.[6] Complex **2** is now often recognized as the second-generation Grubbs catalyst. Following the success, numerous NHC-based Ru catalysts have been synthesized and studied. Some representative examples include (1) replacing the PCy_3 ligand with pyridine to give catalyst **3** that initiated extremely fast, making it an ideal catalyst for living polymerization to produce narrowly dispersed polymers; [7] (2) incorporating an isopropoxybenzylidene ligand to give catalyst **4** to impart increased stability relative to phosphine-containing analogues;[8] (3) tethering the NHC to the Ru center to give a series of catalysts **5** that can produce cyclic polymers.[9]

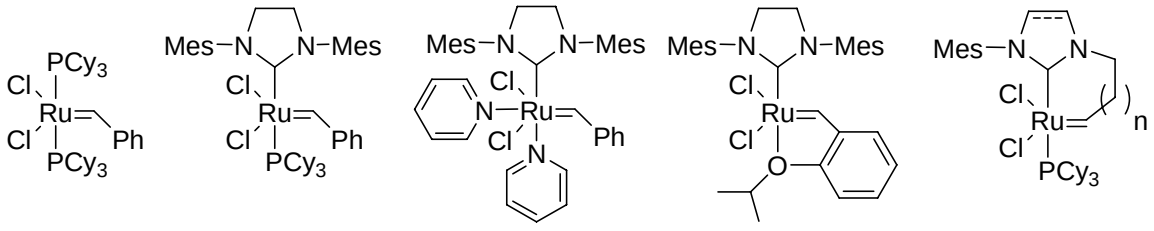

1 **2** **3** **4** **5**

Figure 2. Representative ruthenium-based olefin metathesis catalysts.

Ring-Opening Metathesis Polymerization (ROMP)

As one of the most important polymerizations, ROMP is a chain-growth polymerization in which cyclic olefins are converted to polyalkenamers. The overall reaction involves breaking and reforming olefin double bonds with simultaneous opening of the unsaturated cyclic monomers. Thus, the total amount of unsaturation is retained, and the resulting polymers are comprised of repeating units that contain olefins in their backbones. The release of ring strain provides the driving force for ROMP to proceed. Typical cyclic olefin monomers for ROMP in order of decreasing ring strain include cyclobutene, norbornene, cyclooctene, cyclododecatriene, and cyclopentene, (Figure 3).

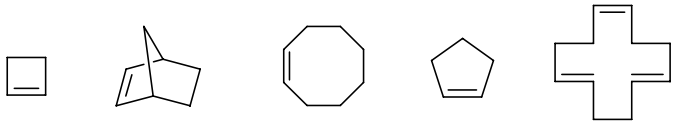

Figure 3. Representative cyclic olefin monomers used in ROMP.

Unhindered backbone olefins in the polyalkenamers can also undergo secondary metathesis since ROMP is equilibrium controlled. Intermolecular secondary metathesis leads to transfer of the active metal center from one polymer chain end to another chain and the total number of polymer chains does not change (Figure 4(a)). The active metal center at a polymer chain end can also react with an internal olefin in its own polymeric backbone, thus producing a macrocycle, and this intramolecular secondary metathesis is often referred as backbiting (Figure 4(b)).[10] To minimize the concentration of cyclic oligomers, polymerizations should be performed at conditions that minimize the relative equilibrium monomer (typically high monomer concentration and low temperatures for exothermic polymerizations). Both intermolecular chain transfer and backbiting result in

broadening of the polymer molecular weight distributions, and should therefore be avoided when living polymerization is desired.

(a)

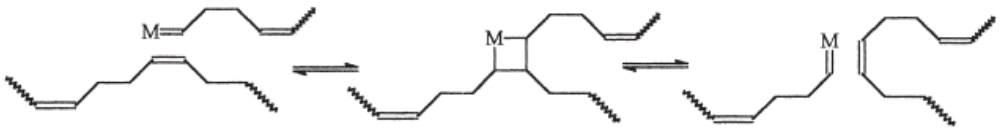

(b)

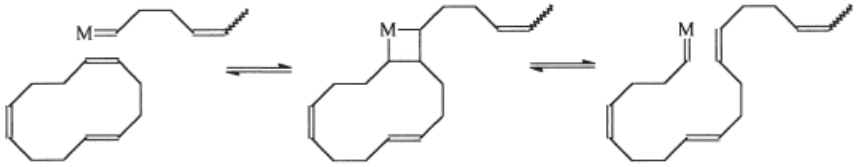

Figure 4. Secondary metathesis reations: (a) intermolecular chain transfer; (b) intramolecular back-biting.

On the other hand, intermolecular chain transfer (CT) can also be advantageous to produce telechelic polymers when an α,γ-difunctional olefin is employed as chain-transfer agent (CTA).[11] In the CT reaction with a symmetric α,γ-difunctional olefin, a propagating polymer chain is terminated with a functional group and forms a new substituted metal alkylidene. This complex subsequently reacts with monomer or a preformed polymer chain and effectively transfers the active species from one chain to another (Figure 5). This process preserves the number of active catalyst centers and leads to symmetric telechelic polymers with a number average functional groups per chain approaching 2. In the absence of chain termination (i.e., decomposition of the active metal center at the chain end), the only non-functional end group comes from the benzylidene or alkylidene in the original catalyst. Therefore, it is important to use a minimal amount of catalyst compared to the CTA. Catalysts **2** and **4** are best suited for ROMP-CT due to their extraordinary activity and high stability. If the catalyst does not

decompose during the course of ROMP, the molecular weight (MW) of the polymer product is controlled by an equilibrium process. Therefore, if the catalyst concentration ($[C]_0$) is chosen such that $[CTA]_0 >> [C]_0$, then the average degree of polymerization (DP) is determined by

$DP = ([M]_0 - [M]_t) / ([CTA]_0 - [CTA]_t)$.

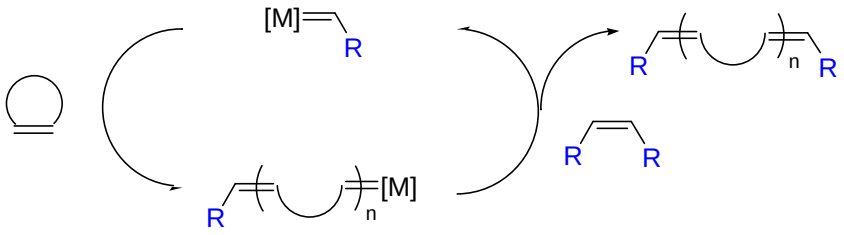

Figure 5. Generic mechanism of chain transfer in ROMP to generate telechelic polymers.

ROMP can also be controlled to behave as a living/controlled polymerization: (1) complete and instantaneous initiation to ensure each polymer chain starts to grow at approximately the same time; (2) irreversible propagation and the propagation rate (k_p) is much smaller than the initiation rate (k_i) to ensure all the polymer chains grow simultaneously; (3) absence of chain termination and chain transfer to ensure all the propagating chain ends remain active. In order to eliminate the secondary metathesis on the polymer backbones, sterically bulky bicyclic monomers, such as substituted norbornenes, are often used. Living ROMP is also possible with monocyclic, unhindered olefins, such as cyclobutene, cyclopentene, and *trans*-cyclooctene, with the use of excess free phosphine ligands to significantly suppress the secondary metathesis.[12] Both catalysts **1** and **3** can mediate living ROMP due to their fast initiation, but catalyst **3** has become the state-of-the-art choice due to its much more improved initiation and activity. The extraordinary activity of catalyst **3** has enabled rapid synthesis of polymers with very low polydispersity indices (PDI) from norbornenes with various functionalities, and full

monomer conversion is usually achieved within minutes.[13] Living ROMP has also significantly simplified the synthesis of block copolymers, simply through sequential addition of different monomers, which do not undergo chain transfer.[14]

Expansion of Polymer Chemistry Toolbox

Besides metathesis polymerizations, polymer chemistry has undergone some other important developments over the last two decades. These relatively new developments, together with the well-known ones, greatly enhanced the ability of polymer chemists to control the molecular weight distribution, functionality, microstructure, and architecture of polymers.

Living Ionic Polymerizations

Developed in the 1960s, ionic polymerizations were once the state-of-the-art living polymerization techniques (for certain types of polymers, still the best techniques to produce the highest-quality polymer products, if performed well). Cationic polymerization is suitable for olefin monomers with electron-donating substituents such as alkoxy and phenyl.[15] Anionic polymerization takes place with monomers possessing electron-withdrawing groups such as nitrile, carbonyl, and phenyl.[16]

Limited monomer functionality, rigorously purified monomer and solvent, and low temperatures are required to suppress termination and chain transfer. A suitable solvent is also important to stabilize the ionic propagating species long enough to propagate into high MW polymers. These stringent requirements make the utility of ionic polymerizations relatively limited.

Controlled Radical Polymerizations

The last 15 years have witnessed the explosive development of controlled radical polymerizations (CRPs) that mainly include atom-transfer radical polymerization (ATRP),[17] reversible addition fragmentation chain-transfer (RAFT) polymerization,[18] and nitroxide mediated radical polymerization (NMRP).[19]

All the CRP methods are based on the same idea: (1) a dynamic equilibrium is established between a low concentration of active propagating chains and a large amount of dormant chains (unable to propagate or terminate) via rapid, reversible chain-end capping or chain transfer reaction; (2) the propagation and deactivation of the active radicals, namely reversible termination or chain transfer reaction, are much faster than any irreversible termination to minimize the chance of irreversible termination and ensure that all polymer chains are growing at approximately the same rate to obtain uniform molecular weight distribution.

ATRP has been the most widely used and versatile CRP method, and it uses a catalytic amount of a transition metal complex, often copper or ruthenium, to reversibly abstract a halogen atom from a polymer chain end, and thereby transform the chain end group into an active propagating radical from a dormant state. This dynamic equilibrium strongly favors the dormant species (K_{eq} = 10^{-9}-10^{-7}). Therefore only a minute concentration of growing free radicals is maintained, and thus bimolecular termination and disproportionation are minimized.

Similarly, in NMRP, unstable alkoxyamine can thermally initiate and the nitroxide radicals reversibly trap the propagating radicals to maintain a low concentration of growing free radicals.

RAFT polymerizations utilize a di- or trithiocarbonyl chain transfer agent (CTA) to degeneratively chain transfer between the propagating chain ends: propagating chain end radical addition to the C=S bond in CTA is followed by rapid reinitiation through S-C bond cleavage to release another propagating chain with an active radical chain end.

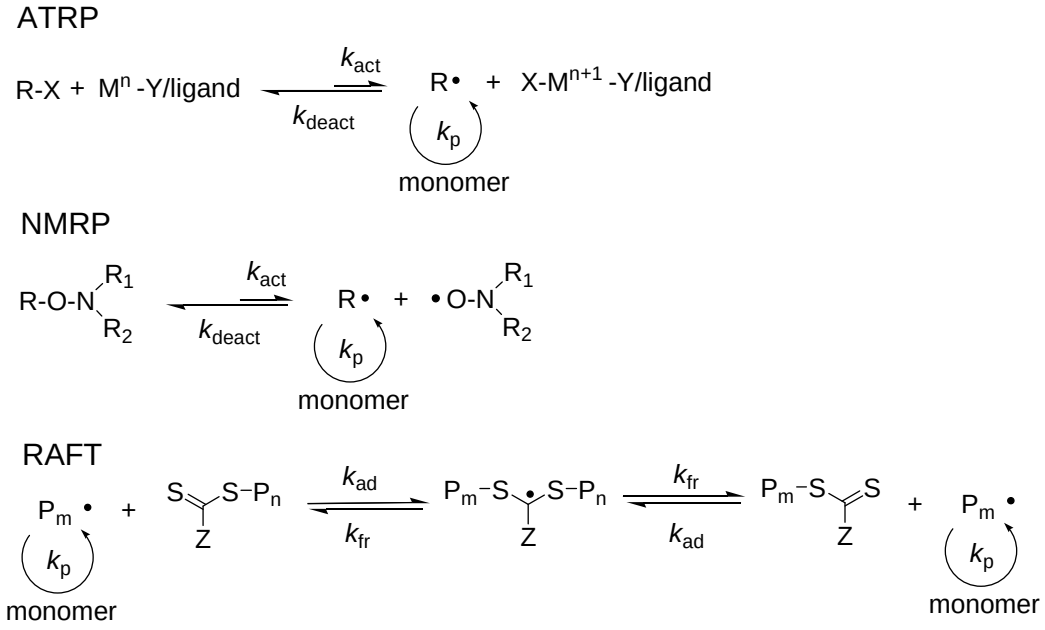

Figure 6. Generic mechanism of controlled radical polymerizations: ATRP, NMRP, and RAFT.

"Click" Chemistry

One of the most noticeable synthetic trends in the past decade is "click" chemistry, a concept first introduced by Sharpless, Kolb, and Finn in 2001,[20] which had an enormous impact on materials synthesis. The basic philosophy of "click" chemistry is to develop reactions that have

- High chemoselectivity
- Quantitative yield with little or no by-products
- Robustness to various experimental conditions

- Fast kinetics
- Functional group tolerance
- Simple and mild reaction conditions

A few modular reactions that meet these criteria involve easy-to-introduce functional groups and often have a large thermodynamic driving force to favor a single reaction product. The most notable "click" reaction is copper-catalyzed Huisgen azide–alkyne cycloadditions (CuAAC). Catalytic amount of copper(I) from various sources can be used to give exclusively 1,4-triazoles. The reaction can also be carried out in air and in water, by formation of copper(I) *in situ* using a one-electron reductant such as sodium ascorbate. In applications where residual copper may be a concern, strained cyclooctynes have been found to spontaneously undergo quantitative and selective cycloaddition with azides even in living biological systems.[21]

Other popular "click" reactions include: radical thiol-ene coupling, activated ester couplings, Michael addition, oxime condensation, anthracene-maleimide Diels-Alder cycloaddition and so on.[22]

Different from small-molecule organic reactions, reactions on or between polymers are challenging in many cases, because of the low concentrations and sterically hindered functional groups on polymers, the presence of a large amount of other functionalities, and the difficulty in purification if side or incomplete reactions occur. Simple, efficient, and selective "click" reactions are ideal to meet these challenges, and satisfy the huge need from polymer chemists to modify, functionalize, or couple polymers in a well-controlled fashion, resulting in the wide application of "click" chemistry in polymer science in the last a few years.

Control of Polymer Architectures

It has long been understood that the polymer architecture has huge implications for the physical properties and applications of polymeric materials. A central theme in polymer science over the last half century has been to develop methods for efficient and accurate control of polymer molecular weights and architectures, and to understand the structure-property relationships of polymer materials.

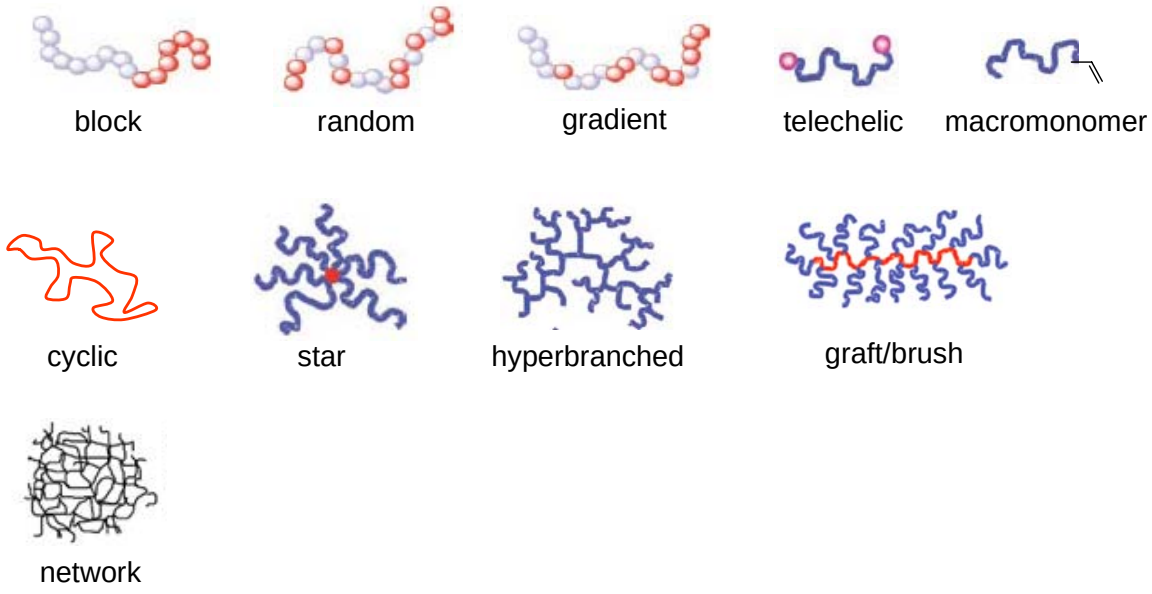

Figure 7. Representative polymer architectures. Partly adapted from reference 25b.

Linear Copolymers

The simplest examples of linear polymer architectures include copolymers of two types of different monomers, A and B. A and B can be arranged in a "block", "random", "alternating", or "gradient" fashion in a linear chain. With the same overall chemical compositions, the arrangement of A and B monomers can dramatically affect the materials properties, such as the viscosity, the solubility, phase transitions temperatures, mechanical properties, optical properties, and association behavior in the melt and solution states.[23]

Telechelic Polymers

The ends of a polymer chain are obviously important positions. Polymers with reactive or functional terminal groups are called telechelic polymers. Polymer terminal groups most often originate from the initiation and the termination steps, and from chain transfer process in some cases.[24] A wide variety of controlled polymerization methods, such as anionic, controlled radical, and metathesis polymerizations, provide precise control of the chain ends. Using functionalized initiators,[25] modifying the existing end groups,[25] and end-capping with functional terminating agents[26] are the most common ways to achieve the desired chain end functionalities.

The end groups of telechelic polymers can be used to attach polymers onto surfaces or to form hybrid conjugates only at the chain ends.[27] The end groups can also be designed to form associating supramolecular polymers or networks.[11c,11d,28] Telechelic polymers are also important precursor polymers for the synthesis of triblock copolymers through chain extension,[29] and for the syntheses of cyclic polymers[30] and model networks[31] through end-linking.

In a special case, when a polymer chain is terminated at only one end with a polymerizable group, this monotelechelic polymer is often referred as “macromonomer” (MM).[32] Macromonomers can be polymerized to prepare more complex polymer structures.

Cyclic Polymers

While end groups of polymers have demonstrated a significant role in many of their properties, the absence of end groups in cyclic polymers make them a unique architecture, mostly for scientific curiosity, but they may find commercial applications if

unique properties can be found from cyclic polymers or mixtures of cyclic and linear polymers. For example, (1) cyclic polymers can be used to test the existing theories of polymer physics established on linear chains, such as the reptation theory in polymer melt and the glass transition of polymers; (2) the absence of end groups may be an advantage in some cases, considering that end groups often affect surface properties and degradation; (3) threaded cyclic polymers may act as mechanical crosslinks in a mixture with linear chains.[33]

Synthetic strategies of cyclic polymers can be divided into two main categories: ring-closure approach and ring-expansion approach.[30,33] The ring-closure approach involves cyclization reaction of telechelic polymers under high (or pseudo-high) dilution conditions to suppress the intermolecular end-linking. Successful macrocyclization has been achieved in both bimolecular coupling of a symmetric telechelic polymer and a bifunctional coupling agent[34] and unimolecular coupling of an asymmetric telechelic polymer with complementary functional end groups[35] (Figure 8). Clean, fast, and high yield coupling reactions are commonly used in macrocyclization to boost the conversion of the coupling step.

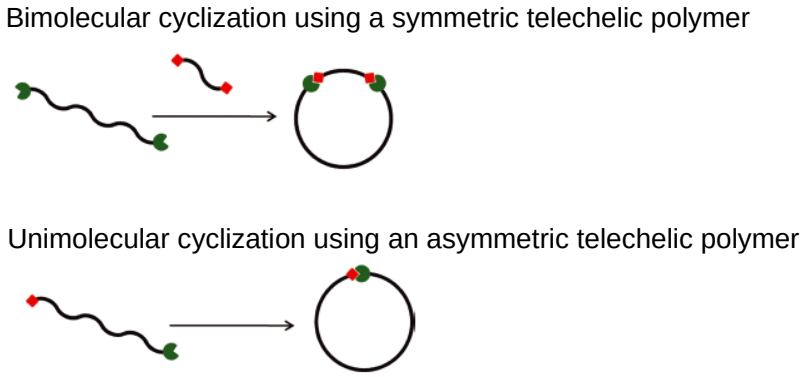

Figure 8. Synthesis of cyclic polymers via cyclization of telechelic polymers. Adapted from reference 30a.

A general issue with the ring-closure approach is that cyclization yields dramatically decreas with increasing MW of the telechelic precursor polymers. Inevitable intermolecular end-linking reactions during macrocyclization lead to the formation of linear chain impurities, which are often difficult and laborious to separate from the cyclic product. Although, a few methods have been developed to strongly favor the intramolecular macrocyclization, such as using biphasic coupling,[36] electrostatic interaction,[37] and addition of poor solvent,[38] and high cyclization efficiencies (>90%) have been reported in some systems. A second limit with the ring-closure approach is the small quantity of cyclic materials that can be produced as a result of the high dilution conditions. Reported macrocyclization reactions are often carried out at milligram scale, making many physical measurements and applications of the cyclic polymer product difficult.

The second strategy toward cyclic polymers is the ring-expansion approach. Ring-expansion polymerizations typically involve a catalyst or initiator that yields a growing cyclic polymer chain, held together by a relatively labile bond (i.e., organometallic or electrostatic). Propagation by insertion of new monomer into this weak bond is driven by thermodynamic factors, such as ring strain in the monomer. The resulting macrocycle may either retain this initiating species or release the catalyst by an intramolecular chain transfer.

The key advantage of the ring-expansion approach is that high dilution is not required to yield cyclic polymers. As a result, this approach is amenable to large scale syntheses. Also, because the cyclic structure is maintained throughout propagation, high molecular weight polymers can be easily prepared without the entropic penalty associated

with the ring-closure approach. The complication of the ring-expansion approach is that, as a catalytic process, the rates of initiation, propagation, chain transfer, and catalyst release (when possible) have to be fine tuned in order to control the MW and purity of the produced cyclic polymers. Furthermore, linear monomer, linear catalyst, or undesired initiator may have to be absent from the reaction system to avoid ring opening during the ring-expansion polymerization.

The cyclic nature of the polymer products is often supported either by molecular characterizations, such as matrix-assisted laser desorption/ionization (MALDI) mass spectrometry, to confirm the absence of end groups, or by materials characterization, based on known properties of cyclic polymers, such as lower intrinsic viscosity and smaller hydrodynamic radius of cyclic polymers compared to their linear analogs *at the same MW*.

However, these characterizations may not reveal the overall purity of the cyclic polymers. Furthermore, the lack of the exact linear polymer analogs may complicate the comparison of the properties. As a result, in most of these studies, the purity of the cyclic polymers was not claimed and protocols to ensure high purity were not studied.

Some of the most important examples using this approach are highlighted below:

In an early example, the Shea group has developed a cyclic borane to initiate the polyhomologation of dimethylsulfoxonium methylide (Figure 9). Methylene insertion occurs only on the two less-hindered carbon-boron bonds on the macrocycle to produce low MW cyclic polymethylene (0.6−2 kDa) with PDIs between 1.1 and 1.6.[39]

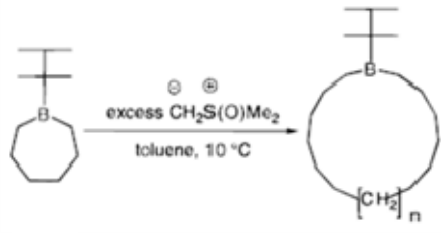

Figure 9. Synthesis of cyclic poly(methylene) from cyclic boranes. Adapted from reference 39.

The groups of Jérome and Kricheldorf have used cyclic tin alkoxide initiators to make cyclic polyesters from lactone monomers.[40] At the end of the polymerization, the tin initiator remains in the cyclic polymer and is subject to hydrolysis. To stabilize the cyclic structure, a small amount of crosslinkable caprolactone was polymerized after the first caprolactone polymerization was finished. Photo-crosslinking the cyclic block copolymer under dilute conditions produced more stable linkage (Figure 10).[40d]

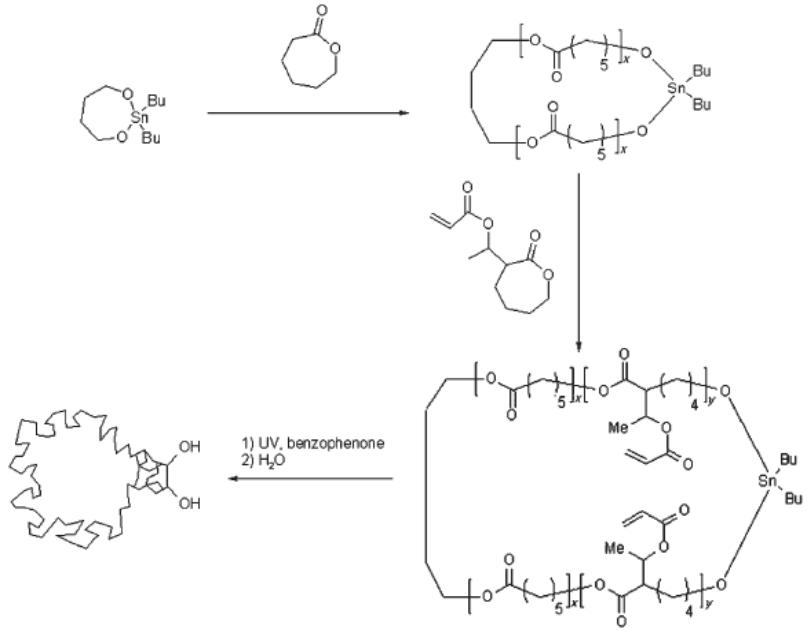

Figure 10. Synthesis of cyclic polycaprolactone block copolymers from a cyclic tin alkoxide initiator and photo-crosslinking to stabilize the cyclic structure. Adapted from reference 40d.

In their research on organocatalysis of lactone polymerization, the groups of Waymouth and Hedrick have found that, in the absence of any alcohol initiators, NHC can mediate the polymerization of lactones to produce cyclic polyesters.[41] The polymerization was believed to occur by nucleophilic attack of the carbene on lactone to generate an alkoxide and acylimidazolium zwitterions, which subsequently propagates by the addition of monomer to the alkoxide of the zwitterionic intermediate. Efficient macrolactonization occurs rapidly as a result of the enforced proximity of the zwitterionic chain ends to generate macrolactones (Figure 11). The produced cyclic polyesters had MW of 7-26 kDa, which was controlled by the ratio of monomer to NHC ([M]/[NHC]), and PDIs < 1.3. Recently, the Zhang group also reported narrowly dispersed cyclic homo and block poly(α-peptoid)s (PDI < 1.2) from NHC catalyzed polymerization of *N*-carboxylanhydrides, presumably operated by the same zwitterionic mechanism.[42]

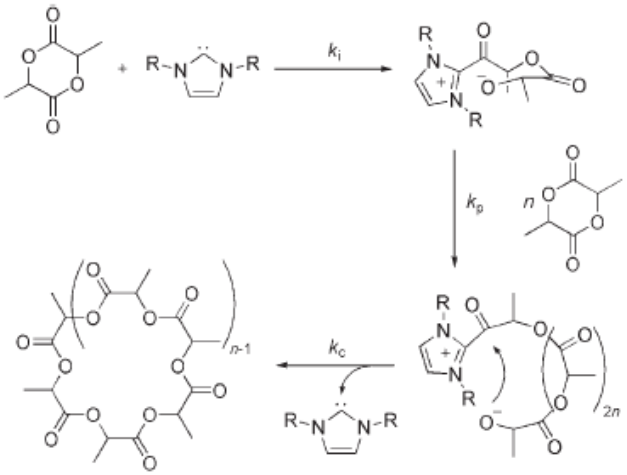

Figure 11. Proposed mechanism for NHC-mediated zwitterionic polymerization of lactide. Adapted from reference 41a.

The Grubbs group has developed a series of cyclic Ru-alkylidene catalysts (Catalyst **5** in Figure 2) that were able to mediate ring-expansion metathesis polymerization (REMP) of cyclic olefins to produce cyclic polymers.[43] A portion of this

thesis is devoted to the study of REMP mechanism and synthesis of cyclic polymers via REMP.

Star Polymers

Star polymers have a globular three-dimensional structure consisting of multiple linear polymers (arms) radiating from the central moiety (core). The preparation of star polymers is usually achieved via living ionic polymerizations, controlled radical polymerizations, and ring-opening polymerizations. The synthetic strategies can be divided into three general synthetic methods: (1) "core-first" approach, where a multifunctional initiator is employed to simultaneously initiate the polymerization to form the arms of the star polymer (Figure 12a); (2) "arm-crosslinking" approach involves the reaction of a macroinitiator or a macromonomer, pre-prepared as the arm, with a difunctional (or higher) crosslinker to form a densely cross-linked core (figure 12b). (3) "Arm coupling" approach involves coupling of end-functionalized polymers or living polymer chains with a multifunctional coupling agent (Figure 12c).[44,45,46]

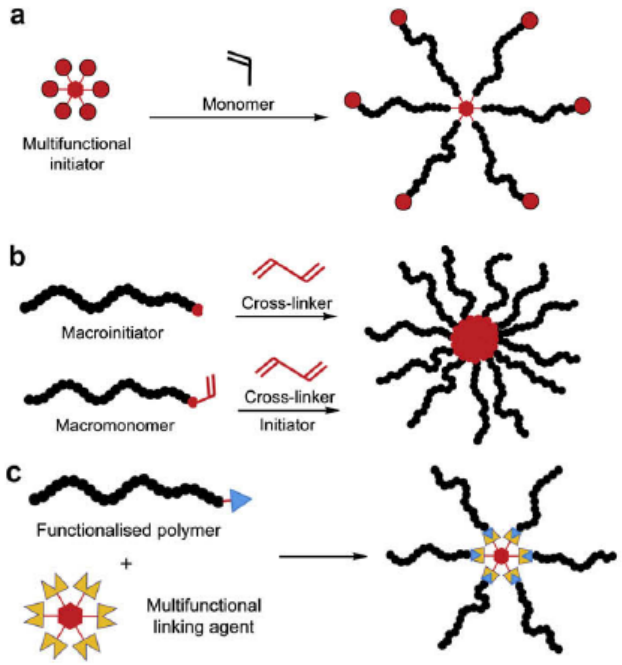

Figure 12. Synthetic approaches toward star polymers. Adapted from reference 45.

Hyperbranched Polymers

Similar to star polymers, hyperbranched polymers are relatively compact and have lower viscosity than their linear counterparts with the same MW because of their small hydrodynamic radius. There are two major approaches to preparing hyperbranched polymers: (1) condensation polymerization of AB_n-type of monomers, where the A group can react with B, and create a branching point; and (2) "self-condensing polymerization" of inimers which contain both a polymerizable group (carbon–carbon double bond) and a group able to initiate polymerization, in the same molecule.[47]

Graft/Comb/Brush Polymers

Graft/comb polymers are a special type of branched polymers in which side chains or side groups are attached to the backbone polymer at various points. Brush polymers are commonly referred to as high MW graft polymers with very dense side chains placed on every backbone repeating unit. For simplicity, the name "brush

polymer" is exclusively used to represent this type of graft polymer architecture. In brush polymers, the high steric crowding of sides chains leads to an extended backbone conformation, instead of random coil as in a linear polymer. The nonspherical macromolecular geometries and molecular lengths that can be up to a few hundred nanometers make brush polymers an attractive unimolecular nano-object to study.[48]

Brush polymers are usually prepared by three grafting methods (Figure 13): "grafting from", "grafting onto", and "grafting through" (i.e., the macromonomer approach): (1) The "grafting from" approach involves the growth of side chains from polymer backbones containing initiation sites (macroinitiators) and has been most explored for a variety of monomers. Importantly, the initiation efficiency from the macroinitiators may be limited due to the high density of initiation sites. (2) The "grafting onto" method allows separate preparation of backbone polymers and side chains, but the grafting becomes progressively difficult with conversion, leading to limited grafting density, even in large excess of side chains. (3) The "grafting through" approach guarantees complete grafting (i.e., one side chain per repeating unit), and it can also afford the most precise and easiest control of side chain length and main chain length, provided that the polymerization of MM is efficient and controlled. However, this is often difficult because of the inherently low concentration of polymerizable groups and the demanding steric hindrance of side chains.[46, 49]

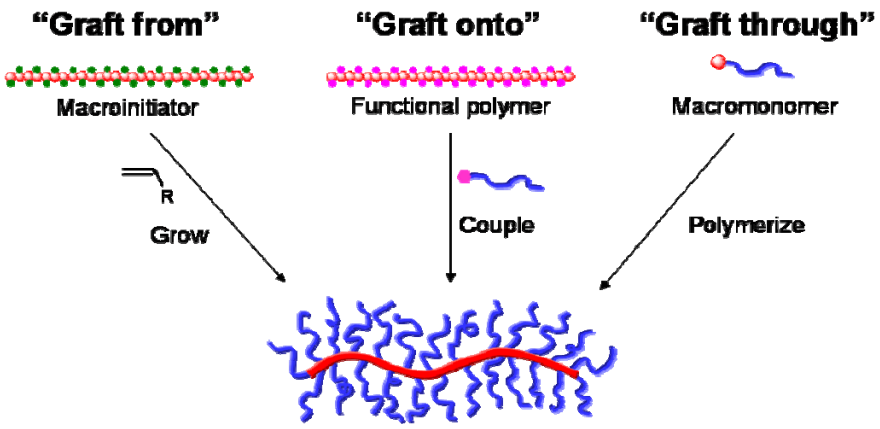

Figure 13. Synthetic approaches toward brush polymers.

A portion of this thesis addresses the challenges to synthesize brush polymers with *ultrahigh MW* and *low PDI*, in *high conversions* and *large quantities*.

Additionally, hybrid polymers combining different architectures are also of great interest for current research.

Thesis Research

To design and synthesize well-defined polymeric materials efficiently with predetermined properties is a constant goal for polymer scientists. This thesis research explores the use of powerful olefin metathesis reactions in the syntheses of complex polymer structures and investigates the physical properties enabled by the resultant new materials.

Chapters 2 and 3 describe the study of a homologous series of "cyclic" catalysts that can mediate REMP to produce cyclic polyalkenamers, including the polymerization mechanism and characterizations of cyclic polymer products.

Chapters 4 and 5 describe the synthesis of various linear brush homopolymers and copolymers via living ROMP of macromonomers and the synthesis of cyclic brush polymers. Several morphological characterizations revealed the extended conformation

of individual brush polymers and the highly ordered self-assembly structures formed by brush copolymers.

Chapter 6 describes the synthesis of well-defined liquid crystalline (LC) networks from telechelic precursor LC polymers. These networks exhibited fast, reversible, low-threshold electro-optic response, revealing the importance of network parameters on the materials performance.

References

(1) *Handbook of Metathesis*; Grubbs, R. H., Ed.; Wiley-VCH: Weinheim, 2003.
(2) Gilliom, L. R.; Grubbs, R. H. *J. Am. Chem. Soc.* **1986**, *108*, 733.
(3) (a) Schrock, R.R. *Acc. Chem. Res.* **1990**, *23*, 158. (b) Feldman, J.; Schrock, R.R. *Prog. Inorg. Chem.* **1991**, *39*, 1.
(4) (a) Nguyen, S. T.; Johnson, L. K.; Grubbs, R. H.; Ziller, J. W. *J. Am. Chem. Soc.* **1992**, *114*. 3974. (b) Nguyen, S. T.; Grubbs, R. H.; Ziller, J. W. *J. Am. Chem. Soc.* **1993**, *115*, 9858. (c) Fu, G. C.; Nguyen, S. T.; Grubbs, R. H. *J. Am. Chem. Soc.* **1993**, *115*, 9856. (d) Schwab, P.; Grubbs, R. H.; Ziller, J. W. *J. Am. Chem. Soc.* **1996**, *118*, 100.
(e) Schwab, P.; France, M. B.; Ziller, J. W.; Grubbs, R. H. *Angew. Chem. Int. Ed.* **1995**, *34*, 2039.
(5) Scholl, M.; Ding, S.; Lee, C. W.; Grubbs, R. H. *Org. Lett.* **1999**, *1*, 953.
(6) Bielawski, C. W.; Grubbs, R. H. *Angew. Chem. Int. Ed.* **2000**, *39*, 2903.
(7) (a) Sanford, M. S.; Love, J. A.; Grubbs, R. H. *Organometallics* **2001**, *20*, 5314.
(b) Love, J. A.; Morgan, J. P.; Trnka, T. M.; Grubbs, R. H. *Angew. Chem., Int. Ed.* **2002**, *41*, 4035. (c) Choi, T. L.; Grubbs, R. H. *Angew. Chem. Int. Ed.* **2003**, *42*, 1743.
(8) Garber, S. B.; Kingsburgy, J. S.; Gray, B. L.; Hoveyda, A. H. *J. Am. Chem. Soc.* **2000**, *122*, 8168.
(9) (a) (a) Bielawski, C. W.; Benitez, D.; Grubbs, R. H. *Science* **2002**, *297*, 2041.
(b) Bielawski, C. W.; Benitez, D.; Grubbs, R. H. *J. Am. Chem. Soc.* **2003**, *125*, 8424.
(c) Boydston, A. J.; Xia, Y.; Kornfield, J. A.; Gorodetskaya, I. A.; Grubbs, R. H. *J. Am. Chem. Soc.* **2008**, 130, 12775. (d) Xia, Y.; Boydston, A. J.; Yao, Y.; Kornfield, J. A.; Gorodetskaya, I. A.; Spiess, H. W.; Grubbs, R. H. *J. Am. Chem. Soc.* **2009**, 131, 2670.
(10) (a) Ofstead, E. A.; Calderon, N. *Makromol. Chem.* **1972**, *154*, 21. (b) Höcker, H.; Müsch, R. *Makromol. Chem.* **1972**, *157*, 201.
(11) (a) Bielawski, C. W.; Morita, T.; Grubbs, R. H. *Macromolecules* **2000**, *33*, 678.
(b) Morita, T.; Maughon, B. R.; Bielawski, C. W.; Grubbs, R. H. *Macromolecules* **2000**, *33*, 6621. (c) Scherman, O. A.; Ligthart, G. B. W. L.; Ohkawa, H.; Sijbesma, R. P.; Meijer, E. W. *Proc. Natl. Acad. Sci. USA* **2006**, *103*, 11850. (d) Higley, M. N.; Pollino, J. M.; Hollembeak, E.; Weck, M. *Chem. Eur. J.* **2005**, *11*, 2946.
(12) (a) Wu, Z.; Wheeler, D. R.; Grubbs, R. H. *J. Am. Chem. Soc.* **1992**, *114*, 146.
(b) Wu, Z.; Grubbs, R. H. *Macromolecules* **1994**, *27*, 6700. (c) Trzaska, S. T.; Lee, L. B. W.; Register, R. A. *Macromolecules* **2000**, *33*, 9215. (d) Walker, R.; Conrad, R. M.; Grubbs, R. H. *Macromolecules* **2009**, *42*, 599.
(13) Choi, T.-L.; Grubbs, R. H. *Angew. Chem. Int. Ed.* **2003**, *42*, 1743.
(14) (a) Camm, K. D.; MartinezCastro, N.; Liu, Y.; Czechura, P.; Snelgrove, J. L.; Fogg, D. E. *J. Am. Chem. Soc.* **2007**, *129*, 4168. (b) Matson, J. B.; Grubbs, R. H. *J. Am. Chem. Soc.* **2008**, *130*, 6731.
(15) Kennedy, J. P. *J. Polym. Sci. Part A: Polym. Chem.* **1999**, *37*, 2285.
(16) Smid, J. *J. Polym. Sci. Part A: Polym. Chem.* **2002**, *40*, 2101.
(17) (a) Matyjaszewski, K.; Xia, J. *Chem. Rev.* **2001**, *101*, 2921. (b) Ouchi, M.; Terashima, T.; Sawamoto, M. *Chem. Rev.* **2009,** *109,* 4963.
(18) (a) Moad, G.; Rizzardo, E.; Thang, S. H. *Acc. Chem. Res.* **2008,** *41,* 1133. (b) Moad, G.; Rizzardo, E.; Thang, S. H. *Polymer* **2008,** *49,* 1079.

(19) (a) Hawker, C. J.; Bosman, A. W.; Harth, E. *Chem. Rev.* **2001**, *101*, 3661.
(b) Sciannamea, V.; Jérôme, R.; Detrembleur, C. *Chem. Rev.* **2008**, *108*, 1104.
(20) Kolb, H. C.; Finn, M. G.; Sharpless, K. B. *Angew. Chem. Int. Ed.* **2001**, *40*, 2004.
(21) For reviews of "click" chemistry in materials synthesis: (a) Lutz, J.-F. *Angew. Chem. Int. Ed.* **2007**, *46*, 1018. (b) Lutz, J.-F. *Angew. Chem. Int. Ed.* **2008**, *47*, 2182.
(22) Iha, R. K.; Wooley, K. L.; Nyström, A. M.; Burke, D. J.; Kade, M. J.; Hawker, C. J. *Chem. Rev.* **2009,** *109,* 5620.
(23) *Introduction to Physical Polymer Science*; Sperling, L. H., 4th ed.; Wiley-VCH: New Jersey, 2006.
(24) Verso, F. L.; Likos, C. N. *Polymer* **2008**, *49*, 1425.
(25) For reviews: (a) Coessens, V.; Pintauer, T.; Matyjaszewski, K. *Prog. Polym. Sci.* **2001**, *26*, 337. (b) Matyjaszewski, K.; Tsarevsky, N. V. *Nature Chem.* **2009**, *1*, 276.
(26) End-capping in anionic polymerization examples: (a) Schmidt, S. C.; Hillmyer, M. A. *Macromolecules* **1999**, *32*, 4794. (b) Henderson, Ian M.; Hayward, Ryan C. *Macromolecules* **2010**, 43, 3249.; End-capping in ROMP examples: (c) Matson, J. B.; Grubbs, R. H. *Macromolecules* **2010**, 43, 213. For review: (d) Hilf, S.; Kilbinger, A. F. M. *Nature Chem.* **2009**, *1*, 537.
(27) (a) Pankewitsch, T.; Vanhoorne, P.; Jérôme, R.; Stamm, M. *Macromolecules* **1996,** *28,* 6986. (b) Šubr, V.; Koňák, Č.; Laga, R.; Ulbrich, K. *Biomacromolecules* **2006**, *7*, 122. (c) Heredia, K. L.; Maynard, H. D. *Org. Biomol. Chem.* **2007**, *5*, 45. (d) Gauthier, M. A.; Klok, H.-A. *Chem. Commun.*, **2008**, 2591. (e) Roth, P. J.; Kim, K.-S.; Bae, S. H.; Sohn, B.-H.; Theato, P.; Zentel, R. *Macromol. Rapid Commun.* **2009**, *30*, 1274. (f) Roth, P. J.; Jochum, F. D.; Zentel, R.; Theato, P. *Biomacromolecules* **2010**, *11,* 238.
(28) Brunsveld, L.; Folmer, B. J. B.; Meijer, E. W.; Sijbesma, R. P. *Chem. Rev.* **2001**, *101*, 4071.
(29) (a) Tong, J. D.; Moineau, G.; Leclère, P.; Brédas, J.L.; Lazzaroni, R.; Jérôme, R. *Macromolecules*, **2000**, *33*, 470. (b) Bielawski, C. W.; Morita, T.; Grubbs, R. H. *Macromolecules* **2000**, *33*, 678. (c) Mahanthappa, M. K.; Bates, F. S.; Hillmyer, M. A. *Macromolecules* **2005**, *38*, 7890.
(30) For reviews: (a) Laurent, B. A.; Grayson, S. M. *Chem. Soc. Rev.*, **2009**, *38*, 2202.
(b) Kricheldorf, H. R. *J. Polym. Sci. Part A: Polym. Chem.* **2010**, *48*, 251.
(31) (a) Patel, S. K.; Malone, S.; Cohen, C.; Gillmor, J. R.; Colby, R. H. *Macromolecules* **1992**, *25*, 5241. (b) Hedden, R. C.; Saxena, H.; Cohen, C. *Macromolecules* **2000**, *33*, 8676. (c) Johnson, J. A.; Lewis, D. R.; Diaz, D. D.; Finn, M. G.; Koberstein, J. T.; Turro, N. J. *J. Am. Chem. Soc.* **2006**, *128*, 6564.
(32) Hadjichristidis, N.; Pitsikalis, M.; Iatrou, H.; Pispas, S. *Macromol. Rapid Commun.* **2003**, *24*, 979.
(33) Semlyen, J. A. *Cyclic Polymers*, 2nd edition; Kluwer Academic Publishers: Boston, 2000.
(34) (a) Roovers, J.; Toporowski, P. M. *Macromolecules* **1983**, *16*, 843. (b) Lepoittevin, B.; Dourges, M. A.; Masure, M.; Hemery, P.; Baran, K.; Cramail, H. *Macromolecules* **2000**, *33*, 8218. (c) Oike, H.; Mouri, T.; Tezuka, Y. *Macromolecules* **2001**, *34*, 6592.
(d) Takano, A.; Kadoi, O.; Hirahara, K.; Kawahara, S.; Isono, Y.; Suzuki, J.; Matsushita, Y. *Macromolecules* **2003**, *36*, 3045. (e) Clark, P. G.; Guidry, E. N.; Chan, W. Y.; Steinmetz, W. E.; Grubbs, R. H. *J. Am. Chem. Soc.* **2010**, *132*, 3405.

(35) (a) Schappacher, M.; Deffieux, A. *Macromolecules* **2001**, *34*, 5827. (b) Lepoittevin, B.; Perrot, X.; Masure, M.; Hemery, P. *Macromolecules* **2001**, *34*, 425. (c) Laurent, B. A.; Grayson, S. M. *J. Am. Chem. Soc.* **2006**, *128*, 4238.
(36)Ishizu, K.; Kanno, H. *Polymer*, **1996**, *37*, 1487.
(37)Oike, H.; Imaizumi, H.; Mouri, T.; Yoshioka, Y.; Uchibori, A.; Tezuka, Y. *J. Am. Chem. Soc.*, **2000**, *122*, 9592.
(38)Yu, G.-E.; Sinnathamby, P.; Price, C.; Booth, C. *Chem. Commun.*, **1996**, 31.
(39)Shea, K. J.; Lee, S. Y.; Busch, B. B. *J. Org. Chem.*, **1998**, *63*, 5746.
(40) (a) Kricheldorf, H. R.; Lee, S. *Macromolecules*, **1995**, *28*, 6718. (b) Kricheldorf, H. R., Al-Masri, M.; Schwarz, G. *Macromolecules*, **2002**, *35*, 8936. (c) Kricheldorf, H. R. *J. Polym. Sci., Part A: Polym. Chem.*, **2004**, *42*, 4723. (d) Li, H.; Debuigne, A.; Jérome, R.; Lecomte, P. *Angew. Chem. Int. Ed.*, **2006**, *45*, 2264.
(41) (a) Culkin, D. A.; Jeong, W.; Csihony, S.; Gomez, E. D.; Balsara, N. P.; Hedrick, J. L.; Waymouth, R. M. *Angew. Chem. Int. Ed.* **2007**, *46*, 2627. (b) Jeong, W.; Hedrick, J. L.; Waymouth, R. M. *J. Am. Chem. Soc.* **2007**, *129*, 8414.
(42) Guo, L.; Zhang, D. *J. Am. Chem. Soc.* **2009**, *131*, 18072.
(43) (a) Bielawski, C. W.; Benitez, D.; Grubbs, R. H. *Science* **2002**, *297*, 2041.
(b) Bielawski, C. W.; Benitez, D.; Grubbs, R. H. *J. Am. Chem. Soc.* **2003**, *125*, 8424.
(c) Boydston, A. J.; Xia, Y.; Kornfield, J. A.; Gorodetskaya, I. A.; Grubbs, R. H. *J. Am. Chem. Soc.* **2008**, *130*, 12775. (d) Xia, Y.; Boydston, A. J.; Yao, Y.; Kornfield, J. A.; Gorodetskaya, I. A.; Spiess, H. W.; Grubbs, R. H. *J. Am. Chem. Soc.* **2009**, 131, 2670.
(44) Kennedy, J. P.; Jacob, S. *Acc. Chem. Res.* **1998,** *31*, 835.
(45) Blencowe, A.; Tan, J. F.; Goh, T. K.; Qiao, G. G. *Polymer* **2009**, *50*, 5.
(46) Hadjichristidis, N.; Pitsikalis, M.; Pispas, S.; Iatrou, H. *Chem. Rev.* **2001,** *101,* 3747.
(47) For review: Voit, B. I.; Lederer, A. *Chem. Rev.* **2009,** *109,* 5924.
(48) Sheiko, S. S.; Möller, M. *Chem. Rev.* **2001**, *101*, 4099.
(49) Zhang, M.; Müller, A. H. E. *J. Polym. Sci., Part A: Polym. Chem.* **2005**, *43*, 3461.

C h a p t e r 2

Cyclic Ruthenium-Alkylidene Catalysts for Ring-Expansion Metathesis Polymerization

Portions of this chapter have been published: Boydston, A. J.; Xia, Y.; Kornfield, J. A.; Gorodetskaya, I. A.; Grubbs, R. H. *J. Am. Chem. Soc.* **2008**, 130, 12775-12782.

Abstract

A series of cyclic Ru-alkylidene catalysts have been prepared and evaluated for their efficiency in ring-expansion metathesis polymerization (REMP). The catalyst structures feature chelating tethers extending from one N-atom of an imidazolylidine ligand to the Ru metal center. The catalyst design is modular in nature, which provided access to Ru-complexes having varying tether lengths, as well as electronically different NHC ligands. Structural impacts of the tether length were unveiled through ^{1}H NMR spectroscopy as well as single-crystal X-ray analyses. Catalyst activities were evaluated via polymerization of cyclooctene, and key data are provided regarding propagation rates, intramolecular chain-transfer, and catalyst stabilities, three areas necessary for the efficient synthesis of cyclic poly(olefin)s via REMP. From these studies, it was determined that while increasing the tether length of the catalyst leads to enhanced rates of polymerization, shorter tethers were found to facilitate intramolecular chain-transfer and release of catalyst from the polymer. Electronic modification of the NHC via backbone saturation was found to enhance polymerization rates to a greater extent than did homologation of the tether. Overall, cyclic Ru-complexes bearing 5- or 6-carbon tethers and saturated NHC ligands were found to be readily synthesized, bench-stable, and highly active catalysts for REMP.

Introduction

The exploration of Ru-based metathesis catalysts has opened doorways to multiple areas of synthetic and polymer chemistry.[1,2] Advances in these areas have been made possible via development of new catalyst scaffolds based on bis(phosphine) complex **1** (Figure 1), or those bearing N-heterocyclic carbene (NHC) ligands such as **2** and **3**. The introduction of catalysts based on **1**–**3**, but predisposed for specific tasks, has further expanded the potential of olefin metathesis. For example, areas such as solid-supported catalysts,[3] symmetric olefin metathesis,[4] tandem catalysis,[5] living polymerization,[1a,6] and stereoselective cross-metathesis (CM) have each benefited from judicious catalyst design and development.[7]

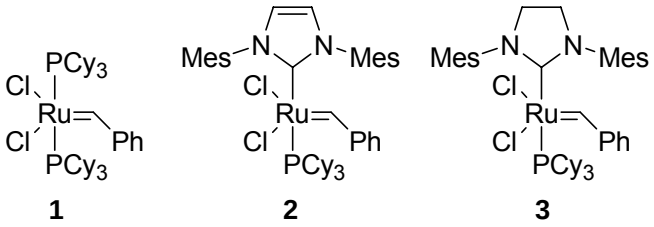

1 **2** **3**

Figure 1. Representative Ru-based metathesis catalysts.

Recently, a Ru-based catalyst design was reported that featured a chelating N-to-Ru tether (Figure 2).[8] Whereas the catalytic activities of **UC-4**–**UC-6** have not been explored, **UC-7** was found to mediate the synthesis of cyclic polymers from cyclic monomers (Scheme 1).[9,10] This ring-expansion metathesis polymerization (REMP) afforded the ability to produce cyclic polymers on large scale from diverse, readily available cyclic monomers.[11,12] While the high catalytic activity of **UC-7** was desirable, caveats were that the synthesis and storage of this compound were complicated by instability. To realize the potential in the area of cyclic polymer chemistry, catalysts

should be readily synthesized in good yields, be easily purified to eliminate any acyclic contaminants, and have an appropriate balance of stability (e.g., during storage as well as polymerizations) and activity. To address issues of stability, we envisioned that catalysts with shorter tether lengths, such as **UC-4**, **UC-5**, and **UC-6**, which contain 4-, 5-, and 6-carbon tethers, respectively, may be advantageous. A potential drawback, however, is that this may be accompanied by decreased catalytic activities. Therefore, we designed catalysts to incorporate two key structural features, shortened tether lengths and saturated NHC backbones, expected to synergistically to provide REMP catalysts of high stabilities and activities.[13]

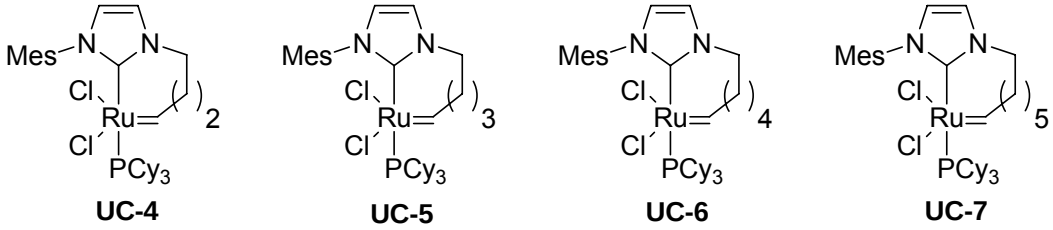

Figure 2. Cyclic Ru-alkylidene metathesis catalysts.

The mechanism by which REMP proceeds may also be elucidated through judicious catalyst design. Initially, REMP was proposed to proceed via a ring-expansion initiation event from a cyclic Ru-alkylidene catalyst (Scheme 1) and propagate as cyclic monomers were incorporated into a growing cyclic polymer. Upon consumption of monomer, a final catalyst release step would provide the original catalyst and the desired cyclic polymer. The polymerization mechanism depicted in scheme 1 has several intriguing features including 1) opening of a chelated Ru-alkylidene catalyst, 2) propagation with the prospect of competing intramolecular chain-transfer events, and 3) a final release of the original catalyst via intramolecular CM.

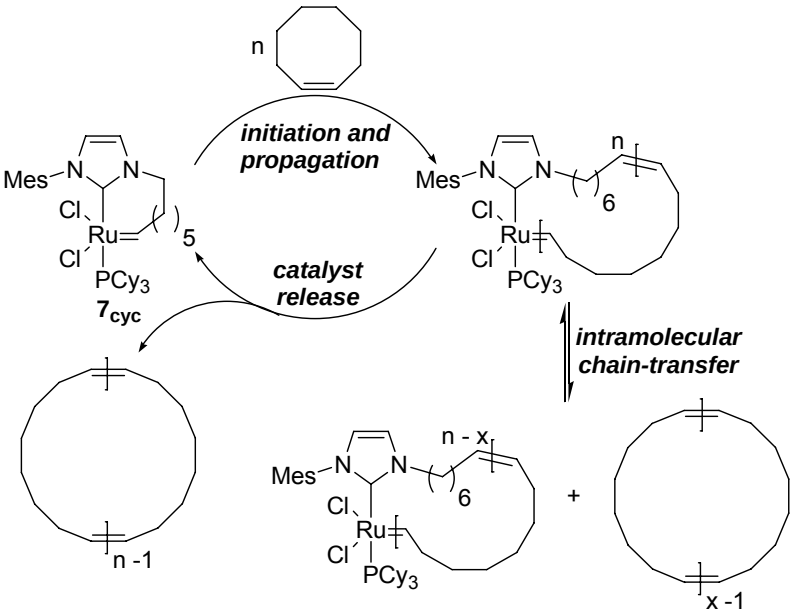

Scheme 1. Proposed REMP catalytic cycle.

Many scenarios are consistent with scheme 1, depending on the relative rates of initiation, propagation, intramolecular chain-transfer, and catalyst release. Initial studies using catalyst **UC-7** demonstrated the ability to control polymer molecular-weight (MW) using the monomer/catalyst loading. This corresponds to a regime in which nearly complete initiation occurs, and catalyst release does not take place prior to complete monomer consumption. Another key observation was that after complete conversion of monomer, the MW of the cyclic polymers progressively decreased in the presence of **UC-7**, indicating significant amounts of intramolecular chain-transfer (Scheme 1). Alternatively, if the rate of propagation is much greater than that of initiation, and the rates of intramolecular chain-transfer and catalyst release are negligible, then all monomer species may be incorporated into a number of macrocycles equal to the number of catalyst molecules that initiated. This last scenario would yield cyclic polymers in which Ru is incorporated into the backbone. Therefore, understanding how the catalyst

design influences the relative kinetics of these processes is central to controlling the nature and distribution of products obtained via REMP.

To better understand each of the mechanistic aspects of REMP, and provide guidance for REMP catalyst design, we sought to investigate a homologous series of cyclic catalysts of varying N-to-Ru tether lengths (Figure 2). The tether length may be central in controlling structural features of the catalyst such as 1) inherent ring-strain in the cyclic Ru-complexes, 2) relative orientations of the NHC and PCy_3 ligands about the metal center, and 3) rotation about the Ru-alkylidene (i.e., Ru=C-R) bond. As will be discussed below, a combination of NMR spectroscopy and single-crystal X-ray analyses of cyclic catalysts ultimately revealed key connections between their structures and activities.

Considering each step in the REMP cycle, it was expected that the tether length ideal for polymerization activity might be unfavorable for catalyst release. Specifically, intramolecular metathesis to reform and release the initial catalyst from the polymer is expected to be most efficient for shorter tether lengths. In contrast, increased tether lengths may be beneficial for polymerization rates, considering longer tethers may increase ring-strain of the catalyst or provide necessary flexibility within the structure. Encouraged by the modular nature of the NHC ligand, and the possibility of controlling REMP catalyst activities via tether length, we prepared and analyzed a homologous series of cyclic REMP catalysts (**UC-4**–**UC-7**, Figure 2), as well as analogues possessing imidazolinylidene ligands. Herein we report the study of their activity in various steps of the REMP cycle, as well key structure-activity relationships.

Results and Discussion

Catalyst Syntheses. The syntheses of complexes **UC-4** and **UC-5** were previously described by Fürstner. To our knowledge, however, their catalytic activity has not been reported. Catalysts **UC-6** and **UC-7** were prepared analogously, as described in scheme 2. The corresponding imidazolium salts (**8**) were first obtained by alkylation of 1-mesitylimidazole. Ligand exchange was then achieved via deprotonation of the imidazolium salt, followed by addition of bis(phosphine) complex **1** (**8**/**1** molar ratio = 2:1) to give "open" complexes **pre-UC-4**–**pre-UC-7**.[,14] In general, ligand exchange proceeded smoothly and the desired non-chelated complexes were isolated in good yields after chromatography on silica gel.[15, 16] Intramolecular metathesis/cyclization was conducted in a PhH/pentane mixture (1:15 v/v) at 70 °C and 0.001 M to give the final "closed" complexes **UC-4**–**UC-7**. Each of the catalysts could be purified by chromatography on silica gel, however, purification of **UC-4**–**UC-6** was more efficiently accomplished via recrystallization from Et_2O/pentane.**Error! Bookmark not defined.**

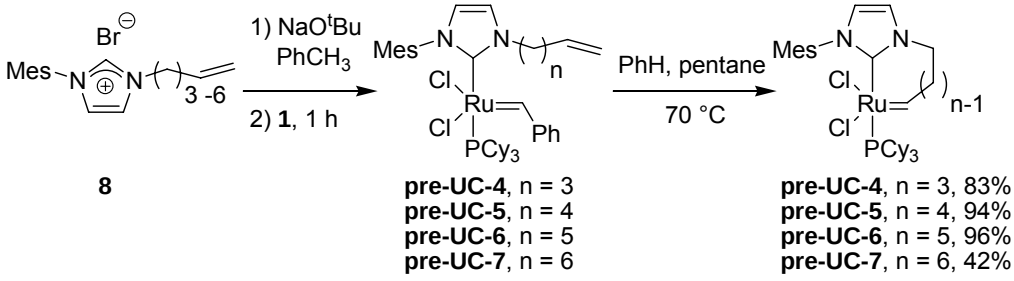

8

pre-UC-4, n = 3
pre-UC-5, n = 4
pre-UC-6, n = 5
pre-UC-7, n = 6

pre-UC-4, n = 3, 83%
pre-UC-5, n = 4, 94%
pre-UC-6, n = 5, 96%
pre-UC-7, n = 6, 42%

Scheme 2. Synthesis of cyclic REMP catalysts **UC-4** – **UC-7**.

We noted that the efficiency of the cyclization of open complexes **pre-UC-4**–**pre-UC-7** to give cyclic catalysts **UC-4**–**UC-7** is highly dependent on the tether length (Table 1). Ostensibly, the ability of an open complex to undergo intra- versus intermolecular metathesis events may give some indication of the tendency for the proposed catalyst

release step in scheme 1. Table 1 summarizes the results of cyclization reactions for each catalyst at 0.01 and 0.001 M. In each case, yields were markedly improved at lower concentration (0.001 M) as determined by ^{1}H NMR analysis of the crude reaction mixtures. At 0.01 M, additional alkylidene peaks were observed via ^{1}H NMR spectroscopy that were upfield of signals characteristic of **1**, **pre-UC-4**–**pre-UC-7**, or **UC-4**–**UC-7**. These signals may be attributed to CM products such as those arising from CM between styrene (formed as a product in the cyclization step), or the terminal olefin of one ligand with the Ru-center of another complex. As expected, these intermolecular metathesis events were significantly diminished at lower concentration. Prolonged reaction times did not result in increased conversion to the desired cyclic species, rather decomposition was observed. It is worth noting that in the case of **pre-UC-7**, no product was observed when the cyclization was conducted at 0.01 M. Therefore, catalyst release during REMP may be slow in comparison with other chain-transfer events when **UC-7** is employed.[17]

Table 1. Cyclization to give cyclic catalysts **UC-4**–**UC-7**[a]

cyclic catalyst	tether length	yield (%)[b]	
		0.01 M	0.001 M
UC-4	4	62	81
UC-5	5	76	97
UC-6	6	81	97
UC-7	7	0	63

[a]Reactions conducted in dry C_6D_6 under N_2 atmosphere at 80 °C for 1 h. [b]Determined by ^{1}H NMR spectroscopy of crude reaction mixtures.

Considering the enhanced activity observed from saturation of the NHC backbone (cf. **2** and **3**), we were motivated to investigate cyclic catalysts with saturated NHC backbones. As depicted in scheme 3, a $PhCH_3$ solution of *N*-mesitylethylenediamine (**9**)[18] was treated with $HC(OEt)_3$ in the presence of catalytic PTSA and stoichiometric

bromo-olefin at 110 °C.[19] This one-pot procedure effected cyclization and alkylation to provide the imidazolinium salts **10** in excellent yields. Unfortunately, attempts at direct deprotonation of **10** using KHMDS in the presence of bis(phosphine) complex **1** were complicated by NHC dimerization and provided low yields of the desired products.[20] Alternatively, treatment of **10** with NaH in $CHCl_3$ cleanly provided neutral adducts **11**.[21] Heating THF solutions of **11** (0.001 M) in the presence of **1** (**11**/**1** molar ratio = 2:1) accomplished ligand exchange as well as cyclization to provide the desired cyclic catalysts **SC-5** and **SC-6** in 46% and 57% overall yields, respectively.[22] Although **SC-5** and **SC-6** were each isolable via chromatography on silica gel, both were found to be crystalline solids and were routinely recrystallized by slow addition of pentane into saturated PhH solutions of the complexes. Similar to **UC-5** and **UC-6**, the saturated catalysts **SC-5** and **SC-6** displayed good stability both in the solid state and in solution.[23]

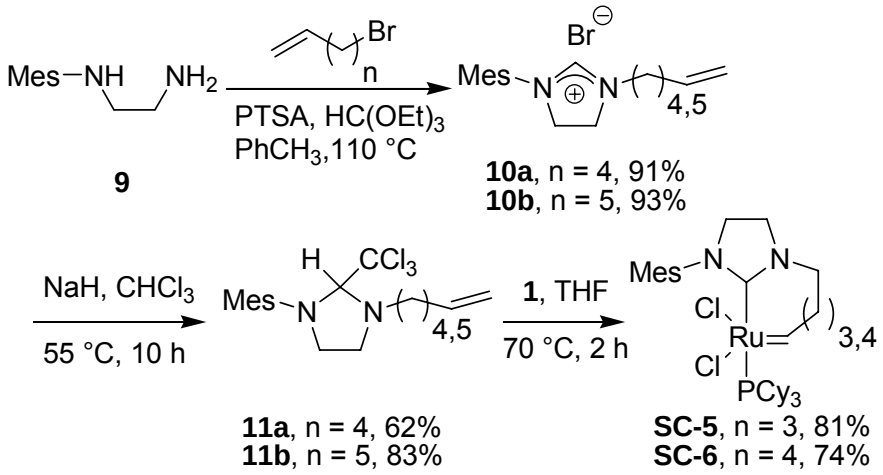

Scheme 3. Synthesis of "saturated" catalysts **SC-5** and **SC-6**.

Structural Analyses. The structural impacts of changing the tether lengths of catalysts **UC-4** – **UC-7** resulted in significant differences in catalyst activities (see polymerization studies below for more discussion). In addition to understanding the structure-activity

relationships pertaining to REMP catalysts, a more general understanding of catalyst architecture may lead to breakthroughs in catalyst design as well as fundamental mechanistic insights of olefin metathesis. Cyclic catalysts **UC-4**–**UC-6** were found to show tether length-dependent trends in three key structural parameters summarized in table 2: 1) rotation about the Ru1-C2 bond, 2) the C1-Ru1-P1 bond angle, and 3) the Ru-C1 bond length (Figure 3).[24]

Table 2. Selected ^{1}H NMR and single-crystal X-ray data for **UC-4**–**UC-7**, **SC-5** and **SC-6**

Catalyst	UC-4[b]	UC-5[b]	SC-5	UC-6	SC-6
δ H2 (ppm)[a]	19.70	20.50	20.39	19.71	19.61
$^{3}J_{H2,P1}$ (Hz)[a]	14.1	10.5	9.3	5.1	5.0
Cl2-Ru1-C2-C3	51.3	26.6	18.3	16.2	21.1
N1-C1-Ru1-C2	156.5	162.2	160.0	153.5	151.2
C1-Ru1-P1	171.0	166.0	165.3	163.3	168.8
N1-C1-Ru1	128.8	127.0	124.3	126.6	124.0
N2-C1-Ru1	127.8	128.9	128.1	129.4	129.5
N1-C1-N2	103.4	104.1	107.5	103.6	107.2
Ru1-C1	2.076	2.091	2.072	2.113	2.084
Ru1-C2	1.812	1.806	1.821	1.823	1.800
Ru1-P1	2.402	2.421	2.417	2.421	2.423

[a]Data taken in C_6D_6 at ambient temperature. [b]See reference 8.

Although many structural features of **UC-4**–**UC-7** are best observed via solid-state analysis, rotation about the Ru1-C2 bond is manifested in the coupling constants between the P1 and H2 atoms in the ^{1}H NMR spectra (Table 2 and Figure 3). Complexes **UC-4** and **UC-5**, which were previously characterized in solution and solid state, displayed coupling constants of $^{3}J_{H2,P1}$ = 14.1 and 10.5 Hz (solvent = C_6D_6), respectively. The smaller coupling constant observed from complex **UC-5**, in comparison with **UC-4**, indicated that the corresponding atoms in the former are closer to a perpendicular

arrangement. Consistent with this trend, a smaller coupling constant was observed in the ^{1}H NMR spectrum of **UC-6** (i.e., $^{3}J_{H2,P1}$ = 5.1 Hz), indicating that the alkylidene proton (H2) was projected nearly perpendicular to the Ru1-P1 bond. The ^{1}H NMR spectrum of **UC-7** revealed a coupling constant of $^{3}J_{H2,P1}$ = 10.2 Hz, which may be ascribed to the increased ring size (cf. **UC-6**) inducing twist about the Ru1-C2 bond.[25]

To further investigate the structures of the cyclic catalysts, we compared single-crystal X-ray data of **UC-4**–**UC-6**, as well as saturated analogues **SC-5** and **SC-6**. The crystal structures of these complexes confirmed a variable degree of rotation about the Ru1-C2 bond, as determined from the Cl2-Ru-C2-C3 dihedral angles (Table 2). Overall, for **UC-4**–**UC-6**, decreased $^{3}J_{H2,P1}$ values corresponded to decreased dihedral angles suggesting that the solution and solid-state structures of the catalysts are similar. It should be noted that while the $^{3}J_{H2,P1}$ values observed from **SC-5** and **SC-6** were consistent with each complex's respective unsaturated analogue, solid-sate analysis revealed that the Cl2-Ru-C2-C3 dihedral angles were not consistent with the trend observed from the unsaturated series.

Stepwise increase in the tether lengths was found to cause increasing nonlinearity in the C1-Ru1-P1 bond angles. Specifically, catalysts **UC-4**, **UC-5**, and **UC-6** have C1-Ru1-P1 bond angles of 171.0°, 166.0°, and 163.3°, respectively. One rationale for this trend may be that increasing the tether length caused the NHC ligand to tilt to accommodate the increased steric demand of the tether. An interesting consequence of this tilt is that the Mes group is forced closer to the PCy_3 group which may account for the increased activity observed upon elongation of the tether (see below for a comparison of catalyst activities). This notion is supported by a discernable increase in the Ru1-P1

bond length as the tether length was increased. The Ru1-C1 bond length also showed consistent increase in response to homologation of the tether. For example, upon extension of the tether, the Ru1-C1 bond length increased from 2.076 Å for **UC-4** to 2.113 Å for **UC-6**. The saturated catalysts, **SC-5** and **UC-6**, showed changes in their Ru1-P1 and Ru1-C1 bond lengths that were consistent with those observed in the unsaturated series.

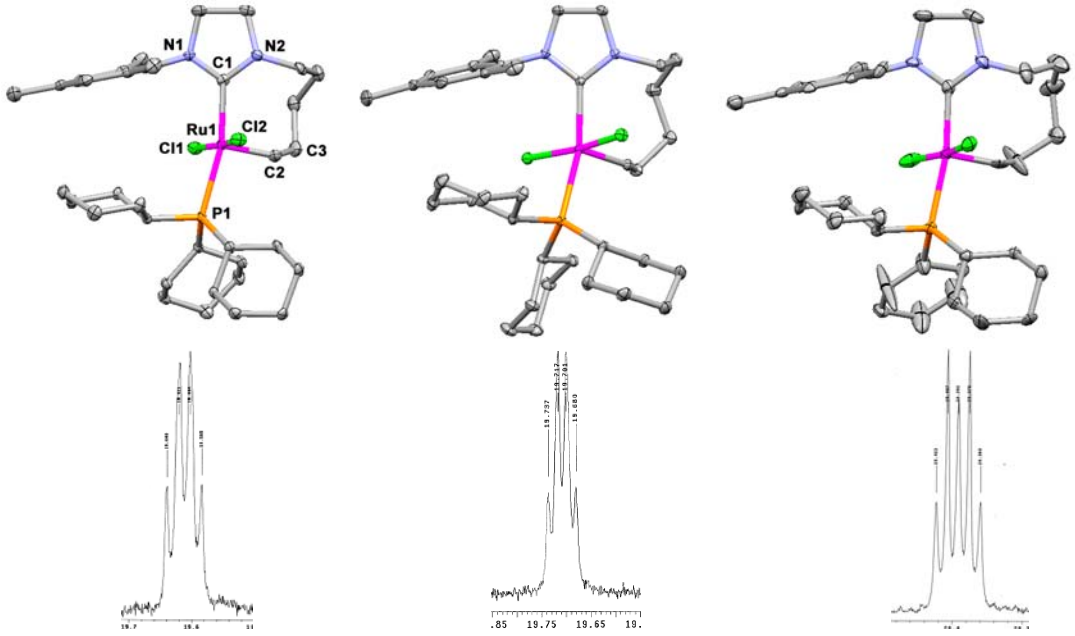

Figure 3. (top): X-ray crystal structures of **SC-5**, **UC-6**, and **SC-6**. Solvent molecules and hydrogens have been removed for clarity. Ellipsoids are drawn at the 50% probability level. (bottom): ^{1}H NMR spectra (C_6D_6) of alkylidene proton of **SC-5**, **UC-6**, and **SC-6**.

Catalyst Release. A unique aspect of REMP, in comparison with ring-*opening* metathesis polymerization (ROMP), is the requirement for an intramolecular chain-transfer event with the olefin nearest to the NHC to release the initial cyclic catalyst and provide a cyclic polymer free of Ru (Scheme 1). While removal of Ru from linear polymers obtained via ROMP can be done efficiently using a terminating group, such as

ethyl vinyl ether, these methods are incompatible with REMP as they would result in linear polymer formation.[26] Given the importance of catalyst release from the cyclic polymers, we investigated each catalyst's propensity to undergo intramolecular cyclization during polymerization that would be indicative of the catalyst's ability to be released from a polymer.

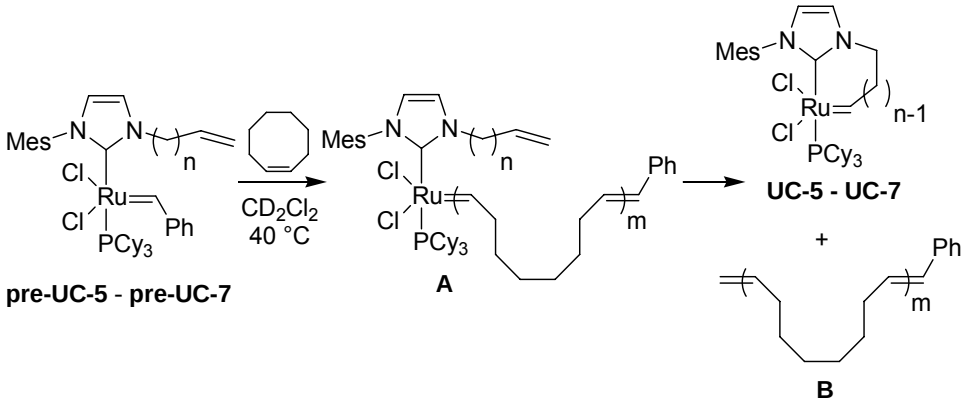

Scheme 4. Proposed species observable upon ROMP of COE using open catalysts **pre-UC-5** – **pre-UC-7**.

We envisioned that conducting polymerizations using "open" catalysts **pre-UC-5** –**pre-UC-7** would provide insight into each catalyst's ability to perform intramolecular CM to release "closed" catalysts **UC-5** – **UC-7**.[27] Propagation via growing Ru-alkylidene species **A** (Scheme 4) would inherently compete with catalyst cyclization (e.g., **A** → **UC-5** + **B**), and provide an indication of each catalyst's propensity to be released from the polymer chain.

To investigate, we conducted polymerizations of COE using open catalysts **pre-UC-5**–**pre-UC-7** in CD_2Cl_2 at 40 °C ($[COE/Ru]_0$ = 250:1, $[COE]_0$ = 0.5 M) and monitored the alkylidene region of the ^1H NMR spectrum as the reactions progressed. Each Ru-complex shown in Scheme 4 was identified by characteristic chemical shifts of the corresponding alkylidene protons. In CD_2Cl_2, complexes **pre-UC-5**–**pre-UC-7** gave

sharp benzylidene resonances as singlets at δ = 19.30 ppm, whereas propagating species (**A**) displayed broad multiplets at δ = 18.69 ppm. Cyclic catalysts **UC-5**, **UC-6**, and **UC-7** displayed signals at δ = 20.23, 19.35, and 19.67 ppm, respectively, with multiplicities matching those in Table 2.

We first examined open catalysts **pre-UC-6** and **pre-UC-7** as these were representative of the most efficient cyclic catalysts (**UC-6** and **UC-7**, respectively) for this series. Catalysts **pre-UC-6** and **pre-UC-7** gave similar results, and polymerization was found to reach completion faster than did cyclization in each case. Specifically, complete conversion of COE was achieved in less than 5 min for each catalyst.[28] The mole fraction of cyclic catalyst (**UC-6**/**UC-7**) observed at this point, however, was only ca. 10%, relative to **pre-UC-6**/**pre-UC-7** (ca. 30%) and **A** (ca. 60%). Continued heating resulted in diminished amounts of **pre-UC-6**/**pre-UC-7** and **UC-6**/**UC-7** in each case, with concomitant increases in the relative amounts of **A**. As will be discussed in the next section, the continued progression to form **A** may have been due to incorporation of free cyclic catalyst into the polymer chains. After ca 1 h, only trace amounts of cyclic species **UC-6**/**UC-7** could be observed. Overall, these results suggested that cyclization is not favored over polymerization for catalysts bearing 6- or 7-membered tethers, and that cyclization to release catalyst **UC-6** or **UC-7** after polymerization is not likely.

We next investigated the behavior of **pre-UC-5** under the same conditions as described above. In contrast to the longer tethered analogues **pre-UC-6** and **pre-UC-7**, polymerization reactions using **pre-UC-5** revealed much faster cyclization relative to polymerization. Figure 4 shows the mole fraction of each catalytic species (**pre-UC-5**, **A**, and **UC-5**) as well as the conversion of COE to PCOE over time. As can be seen, almost

complete formation of cyclic catalyst **UC-5** was observed after ca 45 min, at which time the polymerization had reached only 48% conversion. Moreover, the amount of catalytic species within the polymer chains (**A**) quickly diminished to nearly undetectable amounts. It is clear from the data presented in Figure 6 that cyclization to form **UC-5** is favored over propagation and that the background rate of cyclization (i.e., **pre-UC-5** → **UC-5**) is significant for this catalyst. In addition, the persistent amount of **UC-5** that is observed relative to propagating species (**A**) suggested that incorporation of **UC-5** into existing polymer chains is unlikely.

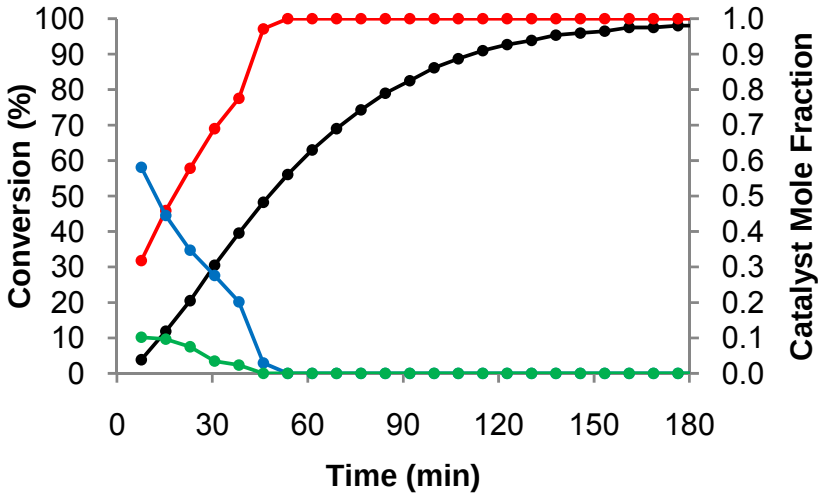

Figure 4. Left axis: Conversion of COE to PCOE using **pre-UC-5** (black). Right axis: Mole fraction of **UC-5** (red), **pre-UC-5** (blue), and **A** (green). Conditions: CD_2Cl_2, 40 °C, [COE/**pre-UC-5**]$_0$ = 250:1, [COE]$_0$ = 0.5 M. Conversion determined by ^{1}H NMR spectroscopy.

Collectively, the experiments investigating the behavior of open catalysts **pre-UC-5** – **pre-UC-7** revealed that controlling the tether lengths of cyclic catalysts may dictate polymerization kinetics with regard to polymer MWs and polydispersities. For example, shorter tether lengths may facilitate intramolecular chain-transfer during polymerization (Scheme 1), ultimately leading to multiple macrocycles produced from a single catalyst species. Alternatively, REMP catalysts displaying little tendency to be

released from a cyclic polymer may provide access to cyclic block copolymers or other advanced macrocycles.

Interaction Between Free Catalyst and Polymer. As mentioned previously, it may be possible for a cyclic catalyst to equilibrate with poly(olefin)s and become incorporated (or reincorporated) into a polymer chain. This equilibrium, depicted in Scheme 5, may be tether length dependent given that ring-opening of the catalyst may be a driving force toward incorporation into the polymer. With regard to REMP, the reversibility of intramolecular chain-transfer and catalyst release (Scheme 1) would result in an equilibrium amount of Ru species contained within the final cyclic polymers. Therefore, understanding each catalyst's affinity toward polymer incorporation is important for understanding the potential purity of the cyclic polymers. To investigate, we prepared linear PCOE via ROMP using acyclic catalyst **3** in the presence of 3-hexene as a chain-transfer agent. This provided a hydrocarbon polymer (M_n = 150 kDa, PDI = 2.1) which closely resembled the PCOE obtained via REMP in composition.[29] The linear PCOE was then treated with each of the cyclic catalysts **UC-5** – **UC-7** (olefin/catalyst molar ratio = 100:1) in CD_2Cl_2 at 40 °C. The equilibration of catalyst and polymer was monitored via ^{1}H NMR spectroscopy using anthracene as an internal standard; key NMR signals of the cyclic catalysts and incorporated species were similar to those observed in the previous section (Scheme 4).

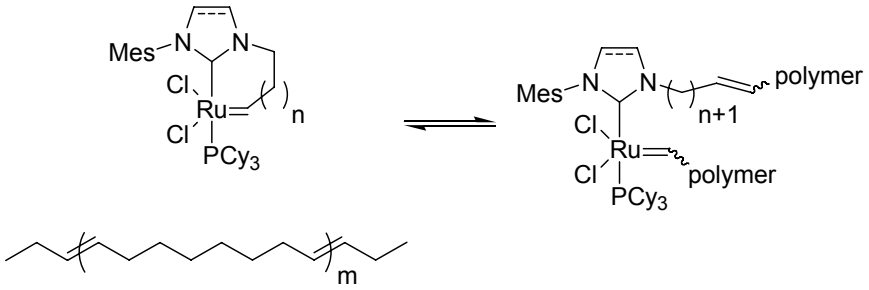

Scheme 5. Equilibration of cyclic catalyst and linear PCOE.

As expected, incorporation of cyclic catalyst into the polymer chain was dependent on the tether length of the catalyst. Specifically, after 1 h ca. 11% of catalyst **UC-7** had become incorporated into the polymer, whereas catalyst **UC-6** showed only 3% incorporation over the same time period. Catalyst **UC-5**, however, revealed no incorporation even after extended periods (up to 6 h). To compare, catalyst **SC-5** was also studied and gave similar results as **UC-5**. Overall, although the amount of incorporated catalyst was small in each case, there appeared to be some equilibration of free catalyst into the poly(olefin) depending upon the length of the catalyst tether.

Conclusions

In summary, we describe the synthesis and characterization of a series of cyclic Ru-alkylidene catalysts with particular focus on their ability to mediate ring-expansion metathesis polymerization. Both catalyst tether length as well as NHC electronics were found to significantly impact different aspects of the polymerization mechanism. Whereas shorter tether lengths were more efficient for catalyst release from the polymer, the caveat for these systems was found to be slower polymerization rates. Fortunately, saturation of the NHC backbone increased polymerization efficiency and effectively balanced activity loss due to shortening of the tether. Catalyst stabilities were found to be good over the course of the polymerization experiments, and pseudo-first order kinetic

plots revealed gradual initiation during the polymerization. The ability to control catalyst activity by a combination of tether length and ligand electronics may lead to new opportunities in olefin metathesis and catalyst design.

Experimental Section

Materials and methods. ^{1}H and ^{13}C NMR spectra were recorded using a Varian Mercury 300 or Varian Inova 500 spectrometer and were routinely run using broadband decoupling. Chemical shifts (δ) are expressed in ppm downfield from tetramethylsilane using the residual protiated solvent as an internal standard (DMSO-d_6, ^{1}H: 2.49 ppm and ^{13}C: 39.5 ppm; $CDCl_3$ ^{1}H: 7.26 ppm and ^{13}C: 77.0 ppm; C_6D_6 ^{1}H: 7.20 ppm and ^{13}C: 128.0 ppm). ^{31}P NMR spectra were externally referenced to 85% H_3PO_4 (0.00 ppm). Coupling constants are expressed in hertz (Hz). THF, CH_2Cl_2, Et_2O, pentane, PhH, $PhCH_3$, and C_6D_6 were obtained from solvent purification columns. CD_2Cl_2 used for NMR-scale experiments was distilled over CaH_2 under N_2 prior to use. $CHCl_3$ was distilled over P_2O_5 under N_2 prior to use. Ru-complex **1** was obtained from Materia, Inc. All other solvents and reagents were of reagent quality and used as obtained from commercial sources. Chromatography was performed with neutral silica gel (TSI Scientific, 230-400mesh, pH 6.5 – 7.0). Crystallographic data have been deposited at the CCDC, 12 Union Road, Cambridge CB2 1EZ, U.K., and copies can be obtained on request, free of charge, by quoting the publication citation and the deposition numbers 687290 (**SC-5**), 683585 (**UC-6**), and 687247 (**SC-6**).

Cyclic complex SC-5. In a Schlenk tube, chloroform adduct **11a** (200 mg, 0.51 mmol) was dissolved in dry THF (515 mL) under at atmosphere of dry N_2. To the solution was added Ru-complex **1** (210 mg, 0.26 mmol). The flask was sealed and the reaction mixture

was stirred in an oil bath at 70 °C for 2 h. Afterward, the cooled reaction mixture was concentrated under vacuum, redissolved in a minimal amount of PhH, and treated dropwise with pentane until crystallization ensued (X-ray analysis was performed on crystals obtained in this manner). The solids were collected by vacuum filtration, rinsed with 5% Et_2O/pentane, and dried under vacuum to provide 147 mg (81% yield) of the desired complex as a tan solid. ^{1}H NMR (500 MHz, C_6D_6): δ 20.39 (dt, $^3J_{H,P}$ = 9.3 Hz, $J_{H,H}$ = 4.5 Hz, 1H), 6.93 (s, 2H), 3.17 (t, J = 10.0 Hz, 2H), 3.10-3.09 (m, 2H), 2.85 (t, J = 10.0 Hz, 2H), 2.75 (br, 2H), 3.71 (s, 6H), 2.60-2.53 (m, 3H), 2.32 (br 2H), 2.23 (s, 3H), 1.95-1.92 (m, 6H), 1.78 (br, 6H), 1.68 (br, 2H), 1.47-1.45 (m, 6H), 1.34-1.29 (m, 10H), 1.19-1.17 (m, 2H). ^{13}C NMR (125 MHz, C_6D_6): δ 216.0 (J_{CP} = 85.9 Hz), 138.4, 137.6, 136.6, 129.9, 57.9 (J_{CP} = 4.9 Hz), 51.2 (J_{CP} = 3.5 Hz), 48.5 (J_{CP} = 2.7 Hz), 47.9, 32.1 (J_{CP} = 15.1 Hz), 29.8, 28.2 (J_{CP} = 10.4 Hz), 27.3, 26.8, 26.7, 21.1, 20.0. ^{31}P NMR (121 MHz, C_6D_6): δ 27.0. HRMS m/z calcd. for $C_{35}H_{57}Cl_2N_2PRu$ [M^+] 708.2680, found 708.2659.

[1-(6-Heptenyl)-3-mesitylimidazolylidene]$RuCl_2$(=CHPh) (PCy_3) (pre-UC-6). Imidazolium bromide **8$_{n=5}$** (400 mg, 1.10 mmol), was suspended in dry $PhCH_3$ (7 mL) under dry N_2. To the solution was added NaOtBu (106 mg, 1.10 mmol) and the resulting mixture was stirred at RT for 12 h. Ru-complex **1** (453 mg, 0.55 mmol) was then added in a single portion and the resulting mixture was stirred for 1 h during which time a color change from purple to brown was observed. Upon completion, the mixture was filtered through a thin pad of TSI silica gel using Et_2O/pentane (1:4 v/v) as eluent. The filtrate was concentrated under vacuum without heating. Purification by column chromatography on TSI silica gel under N_2 pressure (10% Et_2O/pentane) provided 408 mg (90% yield) of the desired compound as a red-purple powder. ^{1}H NMR (major isomer) (300 MHz, C_6D_6):

δ 19.85 (s, 1H), 7.05-6.94 (m, 2H) 6.56-6.55 (m, 1H), 6.31-6.15 (m, 3H), 5.90-5.76 (m, 1H), 5.15-5.03 (m, 2H), 4.70 (t, J = 7.7 Hz, 2H), 2.65-2.53 (m, 4H), 2.13 (s, 3H), 1.97-1.08 (m, 37H), 1.80 (s, 6H). ^{31}P NMR (major isomer) (121 MHz, C_6D_6): δ 34.4. HRMS m/z calcd for $C_{44}H_{65}Cl_2N_2PRu$ [M^+] 824.3306, found 824.3298.

Cyclic complex UC-6. Ru-complex **pre-UC-6** (400 mg, 0.48 mmol), was dissolved in dry PhH (30 mL) and pentane (450 mL) in a Schlenk tube under dry N_2. The mixture was then placed in a oil bath at 70 °C and stirred for 1 h. Upon completion, the solution was cooled to RT, transferred to a round-bottom flask, and concentrated under vacuum without heat. The crude material was triturated with 20% Et_2O/pentane (50 mL) for ca 20 min. The solids were then collected via vacuum filtration, rinsed with pentane, and dried under vacuum to provide 335 mg (96% yield) of the desired compound as a red-brown powder. X-ray quality crystals were obtained by slow addition of pentane to a PhH solution of the complex. ^{1}H NMR (300 MHz, C_6D_6): δ 19.71 (dt, $^3J_{H,P}$ = 5.1 Hz, $J_{H,H}$ = 5.5 Hz, 1H), 6.90 (s, 2H), 6.35 (d, J = 1.8 Hz, 1H), 6.14 (s, 1H), 2.74-2.51 (m, 3H), 2.51 (s, 6H), 2.23 (s, 3H), 1.99-1.31 (m, 40H). ^{13}C NMR (125 MHz, C_6D_6): δ 186.0 (J_{CP} = 84.7 Hz), 138.2, 137.1, 129.4, 128.3, 123.6 (J_{CP} = 2.3 Hz), 120.4, 62.9, 47.0, 32.4 (J_{CP} = 16.9 Hz), 31.5, 29.8, 28.1 (J_{CP} = 10.0 Hz), 26.8, 22.9, 21.1, 19.7. ^{31}P NMR (121 MHz, C_6D_6): δ 33.3. HRMS m/z calcd for $C_{36}H_{57}Cl_2N_2PRu$ [M^+] 720.2680, found 720.2671.

Cyclic complex SC-6. This compound was prepared analogously to **SC-5** from chloroform adduct **11b** (280 mg, 0.69 mmol) and Ru-complex **1** (285 mg, 0.35 mmol) in THF (650 mL) to provide 369 mg (74% yield) of the desired complex as a red-brown solid. X-ray quality crystals were obtained by slow diffusion of pentane into a Et_2O/PhH (20:1 v/v) solution of the complex. ^{1}H NMR (500 MHz, C_6D_6): δ 19.61 (dt, $^3J_{H,P}$ = 5.0 Hz,

$J_{H,H}$ = 5.7 Hz, 1H), 6.93 (s, 2H), 3.33-2.83 (m, 4H), 2.70 (s, 6H), 2.63-2.56 (m, 3H), 2.22 (s, 3H), 1.93-1.30 (m, 40H). ^{13}C NMR (125 MHz, C_6D_6): δ 215.3 (J_{CP} = 80.1 Hz) 137.5, 137.0, 129.9, 129.5, 62.8, 51.7 (J_{CP} = 3.3 Hz), 47.7, 46.9, 32.2 (J_{CP} = 16.5 Hz), 29.7, 28.1 (J_{CP} = 10.1 Hz), 27.9, 26.8, 25.6, 23.6, 21.1. ^{31}P NMR (121 MHz, C_6D_6): δ 30.4. HRMS m/z calcd for $C_{36}H_{59}Cl_2N_2PRu$ [M^+] 722.2837, found 722.2808.

Cyclic complex UC-7. This compound was prepared analogously to **UC-6** from open complex **pre-UC-7** (150 mg, 0.18 mmol) in PhH (10 mL) and pentane (170 mL). Upon completion, the cooled reaction mixture was concentrated under vacuum without heat, then triturated with 20% Et_2O/pentane (10 mL) for ca 20 min. The solids were collected via vacuum filtration and further purification via column chromatography on TSI silica gel under N_2 pressure (30% Et_2O/pentane) provided 56 mg (42% yield) of the desired compound as a light brown powder. ^{1}H NMR (500 MHz, C_6D_6): δ 19.37 (dt, $^3J_{H,P}$ = 10.2 Hz, $J_{H,H}$ = 5.5 Hz, 1H), 6.92 (s, 2H), 6.38 (d, J = 1.5 Hz, 1H), 6.19 (s, 1H), 3.66 (br, 2H), 2.62-2.57 (m, 3H), 2.54 (s, 6H), 2.24 (s, 3H), 2.08-1.61 (m, 24H), 1.50-1.42 (m, 2H), 1.34-1.28 (m, 12H), 1.22-1.17 (m, 2H). ^{13}C NMR (125 MHz, C_6D_6): δ 184.7 (J_{CP} = 97.5 Hz), 138.1, 137.6, 129.2, 128.4, 128.3, 128.1, 127.9, 123.3 (J_{CP} = 3.3 Hz), 119.9, 60.4, 47.1, 32.7 (J_{CP} = 16.1 Hz), 29.9, 28.2 (J_{CP} = 9.5 Hz), 26.8, 26.5, 24.7, 21.1, 20.7, 19.7. ^{31}P NMR (121 MHz, C_6D_6): δ 26.3. HRMS m/z calcd for $C_{37}H_{59}Cl_2N_2PRu$ [M^+] 734.2837, found 734.2814.

1-(6-Heptenyl)-3-mesitylimidazolium bromide ($\mathbf{8_{n=5}}$). This compound was prepared analogously to $\mathbf{8_{n=3,4,6}}$ from *N*-mesitylimidazole (1.00 g, 5.37 mmol) and 1-bromo-6-heptene (1.0 mL, 6.55 mmol) in $PhCH_3$ (20 mL). Upon completion, the reaction mixture was concentrated under vacuum and the crude material was suspended in Et_2O (100 mL)

and vigorously stirred for 12 h to produce a fine white suspension. The solids were collected via vacuum filtration under a stream a N_2 to provide 1.81 g (93% yield) of the desired compound as an off-white powder. (The compound appeared to be hygroscopic, producing a thick, viscous material when collected under air.) ^{1}H NMR (300 MHz, $CDCl_3$): δ 10.31 (dd appearing as t, *J* = 1.5 Hz, 1H), 7.94 (dd apearing as t, *J* = 1.7 Hz, 1H), 7.21 (dd apearing as t, *J* = 1.7 Hz, 1H), 6.94 (s, 2H), 5.76-5.63 (m, 1H), 4.96-4.84 (m, 2H), 4.67 (t, *J* = 7.4 Hz, 2H), 2.29 (s, 3H), 2.01 (s, 6H), 2.01-1.91 (m, 4H) 1.43-1.30 (m, 4H). ^{13}C NMR (125 MHz, $CDCl_3$): δ 141.1, 138.1, 137.8, 134.0, 130.6, 129.7, 123.2, 123.1, 114.7, 50.1, 33.2, 30.2, 28.0, 25.3, 21.0, 17.5. HRMS m/z calcd for $C_{19}H_{27}N_2$ [M^+] 283.2174, found 283.2186.

1-(5-Hexenyl)-3-mesitylimidazolinium bromide (10a). To a solution of $HC(OEt)_3$ (10 mL) and $PhCH_3$ (10 mL) in a 50 mL round-bottom flask was added PTSA•H_2O (39 mg, 0.20 mmol), *N*-mesitylethylenediamine (**9**) (729 mg, 4.09 mmol), and 6-bromo-1-hexene (0.66 mL, 4.91 mmol). The flask was fitted with a H_2O-jacketed condenser and the reaction mixture was stirred under N_2 in an oil bath at 110 °C for 10 h. Afterward, the cooled reation mixture was concentrated under vacuum. The crude product was treated with Et_2O (xx mL) and vigorously stirred for 2 h to produce an off-white slurry. The solids were collected via vacuum filtration, rinsed with Et_2O, and dried under vacuum to provide 1.31 g (91% yield) of the desired compound. ^{1}H NMR (300 MHz, $CDCl_3$): δ 9.50 (s, 1H), 6.87 (s, 2H), 5.80-5.67 (m, 1H), 5.03-4.92 (m, 2H), 4.30-4.11 (m, 4H), 3.94 (t, *J* = 7.2 Hz, 2H), 2.26 (s, 6H), 2.24 (s, 3H), 2.12-2.05 (m, 2H), 1.76-1.66 (m, 2H), 1.49-1.42 (m, 2H). ^{13}C NMR (125 MHz, $CDCl_3$): δ 158.7, 139.9, 137.6, 135.0, 130.4, 129.7, 115.2,

50.9, 48.7, 48.1, 32.8, 26.4, 25.2, 20.8, 17.9. HRMS m/z calcd for $C_{18}H_{27}N_2$ [M^+] 271.2174, found 271.2161.

1-(6-Heptenyl)-3-mesitylimidazolinium bromide (10b). This compound was prepared analogously to **10a** from $HC(OEt)_3$ (7.0 mL), $PhCH_3$ (7.0 mL), PTSA•H_2O (27 mg, 0.14 mmol), *N*-mesitylethylenediamine (**9**) (500 mg, 2.80 mmol), and 7-bromo-1-heptene (0.51 mL, 3.36 mmol) to provide 951 mg (93% yield) of the desired compound. ^{1}H NMR (500 MHz, $CDCl_3$): δ 9.31 (s, 1H), 6.77 (s, 2H), 5.70-5.61 (m, 1H), 4.90-4.81 (m, 2H), 4.20-4.16 (m, 2H), 4.12-4.08 (m, 2H), 3.78 (t, *J* = 7.3 Hz, 2H), 2.16 (s, 3H), 2.15 (s, 6H), 1.96-1.91 (m, 2H), 1.64-1.58 (m, 2H), 1.35-1.30 (m, 2H), 1.27-1.21 (m, 2H). ^{13}C NMR (125 MHz, $CDCl_3$): δ 158.5, 139.7, 138.1, 134.9, 130.3, 129.5, 114.4, 50.8, 48.6, 48.0, 33.1, 27.9, 26.7, 25.3, 20.7, 17.8. HRMS m/z calcd for $C_{19}H_{29}N_2$ [M^+] 285.2325, found 285.2310.

1-(5-Hexenyl)-3-mesityl-2-(trichloromethyl)imidazolidine (11a). Under an atmosphere of dry N_2, imidazolinium bromide **10a** (443 mg, 1.26 mmol) was dissolved in dry $CHCl_3$ (6 mL). NaH (95 wt%, 38 mg, 1.51 mmol) was then added portionwise under a stream of N_2. The resulting mixture was placed in an oil bath at 55 °C and stirred for 10 h. Afterward, the cooled reaction mixture was diluted with Et_2O (100 mL), filtered through a thin pad of silica gel, and concentrated to provide 305 mg (62% yield) of the desired product as a pale yellow oil. ^{1}H NMR (300 MHz, $CDCl_3$): δ 6.86 (s, 1H), 6.85 (s, 1H), 5.91-5.78 (m, 1H), 5.07-4.95 (m, 2H), 4.73 (s, 1H), 3.86-3.78 (m, 1H), 3.62-3.55 (m, 1H), 3.41-3.32 (m, 1H), 3.23-3.16 (m, 1H), 3.10-3.02 (m, 1H), 2.98-2.90 (m, 1H), 2.35 (s, 3H), 2.70 (s, 3H), 2.25 (s, 3H), 2.16-2.09 (m, 2H), 1.68-1.43 (m, 4H). ^{13}C NMR (75 MHz, $CDCl_3$): δ 147.8, 147.7, 142.8, 138.8, 138.7, 134.9, 132.6, 129.9, 129.5, 114.5, 108.2,

94.2, 58.2, 52.9, 52.6, 33.7, 29.7, 26.1, 20.7, 19.8, 19.3. HRMS m/z calcd for $C_{19}H_{27}Cl_3N_2$ [M^+] 388.1240, found 388.1225.

1-(6-Heptenyl)-3-mesityl-2-(trichloromethyl)imidazolidine (11b). This compound was prepared analogously to **11a** from imidazolinium bromide **10b** (730 mg, 2.0 mmol), $CHCl_3$ (8 mL), and NaH (95 wt%, 101 mg, 4.00 mmol) to provide 670 mg (83% yield) of the desired product as a pale yellow oil. ^{1}H NMR (300 MHz, $CDCl_3$): δ 6.88 (s, 1H), 6.86 (s, 1H), 5.92-5.79 (m, 1H), 5.08-4.96 (m, 2H), 4.75 (2, 1H), 3.87-3.80 (m, 1H), 3.65-3.58 (m, 1H), 3.42-3.33 (m, 1H), 3.25-3.17 (m, 1H), 3.10-3.02 (m, 1H), 3.00-2.92 (m, 1H), 2.37 (s, 3H), 2.29 (s, 3H), 2.27 (s, 3H), 2.14-2.05 (m, 2H), 1.68-1.54 (m, 2H), 1.50-1.38 (m, 4H). ^{13}C NMR (75 MHz, $CDCl_3$): δ 142.8, 139.0, 138.6, 134.8, 132.6, 129.9, 129.4, 114.3, 108.2, 94.2, 58.4, 52.9, 52.6, 33.8, 30.1, 28.8, 26.4, 20.7, 19.8, 19.3. HRMS m/z calcd for $C_{20}H_{29}Cl_3N_2$ [M^+] 402.1396, found 402.1382.

References

(1) For general reviews on Ru-catalyzed olefin metathesis, see: (a) Bielawski, C. W.; Grubbs, R. H. *Prog. Polym. Sci.* **2007**, *32*, 1-29. (b) Grubbs, R. H. *Tetrahedron* **2004**, *60*, 7117. (c) Grubbs, R. H. *Handbook of Metathesis*; Wiley-VHC: Weinheim, Germany, 2003. (d) Trkna, T. M.; Grubbs, R. H. *Acc. Chem. Res.* **2001**, *34*, 18. (e) Grubbs, R. H.; Chang, S. *Tetrahedron* **1998**, *54*, 4413. (f) Ivin, K. J.; Mol, J. C. *Olefin Metathesis and Metathesis Polymerization*; Academic Press: San Diego, CA; 1997.

(2) (a) Xia, Y.; Verduzco, R.; Grubbs, R. H.; Kornfield, J. A. *J. Am. Chem. Soc.* **2008**, *130*, 1735. (b) Gorodetskaya, I. A.; Choi, T.-L.; Grubbs, R. H. *J. Am. Chem. Soc.* **2007**, *129*, 12672 (c) Choi, T.-L.; Rutenberg, I. M.; Grubbs, R. H. *Angew. Chem. Int. Ed.* **2002**, *41*, 3839.

(3) (a) Copéret, C.; Basset, J. M. *Adv. Synth. Catal.* **2007**, *349*, 78. (b) Colacino, E.; Martinez, J.; Lamaty, F. *Coord. Chem. Rev.* **2007**, *251*, 726.

(4) (a) Funk, T. W.; Berlin, J. M.; Grubbs, R. H. *J. Am. Chem. Soc.* **2006**, *128*, 1840. (b) Berlin, J. M.; Goldberg, S. D.; Grubbs, R. H. *Angew. Chem. Int. Ed.* **2006**, *45*, 7591.

(5) (a) Louie, J.; Bielawski, C. W.; Grubbs, R. H. *J. Am. Chem. Soc.* **2001**, *123*, 11312. (b) Bielawski, C. W.; Louie, J.; Grubbs, R. H. *J. Am. Chem. Soc.* **2000**, *122*, 12872.

(6) (a) Choi, T.-L.; Grubbs, R. H. *Angew. Chem. Int. Ed.* **2003**, *42*, 1743. (b) Love, J. A.; Morgan, J. P.; Trnka, T. M.; Grubbs, R. H. *Angew. Chem. Int. Ed.* **2002**, *41*, 4035.

(7) (a) Vougioukalakis, G. C.; Grubbs, R. H. *J. Am. Chem. Soc.* **2008**, *130*, 2234. (b) Plietker, B.; Neisius, N. M. *J. Org. Chem.* **2008**, *73*, 3218. (c) Vougioukalakis, G. C.; Grubbs, R. H. *Organometallics* **2007**, *26*, 2469. (d) Vehlow, K.; Maechling, S.; Blechert, S. *Organometallics* **2006**, *25*, 25. (e) Hansen, E. C.; Lee, D. *Org. Lett.* **2004**, *6*, 2035. (f) Chatterjee, A. K.; Choi, T.-L.; Sanders, D. P.; Grubbs, R. H. *J. Am. Chem. Soc.* **2003**, *125*, 11360.

(8) For the synthesis and structural characterization of $\mathbf{4}_{\mathbf{cyc}}$ and $\mathbf{5}_{\mathbf{cyc}}$, see Fürstner, A.; Ackermann, L.; Gabor, B.; Goddard, R.; Lehmann, C. W.; Mynott, R.; Stelzer, F.; Thiel, O. R. *Chem. Eur. J.* **2001**, *7*, 3236.

(9) To name the cyclic catalysts, we use "U" to denote unsaturation in NHC and "S" to denote saturation in NHC, and "C-number" to denote the number of carbon atoms in the cyclized tether arm. For example, "UC-6" refers to cyclic catalyst with unsaturated NHC and 6 carbon atoms in the tether arm. The precyclized, acyclic forms of these catalysts are named with "pre" as the prefix.

(10) (a) Bielawski, C. W.; Benitez, D.; Grubbs, R. H. *J. Am. Chem. Soc.* **2003**, *125*, 8424. (b) Bielawski, C. W.; Benitez, D.; Grubbs, R. H. *Science* **2002**, *297*, 2041.

(11) For additional cyclic polymer syntheses involving ring-expansion approaches, see (a) Darcy A. Culkin, Wonhee Jeong, Szilárd Csihony, Enrique D. Gomez, Nitash P. Balsara, James L. Hedrick, Robert M. Waymouth, *Angew. Chem. Int. Ed.* **2007**, 46, 2627. (b) H. Li, A. Debuigne, R. Jérome, P. Lecomte, *Angew. Chem. Int. Ed.* **2006**, 45, 2264. (c) He, T.; Zheng, G.-H.; Pan, C.-Y. *Macromolecules*

2003, *36*, 5960. (d) Kudo, H.; Makino, S.; Kameyama, A.; Nishikubo, T. *Macromolecules* **2005**, *38*, 5964. (e) Shea, K. J.; Lee, S. Y.; Busch, B. B. *J. Org. Chem.* **1998**, *63*, 5746.

(12) For cyclic polymer syntheses involving ring-closing of telechelic polymers, see (a) Laurent, B. A.; Grayson, S. M. *J. Am. Chem. Soc.* **2006**, *128*, 4238. (b) Oike, H.; Mouri, T.; Tezuka, Y. *Macromolecules* **2001**, *34*, 6229. (c) Alberty, K. A.; Tillman, E.; Carlotti, S.; Bradforth, S. E.; Hogen-Esch, T. E.; Parker, D.; Feast, W. J. *Macromolecules* **2002**, *35*, 3856. (d) Roovers, J. *J. Polym. Sci., Part B: Polym. Phys.* **1988**, *26*, 1251. (e) Roovers, J.; Toporowski, P. M. *Macromolecules* **1983**, *16*, 843. (f) Geiser, D.; Hoeker, H. *Macromolecules* **1980**, *13*, 653.

(13) (a) Sanford, M. S.; Love, J. A.; Grubbs, R. H. *J. Am. Chem. Soc.* **2001**, *123*, 6543. (b) Bielawski, C. W.; Grubbs, R. H. *Angew. Chem. Int. Ed.***2000**, *39*, 2903.

(14) In solution, complexes **pre-UC-4**–**pre-UC-7** appeared to exist as a mixture of two rotamers as shown by two benzylidene signals (ratio ca 10:1). The major isomer appeared as a singlet, analogous to complex **2**, whereas a second signal was observed further downfield as a doublet (e.g., $^{3}J_{H,P}$ = 12.9 Hz for **UC-6**).**Error! Bookmark not defined.**

(15) Purchased from TSI Scientific, 230-400 mesh, neutral pH.

(16) Notably, "open" complexes **pre-UC-4**–**pre-UC-7** were routinely used in subsequent cyclization steps following only filtration through a short silica gel plug and concentration under vacuum. Residual tricyclohexylphosphine was efficiently removed from the cyclized catalysts **UC-4**–**UC-7** during purification.

(17) Additional considerations should be noted: 1) intramolecular cyclization may proceed to directly give an acyclic methylidene complex that is identical to the product that would be obtained between CM of styrene and the cyclic catalyst, and 2) in rare cases, olefin isomerization and cyclization to give small amounts of cyclic catalysts bearing a one-carbon shorter tether were observed.

(18) Perillo, I.; Caterina, M. C.; López, J.; Salerno, A. *Synthesis* **2004**, 851.

(19) For an alternate, two-step procedure for the synthesis of imidazolinium salts bearing one *N*-aryl and one *N'*-alkyl group, see ref 7d.

(20) Attempts at ligand exchange via deprotonation of imidazolinium salts **10** in hexanes were also unsuccessful.

(21) (a) Courchey, F. C.; Sworen, J. C.; Ghiviriga, I.; Abboud, K. A.; Wagener, K. B. *Organometallics* **2006**, *25*, 6074. (b) Trnka, T. M.; Morgan, J. P.; Sanford, M. S.; Wilhem, T. E.; Scholl, M.; Choi, T.-L.; Ding, S.; Day, M. D.; Grubbs, R. H. *J. Am. Chem. Soc.* **2003**, *125*, 2546.

(22) This reaction was found to be solvent-dependent and $PhCH_3$, PhH, pentane, and PhH/pentane mixture gave inferior results.

(23) Unfortunately, attempts to synthesize **SC-7** were unsuccessful.

(24) We were not able to obtain X-ray quality crystals of **UC-7**.

(25) Since single-crystal X-ray data was not obtained for **UC-7**, therefore, it was not possible to determine the direction of the rotation about the Ru1-C2 bond with respect to complexes **UC-4–UC-6**. We speculate that the long tether of **UC-7** may allow for conformations that collectively frustrate crystallization.

(26) Other terminating agents have also been employed, see (a) Matson, J. B.; Grubbs, R. H., *Macromolecules* **2008**, *41*, 5626. (b) Hilf, S.; Berger-Nicoletti, E.; Grubbs, R. H.; Kilbinger, A. F. M. *Angew. Chem. Int. Ed.* **2006**, *45*, 8045. (c) Owen, R. M.; Gestwicki, J. E.; Young, T.; Kiessling, L. L. *Org. Lett.* **2002**, *4*, 2293.

(27) In light of the relatively low activity of **UC-4**, **pre-UC-4** was not evaluated in these experiments.

(28) Under identical conditions, **pre-UC-5**–**pre-UC-7** gave faster conversions of COE to PCOE than the corresponding "closed" systems (**UC-5**–**UC-7**). The higher polymerization activities of **pre-UC-5**–**pre-UC-7** versus **UC-5**–**UC-7** may reflect restricted conformations of the latter.

(29) Molecular-weight data were obtained from triple-angle laser light-scattering and refractive index measurements.

C h a p t e r 3

Ring-Expansion Metathesis Polymerization:

Catalyst Dependent Polymerization Profiles

Portions of this chapter have been published: Xia, Y.; Boydston, A. J.; Yao, Y.; Kornfield, J. A.; Gorodetskaya, I. A.; Spiess, H. W.; Grubbs, R. H. *J. Am. Chem. Soc.* **2009**, 131, 2670-2677.

Abstract

Ring-expansion metathesis polymerization (REMP) mediated by recently developed cyclic Ru catalysts has been studied in detail with a focus on the polymer products obtained under varied reaction conditions and catalyst architectures. Depending upon the nature of the catalyst structure, two distinct molecular weight evolutions were observed. Polymerization conducted with catalysts bearing 6-carbon tethers displayed rapid polymer molecular weight growth which reached a maximum value at ca 70% monomer conversion, resembling chain-growth polymerization mechanism. In contrast, 5-carbon tethered catalysts lead to molecular weight growth that resembled a step-growth mechanism with a steep increase occurring only after 95% monomer conversion. The underlying reason for these mechanistic differences appeared to be ready release of 5-carbon tethered catalysts from growing polymer rings, which competed significantly with propagation. Owing to reversible chain transfer and the lack of end groups in REMP, the final molecular weights of cyclic polymers was controlled by thermodynamic equilibria. Large ring sizes in the range of 60 – 120 kDa were observed at equilibrium for polycyclooctene and polycyclododecatriene, which were found to be independent of catalyst structure and initial monomer/catalyst ratio. While 6-carbon tethered catalysts slowly incorporated into the formed cyclic polymer, the incorporation of 5-carbon tethered catalysts was minimal, as revealed by ICP-MS. Further polymer analysis was conducted using melt-state magic-angle spinning ^{13}C NMR spectroscopy and matrix-assisted laser desorption ionization mass spectrometry of both linear and cyclic polymers, which revealed little or no chain ends for the latter topology.

Introduction

Cyclic polymers have been a fascinating macromolecular architecture for synthetic chemists, as well as materials scientists and physicists, since the discovery of circular DNA.[1-2] Constraining a macromolecule into a cyclic topology can result in unique properties in comparison with linear analogues such as lower viscosities, smaller hydrodynamic radii, and increased functional group density.[1-3] Furthermore, cyclic polymers may challenge and expand fundamental knowledge regarding polymer properties as they relate to the presence and absence of chain ends. These characteristics make cyclic polymers interesting targets for studying fundamental aspects of property-topology relationships as well as new resources in materials science. Despite considerable recent development in the area of cyclic polymers, the full potential of these materials is yet to be realized. Further advancement requires the ability to efficiently prepare large-scale quantities of cyclic polymers spanning a diverse range of functionality and controlled molecular weights.

From a synthetic standpoint, cyclic polymers present a unique challenge in polymer chemistry. Successful production of large macrocycles has traditionally been accomplished by macrocyclization of appropriately end-functionalized telechelic polymers.[4] Although this approach is compatible with both symmetric[5-12] and unsymmetric[13-16] telechelic polymers, as well as triblock copolymers,[17-18] inherent limitations still persist. Specifically, macrocyclization is generally limited to low polymers (i.e., <10 kDa), and requires high-dilution conditions to suppress intermolecular reaction of end groups. A recent breakthrough in obtaining high molecular weight cyclic polymers utilized macrocyclization of triblock copolymers under high dilution

conditions.[17-18] Using an ABC triblock system in which the A and C blocks comprised complementary coupling partners, this approach provided a mixture of linear and cyclic polymers of up to 96 kDa. The cyclization efficiency for these high molecular weight triblocks was much greater than that typically observed for traditional macrocyclization of telechelic polymers due to the greatly increased effective concentration of functional groups in the A and C blocks of the former. Other cyclic polymer syntheses include those relying on back-biting events during ring-chain equilibria[19-20] or linear living polymerizations.[21] The scope of such methods, however, remains narrow in comparison with the macrocyclization methods previously mentioned.

Complementary to the "grow-then-cyclize" approach of macrocyclization, an alternative strategy, which may be viewed as a "grow-while-cyclic" method, involves ring-expansion of cyclic monomers.[22-30] For example, Pd-mediated polymerization of methylidenecyclopropanes was demonstrated by Osakada, and achieved metallacycles of 5.3 kDa.[25] The prospect of high fidelity ring-expansion methodology offers the potential for formation of pure cyclic polymers free of linear contaminants and to improve the efficiency with which such materials are produced.

The series of cyclic Ru-alkylidene catalysts developed in the Grubbs group (Figure 1), as discussed in Chapter 1, resembled olefin metathesis catalyst **1**, and were able to mediate ring-expansion metathesis polymerization (REMP) of cyclic olefins to produce cyclic polymers.[22,29-30] Overall, REMP has several distinct advantages, such as: 1) the potential to produce large quantities of cyclic polymers from readily available cyclic monomers; 2) tolerance for high concentration, including bulk polymerizations; 3) the

ability to produce homopolymers without linkage groups, including pure hydrocarbon macrocycles; and 4) access to a broad range of molecular weights, extending up to 10^6 Da.

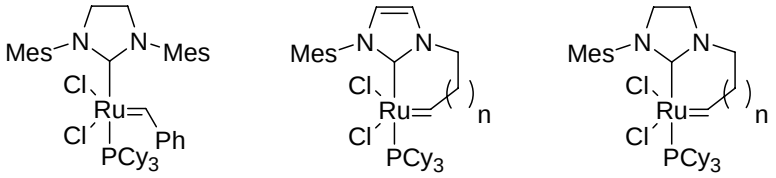

1 **UC-5**, n = 3 **UC-6**, n = 4 **SC-5**, n = 3 **SC-6**, n = 4

Figure 1. Olefin metathesis catalyst **1** and cyclic REMP catalysts.

Capitalizing on the attributes mentioned above requires deeper insights into the mechanism of REMP and an ability to control polymer molecular weights and product distribution by guiding metathesis events within the catalytic cycle. The activities of Ru-based metathesis catalysts can be finely tuned via structural modulation,[31-34] and we envisioned that the specific structural differences in cyclic catalysts (Figure 1) may offer a means to guide the relative rates of different metathesis events involved in REMP, as indicated by our catalyst-focused study in chapter 1. The most apparent mechanistic steps involved in REMP include catalyst initiation, propagation, catalyst release, and intramolecular chain transfer (Figure 2). The rate of initiation (given rate constant k_i) determines the number of catalyst molecules which enter the catalytic cycle, and may also influence the total number of polymer rings which are ultimately formed. Chain propagation, represented by the rate constant k_p, is expected to be independent of catalyst tether length and dependent on NHC electronics (i.e., saturated versus unsaturated backbones). Due to the possibility of catalyst release (with rate constant k_r) and re-incorporation (k_{-r}) during REMP, the value of k_p cannot be directly determined based on the overall polymerization rates alone. Importantly, it is the relative rates of each of these events that will dictate the kinetically controlled product distribution.

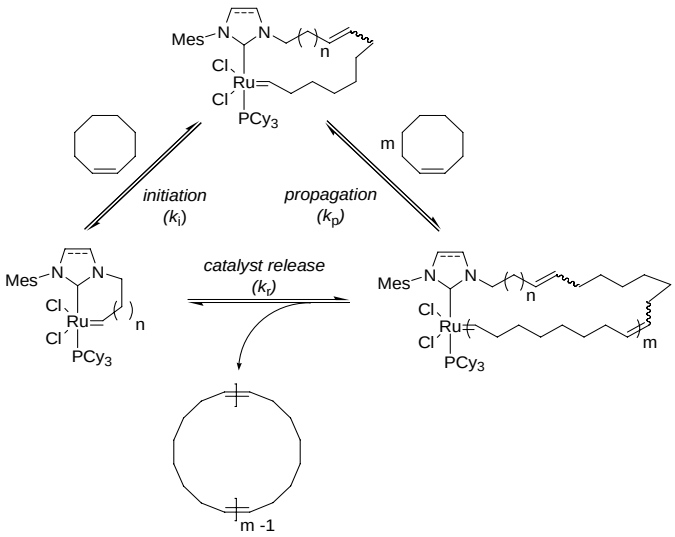

Figure 2. Key mechanistic steps involved in REMP.

In a simplified case, the average degree of polymerization (DP) would be given by $DP = k_p[\text{monomer}]/k_r$ (1)

In such cases, chain growth mechanism would be expected to dominate when $k_p[\text{monomer}] >> k_r$. In contrast, for $k_p[\text{monomer}] \sim k_r$, step growth molecular weight increase would be expected. Both intra- and intermolecular chain transfer events, however, must also be considered during REMP, and therefore Eq (1) cannot be applied to polymerization involving such events. As depicted in figure 3, the ability of an incorporated (i.e., propagating) catalyst species to interact with olefins within the polymer backbone, in a manner that does not result in release of the original catalyst, may be regarded as polymer "pinching" and is assigned the rate constant k_t. Polymer pinching would yield two separate macrocycles of reduced, and not necessarily equal, molecular weight. Dependent upon the number and placement of Ru complexes in the initial ring, at least one of the ensuing macrocycles would contain an active catalyst species and could either undergo chain growth or further pinching. Intermolecular chain transfer (k_{-t}), which may be viewed as the reverse of polymer pinching or polymer "fusion", would result in

considerable molecular weight growth since two large ring systems are being combined. Notably, the reversibility of olefin metathesis provides a potential avenue toward thermodynamic molecular weight control over "endless" polymers via polymer pinching and macrocyclic combination.

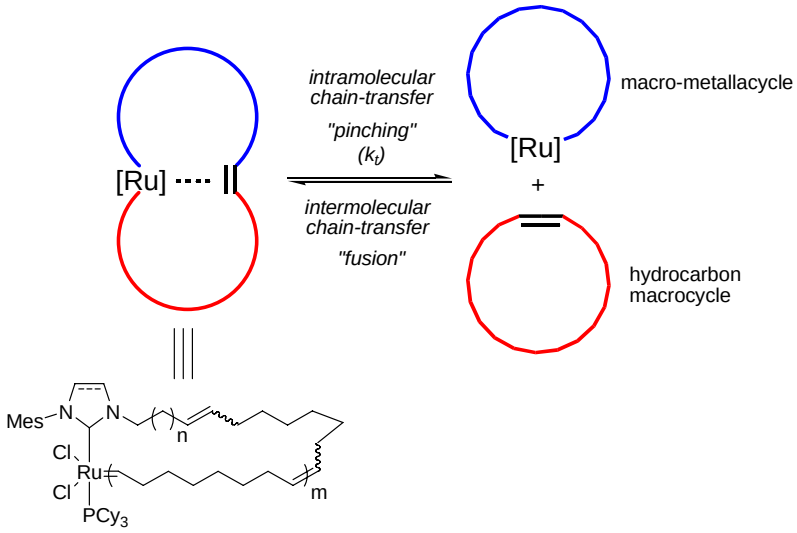

Figure 3. Depiction of reversible polymer "pinching" via intramolecular chain transfer and "fusion" via intermolecular chain transfer.

We envisioned that catalyst structure and reaction conditions could be tuned to control the relative values of k_i, k_p, k_r and k_t and ultimately facilitate access to different kinetically controlled polymer product distributions. The origins of the faster conversions of monomer to polymer, however, may be due to faster initiation, slower catalyst release, faster propagation, or some combination thereof. Catalysts bearing 5-carbon tethers (i.e., **UC-5** and **SC-5**) showed no incorporation into the polymer during polymerizations, suggesting an equilibrium had been established that strongly favored a non-incorporated resting state of the cyclic catalysts. This observation corresponds to catalyst behavior involving initiation, incorporation of monomer units, and catalyst release all prior to complete consumption of monomer; therefore the catalyst does not reside in the formed

polymer. This would be expected to provide multiple polymer macrocycles from each catalyst molecule, and potentially display molecular weight growth reminiscent of step-growth mechanisms.

Herein, predictions regarding polymer structure based on our previous catalyst-focused investigations are tested by examining polymer products during and after polymerization. Collectively, the results demonstrate how different catalyst architectures may be used to control the kinetic profiles of REMP. We describe herein comparative studies of cyclic polymers obtained via REMP of cyclooctene (COE), cyclododecatriene (CDT), and cyclooctene macrocycles (e.g., cyclic cyclooctene trimer), with particular focus on catalyst initiation rates, polymer molecular weight evolution during and after polymerization, quantification of Ru in the cyclic polymer products, and application of melt-state ^{13}C NMR spectroscopy for the characterization of cyclic polymers.

Results and Discussion

Initiation. Catalyst initiation is an important parameter, governing the amount of catalyst that enters the REMP cycle and thus the number of growing chains in solution. In the case of REMP, catalyst release during polymerization may also influence the overall rate of conversion because it competes with propagation, thus it is important to examine the catalyst initiation rates independently. Furthermore, resting state and propagating REMP catalyst species are different in nature, and it has been observed that initiation rates of Ru complexes are not always directly proportional to their olefin metathesis activities.[33]

To investigate REMP catalyst initiation rates, we measured the initiation kinetics by monitoring the stoichiometric metathesis reaction of **1**, **UC-5**, **SC-5**, **UC-6** and **SC-6** each with butyl vinyl ether (BVE).[33-34] Each catalyst was treated with an excess of BVE

(30 equiv relative to [Ru]) in C_6D_6 at 60 °C and the reaction progress was monitored by ^{1}H NMR spectroscopy. Regioselective conversion of the alkylidene complexes (**A**) to the corresponding Fischer carbenes (**B**) was observed for each catalyst and key data are summarized in Table 1. All reactions showed clean first-order kinetics over the time investigated.

Table 1. Initiation kinetics via ^{1}H NMR spectroscopy[a]

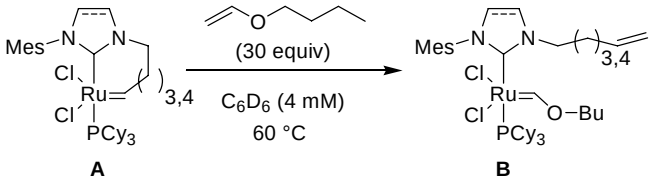

A **B**

catalyst	k_{obsd} (s^{-1})	k_{rel}[b]
1	8.2×10^{-3}	1
SC-5	1.1×10^{-2}	1.3
UC-5	2.4×10^{-3}	0.29
SC-6	4.2×10^{-4}	0.051
UC-6	5.0×10^{-5}	0.0061

[a]Conditions: $[Ru]_0 = 0.004$ M in C_6D_6 at 60 °C under N_2 (sealed tube); $[BVE/Ru]_0 = 30:1$.
[b]k_{rel} is the relative rate constant with respect to catalyst **1**.

The initiation rates showed a strong dependence on the catalyst structure (Table 1). Both **UC-5** and **SC-5** displayed dramatically increased initiation rates in comparison with their 6-carbon tether counterparts, **UC-6** and **SC-6**. Specifically, shortening the tether length by one carbon atom increased the initiation rate by 25 and 48 times for catalysts with saturated and unsaturated NHCs, respectively. In addition, saturation of the NHC backbone also improved initiation as reported for other Ru-NHC complexes.[33] Notably, **SC-5** was found to initiate slightly faster than complex **1** under identical conditions.

Rate of Polymerization. To compare the rate of polymerization for **UC-4** – **UC-7** in REMP, we examined their relative efficiencies in the polymerization of cyclooctene (COE) to poly(cyclooctene) (PCOE). As can be seen from the data presented in Figure 4, the relative efficiencies of the catalysts showed a strong dependence on the length of the chelating tether. In general, increased tether length was accompanied by an increase in catalytic activity. For example, comparison of the unsaturated catalysts revealed the time required to reach >95% conversion was nearly 24 h for **UC-4** (green line), approximately 8 h for **UC-5** (purple line) and **UC-6** (blue line), and less than1 h for **UC-7** (red line).

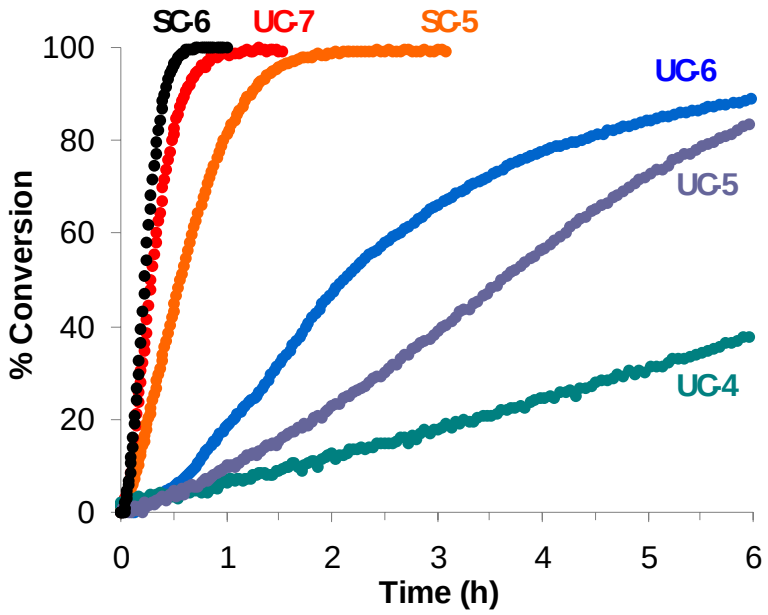

Figure 4. REMP of COE using catalysts **UC-4** (green), **UC-5** (purple), **SC-5** (orange), **UC-6** (blue), **SC6** (black), and **UC-7** (red). Conditions: CD_2Cl_2, 40 °C, $[M/C]_0$ = 1000:1, $[M]_0$ = 0.5 M. Conversion determined by ^1H NMR spectroscopy.

Saturation of the NHC backbone was found to dramatically increase catalyst activity. As expected, **SC-5** and **SC-6** each displayed faster polymerization rates than their unsaturated analogues **UC-5** and **UC-6**, respectively (Figure 4). Surprisingly, the polymerization rate acceleration resulting from NHC saturation appeared to be greater

than for homologation of the tether length. Specifically, **SC-6** was found to achieve >95% conversion in shorter reaction times than did **UC-7**. Similarly, **SC-5** was found to be a more active polymerization catalyst than **UC-6**. Overall, the data revealed that judicious combinations of shorter tether lengths (i.e., 5- or 6-carbon tethers) and NHC backbone saturation (e.g., **SC-5** and **SC-6**) provide a desirable balance of catalyst stabilities and activities.

Interestingly, the effects of ligand structure on relative rates of polymerization do not correspond directly with the observed initiation rates. In particular, the observed rates of polymerization were in the order of **SC-6** > **SC-5** > **UC-6** > **UC-5**, however, the significantly faster initiation of the C-5 catalysts is surprising. After the insertion of the first monomer, further insertions are not expected to depend on a single carbon difference in the size of the ring. Therefore, slower polymerization for C-5 vs. C-6 analogues is not attributed to a difference in the rate constant for monomer addition. Instead, the decreased polymerization rate of C-5 catalysts—in spite of their faster initiation—supports our previous hypothesis that the catalyst release is strongly favored over polymer propagation for these systems.

Catalyst stability takes on particular importance in REMP as decomposition of the catalyst before, during, or after polymerization could potentially lead to linear polymers, instead of the envisioned macrocycles. In addition, relative stabilities are important factors in the general development of new metathesis catalysts. Furthermore, it has been observed in some systems that catalyst stability and activity are inversely related.[35] To explore the stabilities of REMP catalysts **UC-4** – **UC-7** during polymerization reactions, we plotted the ln([COE]) versus time for REMP of COE (Figure 5). The logarithmic plots

were found to be linear (R^2 values ranged from 0.969 to 0.997) between 20% and 80% conversion of COE to PCOE, indicating that catalyst decomposition was negligible in all cases during the time of the polymerization reactions. Closer examination of the plots revealed that the only discernable deviations from linearity (i.e., pseudo-first-order rate kinetics) involved apparent increases in the rate of monomer consumption. This observation can be rationalized by a relatively slow initiation period which would manifest in a gradual increase in the number of propagating polymer chains, and concomitant increase in the rate of conversion.

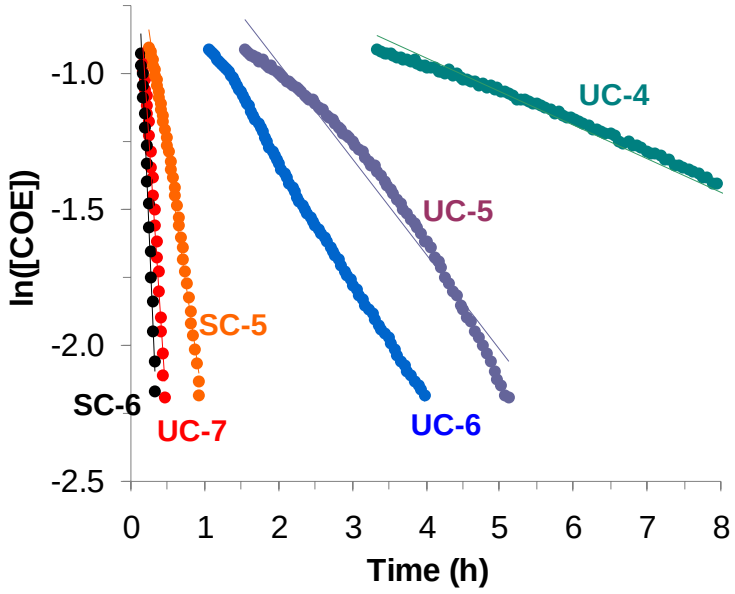

Figure 5. Log plots for REMP of COE using catalysts **UC-4** (green), **UC-5** (purple), **SC-5** (orange), **UC-6** (blue), **SC-6** (black), and **UC-7** (red). Linear least-squares fitting gave R^2 values of: **UC-4**, 0.997; **UC-5**, 0.969; **SC-5**, 0.991; **UC-6**, 0.998; **SC-6**, 0.990; and **UC-7**, 0.991. Conditions: CD_2Cl_2, 40 °C, $[M/C]_0$ = 1000:1, $[M]_0$ = 0.5 M. Conversion determined by ^{1}H NMR spectroscopy.

Molecular Weight Growth and Decline. The molecular weight evolution during polymerization, and equilibration of the cyclic polymers after complete monomer consumption, can shed light on the relative values of k_p, k_r and k_t. For a specific monomer,

different catalysts may be useful for guiding the molecular weight evolution of the cyclic polymers.

We monitored the molecular weight of PCOE during the REMP of COE using cyclic catalysts **UC-6**, **SC-6**, **UC-5**, and **SC-5**. Tether length was found to strongly affect the molecular weight versus conversion profiles (Figure 6), and in all cases the polydispersity indices (PDIs) ranged from 1.3 to 1.8. Catalysts **UC-6** and **SC-6** each delivered a large increase in molecular weight at the beginning of the polymerizations. Additionally, sharp increases in solution viscosities were observed within 1 h. PCOE obtained using **UC-6** displayed a peak molecular weight of 667 kDa when conversion reached 69%, followed by a drop in molecular weight such that at 100% conversion the molecular weight was found to be 393 kDa. Saturated catalyst **SC-6** displayed rapid molecular weight growth such that aliquots drawn prior to complete consumption of monomer provided polymers of sufficiently high molecular weight that they precluded molecular weight analysis via our GPC instrumentation. Thus, for comparison with the other catalyst systems, we use the first M_w obtained of 1260 kDa at 100% conversion. The observed molecular weight evolution for **UC-6** and **SC-6** under these conditions corresponds to polymerization rates that are significantly greater than those of catalyst release or other intramolecular chain transfer reactions. As the concentration of monomer decreased and that of polymer increased, propagation slowed sufficiently such that polymer pinching (k_t) became competitive resulting in molecular weight decline, as discussed in the next section.

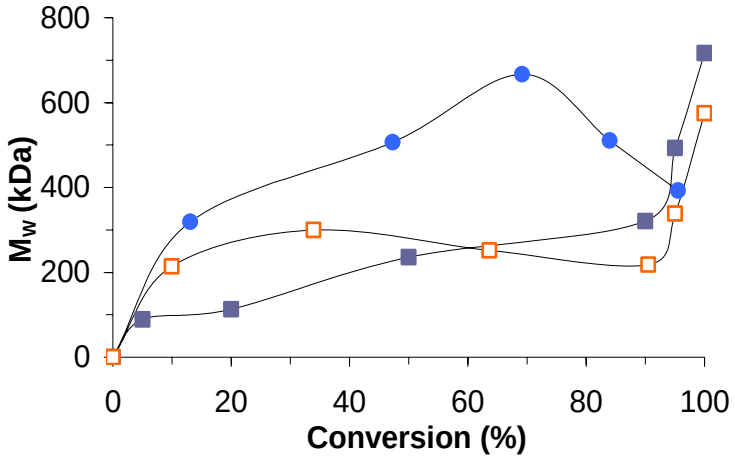

Figure 6. Weight-average molecular weight versus monomer conversion for the polymerization of COE using catalysts **UC-6** (●), **UC-5** (■), and **SC-5** (□). Conditions: $[COE]_0$ = 0.5 M in CH_2Cl_2 at 40 °C; $[COE/Ru]_0$ = 1000:1. (Polymer peaks were used to determine the molecular weight when separate oligomer peaks coexisted at low conversions using **UC-5** and **SC-5**.)

Interestingly, **UC-5** and **SC-5** were found to give strikingly different molecular weight growth profiles than their homologues **UC-6** and **SC-6** (Figure 6). In addition, the reaction mixtures did not show noticeable increase in viscosity until nearly complete monomer consumption, when rapid increase in viscosity was observed. In each case PCOE molecular weight increased sharply at low conversion (i.e., <10%) with noticeable amounts of oligomeric species detected by GPC analysis. Following this initial molecular weight increase, more gradual change in molecular weight, and concomitant decrease in the relative amounts of oligomer, were observed until approximately 90% conversion was achieved. At this point, sharp increases in molecular weight were observed reaching 575 and 717 kDa for **UC-5** and **SC-5**, respectively, at 100% conversion. The molecular weight evolution observed using the C-5 catalysts indicated a greater tendency for catalyst release during polymerization than their C-6 counterparts. Since the relative rates of monomer insertion and catalyst release regulate the kinetic molecular weight in REMP,

at high monomer concentrations propagation occurred faster than catalyst release, and thus polymeric species were observed even at low conversions. The rate of catalyst release, however, quickly became dominant as monomer concentration declined. The steep increase in molecular weight at high conversion suggested that macrocycles were combined via intermolecular chain-transfer events while remaining monomer continued to be incorporated. Notably, this data supports the notion that **UC-5** and **SC-5** each established an equilibrium during polymerization that strongly favored a non-incorporated resting state of the catalyst.

Once all of the monomer is consumed during REMP, the catalyst may continue to perform intra- and intermolecular chain transfer events on macrocyclic species, facilitating molecular weight equilibration. In the absence of end groups, the molecular weight of the final polymers at equilibrium should correspond to the ring size having the lowest thermodynamic energy under the experimental conditions. This differs from many linear polymerizations, including ring-opening metathesis polymerization (ROMP) in which the molecular weight is regulated by the amount of end groups present in the system, which are often from the initiator or chain transfer agent.

To investigate the molecular weight equilibration, we monitored the M_w of the polymers after 100% monomer conversion. Each of the catalysts studied eventually arrived at PCOE M_ws ranging from 300–500 kDa (Figure 7). The broad range of final M_ws suggested that the equilibration had stopped, for example due to catalyst death. To continue the equilibration, we isolated the cyclic PCOE via precipitation into excess acetone. After redissolving and precipitating the polymer successively three times to remove residual catalyst, the polymer was redissolved in CH_2Cl_2 with an olefin

concentration of 0.5 M. Polymer solutions were then treated with REMP catalyst and heated at 40 °C. After 12 h, PCOE was iteratively precipitated three times into acetone and analyzed by GPC to determine the PCOE M_w. The process of polymer isolation, analysis, and subjection to polymerization conditions was repeated three times while maintaining an olefin concentration of 0.5 M in each round, until the change in M_w was minimal. As shown in Figure 8, the PCOE M_w declined rapidly during the first cycle, then more slowly in subsequent cycles, ultimately approaching a value of 60 kDa. The entire process was repeated using $PhCH_3$ in place of CH_2Cl_2, which lead to a final M_w of 100 kDa.

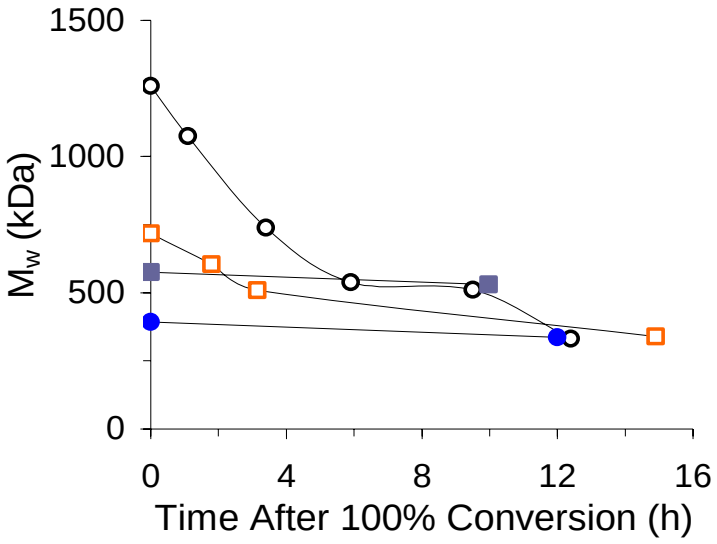

Figure 7. Equilibration of molecular weight of PCOE after 100% monomer conversion was obtained via REMP using catalysts **UC-6** (●), **SC-6** (○), **UC-5** (■), and **SC-5** (□). Conditions: $[COE]_0$ = 0.5 M in CH_2Cl_2 at 40 °C; $[COE/Ru]_0$ = 1000:1.

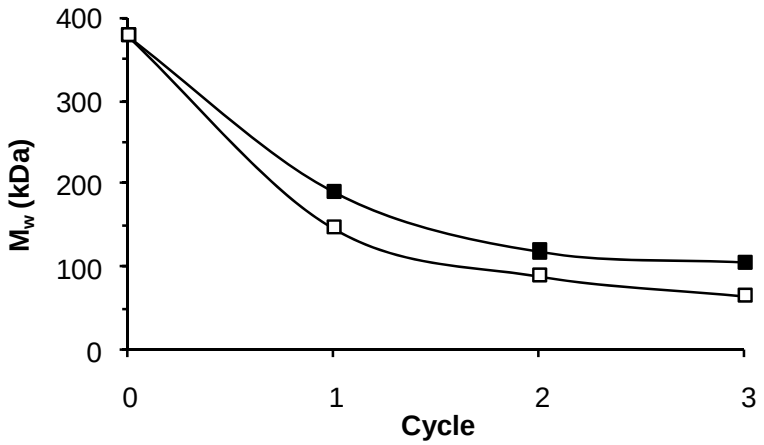

Figure 8. Molecular weight equilibrium of PCOE. Conditions: **SC-5** was repeatedly added at [olefin/Ru] = 500 to isolated PCOE, PCOE dissolved at 0.5 M (olefin concentration), 12 h, 40 °C in $PhCH_3$ (■) and in CH_2Cl_2 (□).

As mentioned previously, if the molecular weight evolution in REMP was approaching a thermodynamically stable state, catalyst loading should only impact the rate at which the equilibrium molecular weight is reached. Using similar conditions to those described above, but with varying initial monomer to catalyst ratios ($[M/Ru]_0$), we examined the molecular weight dependence on this variable. As shown in table 2, the $[M/Ru]_0$ did not linearly correlate with the final molecular weights obtained from the cyclic PCOE. Specifically, a $[M/Ru]_0$ of 1000:1 resulted in a PCOE molecular weight of 380 kDa, reflecting catalyst death prior to complete molecular weight equilibration (see above). Using $[M/Ru]_0$ of 300:1 or 100:1, however, resulted in a PCOE molecular weight of 150 and 100 kDa, respectively. Notably, the difference in molecular weights did not directly reflect the difference in $[M/Ru]_0$ used. Further reduction of the $[M/Ru]_0$ to 33:1 gave PCOE having a molecular weight of 70 kDa. Collectively, the results suggested that in the absence of considerable catalyst death, the final molecular weight more closely reflected thermodynamic equilibration, rather than $[M/Ru]_0$.

Table 2. Effect of **UC-6** catalyst loading on PCOE molecular weight[a]

$[M/Ru]_0$	M_w (kDa)	PDI
1000	380	1.6
300	150	1.5
100	100	1.8
33	70	1.6

[a]Conditions: $[COE]_0$ = 0.5 M in CH_2Cl_2 at 40 °C for 12 h.

We next explored the impact of monomer structure on the molecular weight evolution during REMP. Monomer characteristics, such as ring strain and olefin density, may strongly affect the relative rates of propagation and chain transfer. Therefore, we studied REMP of cyclododecatriene (CDT), which has less strain than COE and twice the olefin density, and would be expected to slow propagation but facilitate chain transfer. To test the hypothesis that REMP of CDT using C-5 catalysts would exhibit efficient catalyst release and as a result more step like molecular weight growth than REMP of COE, the molecular weight evolution was studied for CDT in CH_2Cl_2 (0.3 M) at 40 °C using $[CDT/\mathbf{SC\text{-}5}]_0$ = 500:1. The total monomer concentration was reduced in comparison with the experiments described above using COE ($[COE]_0$ = 0.5 M). The reduced monomer concentration is also expected to favor catalyst release over propagation.

Strikingly, although the monomer conversion reached completion in 4 h, only oligomeric species were observed suggesting that propagation is slower than catalyst release. Polymeric species were detectable by GPC only when conversion began to approach 90% (Figure 9), and relative amounts were significantly less than that of oligomeric species. Continued GPC analysis revealed that a polymer peak gradually

became dominant over lower molecular weight oligomers 8 h after full monomer conversion. After all the monomer was converted to oligomers, these small rings then coalesced into thermodynamically favored cyclic polymers through intermolecular chain transfer. Thus, the propagation of CDT at 0.3 M was sufficiently slower than chain transfer, leading to the observed step-growth type polymerization profile.

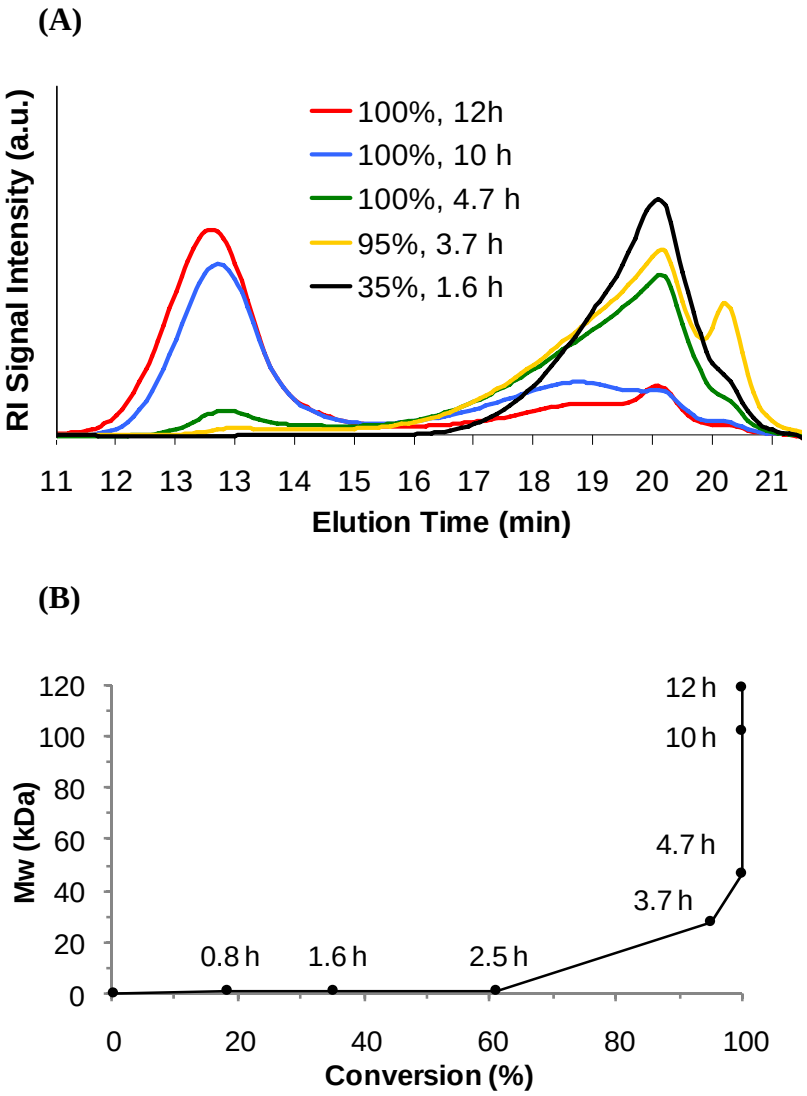

Figure 9. (A) GPC traces of REMP of CDT using **SC-5** at different conversions. (B) molecular weight vs. monomer conversion for REMP of CDT using **SC-5**. $[CDT]_0$ = 0.3 M in CH_2Cl_2, $[CDT/\mathbf{SC\text{-}5}]_0$ = 500:1, 40 °C. Aliquots were withdrawn at the indicated times and immediately treated with ethyl vinyl ether. Conversions were determined by ^1H NMR spectroscopy prior to GPC analysis. After the formation of polymeric species above 95% conversion, only the polymer peaks were selected to determine the molecular weight in figure 9B.

In contrast to REMP of CDT using **SC-5**, **SC-6** produced polymeric species even at low conversions, in addition to significant amounts of oligomer. This is in accord with the faster propagation previously observed from **SC-6** (cf. **SC-5**) in combination with sluggish catalyst release. Moreover, intramolecular chain transfer would be expected to

occur equally efficiently from either an incorporated **SC-5** or **SC-6** species. Therefore, the stunted molecular weight growth observed from **SC-5** can likely be ascribed specifically to increased catalyst release in comparison with **SC-6**, as opposed to ring "pinching" via intra-chain metathesis events.

The molecular weight growth observed at high conversion when using **UC-5** or **SC-5** (Figures 6 and 9) suggested that these catalysts were capable of mediating intermolecular chain transfer between oligomeric macrocycles to achieve polymers of higher molecular weight. This was surprising considering that this required REMP of large, unstrained cyclic olefins. We envisioned REMP of relatively large monomers should then also equilibrate to high molecular weight polymer, despite relatively low disparity in the ring strain of each species.

To obtain appropriate monomers, we took advantage of the entropically driven ring-chain equilibria in ROMP, where unstrained macrocycles are preferentially formed below the critical monomer concentration.[20,36-40] We prepared COE macrocycles at 0.1 M, using **SC-5** as the catalyst to avoid potential linear contamination. Analysis of the product mixture via ^{1}H NMR spectroscopy, GC-MS, and GPC collectively indicated that no linear contaminants or polymeric species were present. When solutions of COE macrocycles in $PhCH_3$ (olefin concentration = 0.5 M) were heated at 40 °C in the presence of **SC-5**, the reaction mixtures became more viscous indicating an increase in molecular weight. After 12 h, the PCOE was isolated in 70% yield via precipitation into acetone. GPC analysis revealed a M_w of 100 kDa, consistent with the results of the molecular weight equilibration starting from high molecular weight PCOE (see above). The same final M_w was obtained for $[\text{olefin/Ru}]_0$ = 500:1 and 150:1, and remained

unchanged upon isolation of polymer and re-injection of new catalyst under the same experimental conditions, suggesting that the ring sizes had reached the most thermodynamically stable state under these conditions.

Determination of Residual Ruthenium. As described previously, incomplete catalyst release from cyclic polymers will result in residual Ru within the polymer backbone. In addition to compromising the overall purity of the polymer products, the metal centers may decompose during subsequent workup, processing, or reactions. Unfortunately, catalyst cleavage using terminating agents such as ethyl vinyl ether, which are widely used to cleave catalyst off polymer prepared via ROMP, cannot remove the incorporated catalyst from the polymer and may also introduce linear impurity.

Therefore, the determination of the residual Ru content in the cyclic polymers obtained via REMP is crucial. Our conclusions thus far have been that catalyst release (i.e., to reform the initial cyclic catalyst) is favored for 5-carbon tethered complexes (e.g., **UC-5** and **SC-5**), and disfavored for complexes bearing longer tethers. Although solution NMR spectroscopy and kinetic data corroborate these findings, we sought a more accurate means to determine the amount of residual Ru in the cyclic polymers. Thus, we prepared samples of PCOE from various cyclic catalysts and analyzed the residual Ru content via inductively coupled plasma mass spectroscopy (ICP-MS). For comparison, linear polymer samples prepared using complex **1** were also analyzed.

Polymerizations were conducted using COE monomer (0.5 M in CH_2Cl_2) and $[M/Ru]_0 = 1000:1$. Upon completion, reaction mixtures were diluted to half concentration with CH_2Cl_2 and cooled to 0 °C causing crystallization of PCOE out of solution. The PCOE was collected and recrystallized three times from CH_2Cl_2 to remove most of the

unbound catalyst. To produce solutions for analysis via ICP-MS, polymer samples were digested in a mixture of concentrated H_2SO_4 and concentrated HNO_3 for 2 days at 70 °C, during which time complete dissolution of polymer was achieved. ICP-MS experiments were conducted in duplicate and a calibration curve was used to determine the amount of Ru in each sample; key data are summarized in Table 3.

The theoretical maximum Ru that could be present in the polymers at a $[M/Ru]_0$ = 1000:1 is 6,550 ppm. PCOE prepared from **UC-5, SC-5** and **UC-6** (entries 3 – 5) were found to contain similar residual Ru content of only ca 230 ppm Ru. In contrast, PCOE prepared using **SC-6** (entry 6) was found to contain 609 ppm Ru. This is consistent with previous NMR spectroscopic experiments which indicated that **SC-6** can gradually incorporate into the polymer backbone, while the incorporation of **UC-5** and **SC-5** was not observed and the incorporation of **UC-6** was only minimal at elevated temperatures. Considering that a small amount of residual Ru was detectable even when complex **1** was used and catalyst cleavage was performed at the end of ROMP (entries 1 and 2), we speculate that the consistent amounts of residual Ru from samples prepared using **UC-5**, **SC-5** and **UC-6** may reflect unbound, physically trapped metal species.

Table 3. Residual Ru amounts in PCOE (ppm) prepared by different catalysts after crystallization of polymer from solution[a]

Entry	Catalyst	M_w of PCOE (kDa)	[Ru] (ppm)[b]
1	**1**[c]	80	151 ± 8
2	**1**[d]	80	137 ± 10
3	**UC-5**	560	236 ± 6
4	**SC-5**	500	237 ± 37
5	**UC-6**	340	219 ± 20
6	**SC-6**	380	609 ± 42

[a]Polymerization conditions: CH_2Cl_2, 40 °C, $[M/Ru]_0$ = 1000:1, $[M]_0$ = 0.5 M, 12 h. Excess ethyl vinyl ether was added at the end of polymerization only when **1** was used. [b]Analyzed by ICP-MS, experiments conducted in duplicate and averaged. [c]Crystallized once at 0 °C from CH_2Cl_2. [d]Crystallized three times at 0 °C from CH_2Cl_2.

Polymer Characterization. A significant challenge in characterization of REMP polymers is the confirmation of a ring topology. Differences between cyclic and linear analogues are typically elucidated via a combination of known solution properties of cyclic polymers, such as longer GPC retention times, smaller hydrodynamic radii, and lower intrinsic viscosities.[5-16,19,21-28] However, clear comparison of these properties requires the use of linear and cyclic polymers at exactly the same MW (i.e., linear precursor polymer and the cyclized cyclic polymer, if prepared via the end-linking strategy). Because REMP does not involve linear precursor polymers and it produces polymers with relatively broad MW distribution, linear polymers have to be prepared separately and it is difficult, if not impossible, to match the exact MW and MW distribution with the cyclic polymer. Although GPC coupled with a triple-detection system could provide this comparison by taking each slice of the polymer peak to

calculate the absolute MW of each point from light scattering, complications may occur, as discussed in the Appendix.

Therefore, we explored melt-state magic-angle spinning (MAS) NMR spectroscopy and mass spectroscopy analyses as viable methods for detecting linear polymer contaminants.

NMR analysis. ^{13}C NMR spectroscopy is one of the few methods that can provide quantitative information about polymer topology and microstructure, and has been widely used for the determination of branch content and tacticity of polyolefins.[41-45] The sensitivity of solution-state NMR spectroscopy is limited due to the low concentration of ^{13}C nuclei, and bulk samples typically suffer severe line broadening. Recently, optimized melt-state MAS NMR methodology has been developed to combine high spin concentrations and motional averaging of line broadening interactions that allows for quantitative analysis of minute chain units (e.g., long-chain branch junctions in polyethylene). Sensitivities for this technique are high, reaching 1 branch per 100,000 CH_2 groups.[42]

Herein, we extended this highly sensitive technique to compare linear (L) and cyclic (C) PCOE prepared from complex **1** and **UC-6**, respectively. GPC analysis revealed a M_w of 220 kDa for the L-PCOE, corresponding to a DP of 2,000, and a M_w of 114 kDa (DP = 1,040) for the C-PCOE. Notably, the lower DP of the C-PCOE in comparison with the L-CPOE should facilitate the detection of linear contaminants in the former. The polymer samples were melted in a sealed zirconia rotor under N_2 at 70 °C and melt-state MAS ^{13}C NMR spectra were recorded using a 7 mm MAS probe at 70 °C for ca. 13 h. The L-PCOE and C-PCOE were found to have similar trans/cis olefin ratios

(3.5:1 for L-PCOE and 4.2:1 for C-PCOE), calculated from the intense peaks from the polymer olefinic (δ = 132-129 ppm) and methylene (δ = 34-27 ppm) carbon resonances (Figure 10). These values were consistent with those obtained via solution-state ^{1}H NMR spectroscopy. End groups in the L-CPOE sample manifested additional peaks in both the olefinic and alkyl regions of the spectrum. In contrast, these signals were not detectable for the C-PCOE, indicating a lack of end groups as expected for the cyclic topology. Considering the sensitivity of this technique, and the DP of the C-PCOE, the results indicate that no greater than 1 in 10 chains contain end groups. In other words, the sample obtained from **UC-6** was found to be >90% cyclic.

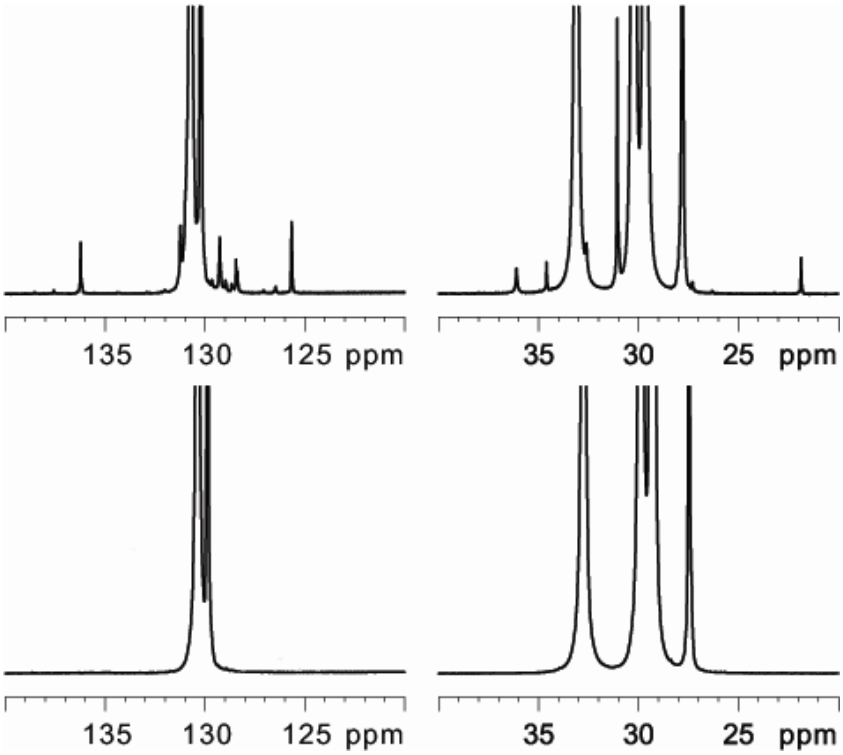

Figure 10. Melt-state ^{13}C NMR spectra of linear PCOE olefinic region (top left), linear PCOE aliphatic region (top right), cyclic PCOE olefinic region (bottom left), and cyclic PCOE aliphatic region (bottom right). Linear PCOE M_w = 220 kDa; Cyclic PCOE M_w = 114 kDa.

MS analysis. We used matrix-assisted laser desorption ionization time-of-flight mass spectrometry (MALDI-TOF MS) to detect the possible end groups of polymers. Due to the extremely difficult ionization of high MW hydrocarbon polymers, poly(5-acetoxy-cyclooctene) (PCOE-OAc) was used for MALDI MS test. Both cyclic and linear PCOE-OAc was prepared under similar conditions, except for the catalyst used, with MW at ~100 kDa (Figure 11).

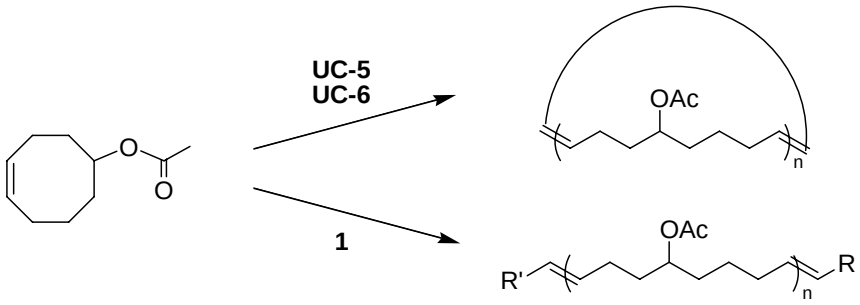

Figure 11. Synthesis of cyclic and linear poly(5-acetoxy-cyclooctene).

The high MW portion of PCOE-OAc was still difficult to ionize, and we obtained the spectra only for relative low MW regions (<5 kDa). MALDI-TOF mass spectrum of the cyclic PCOAc showed only the molecular ions for the sodium-complexed cyclic structure spaced in 168 Da, the molecular weight of the monomer; no other peaks with significant intensity were observed, which indicated the absence of linear structures in the range of molecular ions less than m/z 5000 (Figure 12 left). In contrast, the linear PCOE-OAc showed a group of peaks for each degree of polymerization (DP) (Figure 12 right). The assignment of end groups for these masses was difficult, but these peaks may be due to various end group decomposition during the ionization process.

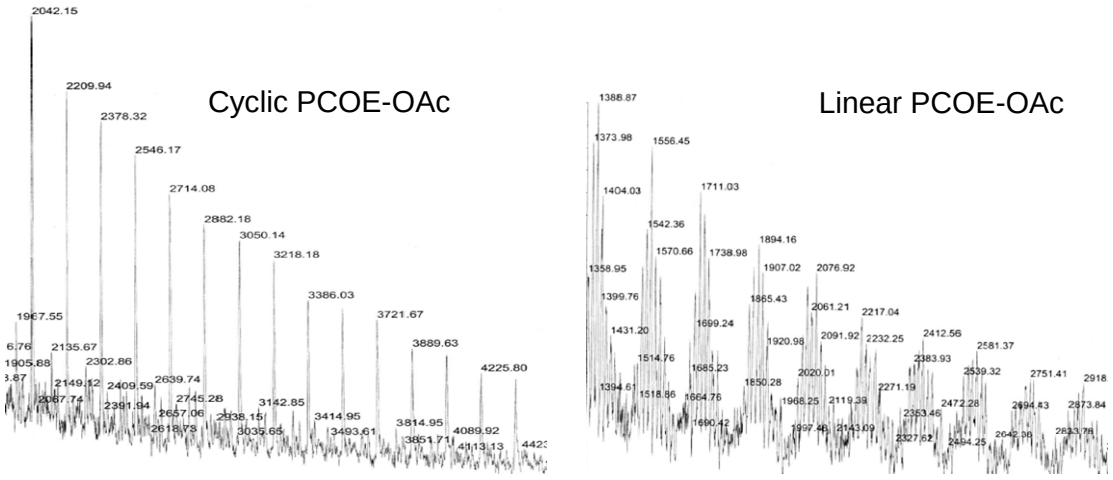

Figure 12. MALDI-TOF mass spectra of cyclic (left) and linear (right) poly(5-acetoxy-cyclooctene). Conditions: cyclic: [M/**UC-6**] = 200, M_w = 105 kDa and linear: [M/**1**] = 500, M_w = 81 kDa, at 40 °C in DCM.

Conclusions

Ring-expansion metathesis polymerization (REMP) has been studied in detail using monomers of varied ring strain and degrees of unsaturation, in combination with cyclic Ru catalysts of varying architecture. Each key step in the proposed REMP catalytic cycle (initiation, propagation, and catalyst release or chain transfer), was probed using different catalysts. The order of initiation rates did not directly correspond to previously observed rates of polymerization, and specifically, C-5 catalysts gave faster initiation than did C-6 analogues. The catalyst tether length was found to have a significant impact on the polymerization profile: REMP using C-5 catalysts showed a step-growth like mechanism, as a result of the fast catalyst release that competed with propagation. In contrast, REMP using C-6 catalysts showed a chain-growth like mechanism, and it gave high-molecular-weight polymer before full monomer conversion due to significantly faster propagation relative to catalyst release or chain transfer. The catalyst structure controls the kinetic molecular weight of their polymer product, but after full monomer conversion the molecular weight of PCOE was found to approach an equilibrium value

that was independent of catalyst structure and initial monomer/catalyst ratios. ICP-MS analysis concluded that low levels of residual Ru were present in the cyclic polymer samples when either catalyst release was efficient (i.e., **UC-5** or **SC-5**) or catalyst incorporation was slow (i.e., **UC-6**). The cyclic nature of the polymer products was supported by high-sensitivity melt-state ^{13}C NMR spectroscopy and MALDI-TOF MS The reported results provide insights into the mechanism of REMP and will guide the synthesis of functional cyclic polymers and development of novel materials based on such materials.

Experimental Section

Materials and instrumentation. CH_2Cl_2, $PhCH_3$ and C_6D_6 were obtained from solvent purification columns. CD_2Cl_2 used for NMR scale experiments was distilled from CaH_2 under N_2 prior to use. Ru complex **1** was obtained from Materia, Inc. Cyclooctene and *cis*, *trans*, *trans*-cyclododecatriene were fractionally distilled before use. All other solvents and reagents were of reagent quality and used as obtained from commercial sources. Cyclic Ru catalysts were synthesized as described previously and stored in a glove box filled with N_2.[22] Solution state ^1H and ^{13}C NMR spectra were recorded using a Varian Mercury 300 or Varian Inova 500 spectrometer and were routinely run using broadband decoupling. Chemical shifts (δ) are expressed in ppm downfield from tetramethylsilane using the residual protiated solvent as an internal standard.

Melt-state ^{13}C NMR spectroscopy was recorded using a Bruker Avance 500 dedicated solid-state NMR spectrometer operating at a proton and carbon Larmor frequency of 500.13 and 125.75 MHz respectively. All measurements were undertaken with a commercial Bruker, ^{13}C-^1H optimized, high temperature, 7 mm magic-angle spinning

(MAS) probehead using zirconia rotors and rotor caps with ca. 200 mg of PCOE packed inside. N_2 gas was used for all pneumatics to limit thermal oxidation. All measurements were conducted at $\omega_r/2\pi$ = 3 kHz spinning speed at 70 °C sample temperature, whilst compensating for thermal MAS effects. Single pulse excitation spectra were acquired using 10 μs ^{13}C π/2 excitation pulses and π pulse-train heteronuclear dipolar decoupling. For both linear and cyclic PCOEs, 200 mg of polymer was used and 21,000 scans were accumulated with a 2 s recycle delay resulting in a measurement time of 13 h 35 min per sample. The spectra were normalized according to the total intensity of olefinic peaks (δ = 132-129 ppm) to compare the presence of end groups.

Gel permeation chromatography (GPC) was carried out in THF on two PLgel 5 μm mixed-C columns (Polymer Labs) connected in series with a DAWN EOS multi-angle laser light-scattering (MALLS) detector and an Optilab DSP differential refractometer (both from Wyatt Technology). No calibration standards were used, and d*n*/d*c* values were obtained for each injection by assuming 100% mass elution from the columns.

Inductively coupled plasma mass spectroscopy (ICP-MS) was conducted on a Hewlett-Packard 4500 ICP mass spectrometer (Agilent Technologies) with a CETAC ASX-500 autosampler (CETAC). PlasmaCal Ru and Rh standard solutions were used for calibration and DigitTUBEs were used for sample digestion. For sample preparation, 25 mg of polymer was accurately weighed using a microbalance and digested in a mixture of 3 mL of concentrated nitric acid and 2 mL of concentrated sulfuric acid at 70 °C for 2 days. To each digested solution was added 1 mL of a 10 ppm Rh solution, used as an internal standard for Ru. Each solution was diluted to 50 mL using DI water before analysis.

NMR initiation kinetics. The Ru catalyst (0.0028 mmol) was dissolved in C_6D_6 (0.7 mL) in an NMR tube fitted with a screw cap containing a rubber septum. The resulting solution was equilibrated in the NMR probe at 60 °C, and BVE (30 equiv relative to [Ru]) was injected into the NMR tube. Reactions were monitored by measuring the peak integration of the starting Ru-alkylidene as a function of time.

General procedure for REMP of cyclooctene. In a typical experiment, an oven-dried 40 mL vial with a Teflon-lined screw cap was charged with degassed COE (1.0 g, 9.1 mmol) and a stir bar. Under an argon atmosphere, 18 mL (0.5 M for the monomer) of dry, degassed CH_2Cl_2 or $PhCH_3$ was added via syringe. In a separate oven-dried vial, a catalyst stock solution was prepared in dry, degassed CH_2Cl_2 or $PhCH_3$ under an atmosphere of argon. The desired amount of catalyst was injected to the monomer solution under argon to initiate the polymerization at 40 °C. Aliquots (0.5 mL) were removed using a degassed syringe at desired time intervals and chilled with dry ice. At the end of polymerization, the solution was diluted to half concentration and was either added dropwise into 300 mL of stirred MeOH or acetone, or cooled to 0 °C in a refrigerator, and the resulting precipitate was collected by centrifugation. Isolated polymer was redissolved in THF at room temperature and reprecipitated and collected two additional times. The isolated white polymer was dried under high vacuum.

Synthesis of macrocyclic cyclooctene oligomer using SC-5. A 50 mL round-bottom flask filled with argon was charged with 0.3 g degassed COE and 30 mL degassed $PhCH_3$ (0.1 M). In a separate vial, an **SC-5** stock solution was prepared in degassed $PhCH_3$ under an atmosphere of argon. 2 mg **SC-5** ($[COE/\mathbf{SC\text{-}5}]_0 = 1000$) was injected into the flask. After stirring at 40 °C for 10 h, NMR showed complete conversion, and one drop of ethyl

vinyl ether was added to quench the reaction. After 1 h, all the solvent was removed under vacuum and the product passed a short silica plug eluting with hexanes to remove the catalyst. The volatiles were removed *in vacuo* to yield 0.2 g clear thick oil. ^{1}H-NMR: δ 5.4-5.2 (m, 2H), 2.1-1.9 (m, 4H), 1.4-1.2 (m, 8H). ^{13}C-NMR: δ130.4, 129.9, 32.8, 30.0, 29.9, 29.4, 29.3, 27.5.

References

(1) Semlyen, J. A. *Large Ring Molecules* **1996**.

(2) Semlyen, J. A. *Cyclic Polymers, 2nd ed.* **2000**.

(3) Zimm, B. H.; Stockmayer, W. H. *J. Chem. Phys.* **1949**, *17*, 1301.

(4) Hadjichristidis, N.; Pitsikalis, M.; Pispas, S.; Iatrou, H. *Chem. Rev.* **2001**, *101*, 3747.

(5) Tezuka, Y.; Fujiyama, K. *J. Am. Chem. Soc.* **2005**, *127*, 6266.

(6) Takano, A.; Kadoi, O.; Hirahara, K.; Kawahara, S.; Isono, Y.; Suzuki, J.; Matsushita, Y. *Macromolecules* **2003**, *36*, 3045.

(7) Oike, H.; Mouri, T.; Tezuka, Y. *Macromolecules* **2001**, *34*, 6592.

(8) Lepoittevin, B.; Dourges, M. A.; Masure, M.; Hemery, P.; Baran, K.; Cramail, H. *Macromolecules* **2000**, *33*, 8218.

(9) Gan, Y.; Dong, D.; Carlotti, S.; Hogen-Esch, T. E. *J. Am. Chem. Soc.* **2000**, *122*, 2130.

(10) Yu, G.-E.; Sinnathamby, P.; Price, C.; Booth, C. *Chem. Commun.* **1996**, 31.

(11) Roovers, J.; Toporowski, P. M. *Macromolecules* **1983**, *16*, 843.

(12) Clark, P. G. G., E. N.; Chan, W. Y.; Steinmetz, W. E.; Grubbs, R. H. *J. Am. Chem. Soc.* **2010**, *132*, 3405.

(13) Qiu, X. P.; Tanaka, F.; Winnik, F. M. *Macromolecules* **2007**, *40*, 7069.

(14) Laurent, B. A.; Grayson, S. M. *J. Am. Chem. Soc.* **2006**, *128*, 4238.

(15) Schappacher, M.; Deffieux, A. *Macromolecules* **2001**, *34*, 5827.

(16) Lepoittevin, B.; Perrot, X.; Masure, M.; Hemery, P. *Macromolecules* **2001**, *34*, 425.

(17) Schappacher, M.; Deffieux, A. *Science* **2008**, *319*, 1512.

(18) Schappacher, M.; Deffieux, A. *J. Am. Chem. Soc.* **2008**, *130*, 14684.

(19) Kress, J. *J. Mol. Catal.* **1995**, *102*, 7.

(20) Reif, L.; Hocker, H. *Macromolecules* **1984**, *17*, 952.

(21) He, T.; Zheng, G. H.; Pan, C. Y. *Macromolecules* **2003**, *36*, 5960.

(22) Boydston, A. J.; Xia, Y.; Kornfield, J. A.; Gorodetskaya, I. A.; Grubbs, R. H. *J. Am. Chem. Soc.* **2008**, *130*, 12775.

(23) Jeong, W.; Hedrick, J. L.; Waymouth, R. M. *J. Am. Chem. Soc.* **2007**, *129*, 8414.

(24) Darcy A Culkin; Wonhee Jeong; Szilard Csihony; Enrique D. Gomez; Nitash P. Balsara; James L. Hedrick; Waymouth, R. M. *Angew. Chem. Int. Ed.* **2007**, *46*, 2627.

(25) Takeuchi, D.; Inoue, A.; Osakada, K.; Kobayashi, M.; Yamaguchi, K. *Organometallics* **2006**, *25*, 4062.

(26) Li, H.; Debuigne, A.; Jerome, R.; Lecomte, P. *Angew. Chem. Int. Ed.* **2006**, *45*, 2264.

(27) Kudo, H.; Makino, S.; Kameyama, A.; Nishikubo, T. *Macromolecules* **2005**, *38*, 5964.

(28) Kricheldorf, H. R. *J. Polym. Sci. Part A: Polym. Chem.* **2004**, *42*, 4723.

(29) Bielawski, C. W.; Benitez, D.; Grubbs, R. H. *J. Am. Chem. Soc.* **2003**, *125*, 8424.

(30) Bielawski, C. W.; Benitez, D.; Grubbs, R. H. *Science* **2002**, *297*, 2041.

(31) Ulman, M.; Grubbs, R. H. *Organometallics* **1998**, *17*, 2484.

(32) Bielawski, C. W.; Grubbs, R. H. *Angew. Chem. Int. Ed.* **2000**, *39*, 2903.

(33) Sanford, M. S.; Love, J. A.; Grubbs, R. H. *J. Am. Chem. Soc.* **2001**, *123*, 6543.

(34) Love, J. A.; Sanford, M. S.; Day, M. W.; Grubbs, R. H. *J. Am. Chem. Soc.* **2003**, *125*, 10103.

(35) Ritter, T. H., A.; Wenzel, A. G.; Funk, T. W.; Grubbs, R. H. *Organometallics* **2006**, *25*, 5740.

(36) Hocker, H.; Reimann, W.; Riebel, K.; Szentivanyi, Z. *Makromol. Chem.* **1976**, *177*, 1707.

(37) Chen, Z.-R.; Claverie, J. P.; Grubbs, R. H.; Kornfield, J. A. *Macromolecules* **1995**, *28*, 2147.

(38) Marmo, J. C.; Wagener, K. B. *Macromolecules* **1995**, *28*, 2602.

(39) Hodge, P.; Kamau, S. D. *Angew. Chem. Int. Ed.* **2003**, *42*, 2412.

(40) Kamau, S. D.; Hodge, P.; Hall, A. J.; Dad, S.; Ben-Haida, A. *Polymer* **2007**, *48*, 6808.

(41) Min, E. Y. J.; Byers, J. A.; Bercaw, J. E. *Organometallics* **2008**, *27*, 2179.

(42) Klimke, K.; Parkinson, M.; Piel, C.; Kaminsky, W.; Spiess, H. W.; Wilhelm, M. *Macromol. Chem. Phys.* **2006**, *207*, 382.

(43) Byers, J. A.; Bercaw, J. E. *Proc. Natl. Acad. Sci. USA* **2006**, *103*, 15303.

(44) Yoder, J. C.; Bercaw, J. E. *J. Am. Chem. Soc.* **2002**, *124*, 2548.

(45) Wood-Adams, P. M.; Dealy, J. M.; deGroot, A. W.; Redwine, O. D. *Macromolecules* **2000**, *33*, 7489.

C h a p t e r 4

Efficient Syntheses of Linear and Cyclic Brush Polymers via Ring-Opening Metathesis Polymerization of Macromonomers

Portions of this chapter have been published: Xia, Y.; Kornfield, J. A.; Grubbs, R. H. *Macromolecules* **2009**, 42, 3761-3766.

Abstract

Various macromonomers (MMs) were efficiently synthesized through the copper-catalyzed "click" coupling of a norbornene moiety to the chain end of poly(methylacrylate), poly(*t*-butylacrylate), and polystyrene that were prepared using atom transfer radical polymerization. Ring-opening metathesis polymerization (ROMP) of these MMs was carried out using the highly active, fast-initiating ruthenium catalyst $(H_2IMes)(pyr)_2(Cl)_2RuCHPh$ in THF at room temperature. ROMP of MMs was found to be living with almost quantitative conversions (>90%) of MMs, producing brush polymers with very low polydispersity indices of 1.01−1.07 and high M_ns of 200−2600 kDa. The efficient ROMP of such MMs provides facile access to a variety of brush polymers and overcomes previous difficulties in the controlled polymerization of MMs. Atomic force microscopy (AFM) of the brush polymer products revealed extended, wormlike shapes as a result of significant steric repulsion of densely grafted side chains.

When cyclic catalysts were used to polymerize these MMs, cyclic brush polymers were clearly observed using AFM together with linear brush polymer impurities.

Introduction

With our knowledge of REMP mechanism on relatively simple monomers, we moved our attention to the confirmation of the cyclic topology of REMP polymers. Besides the chemical structure-based and property-based characterizations, the most convincing evidence would be to directly image cyclic polymers. However, flexible polymers adopt a random-coil conformation, making it impossible to distinguish different topologies when imaged. Therefore, the polymer backbone has to be forced to adopt an extended conformation and needs to be grafted with side chains to make it thicker and larger to facilitate molecular imaging. Bottle-brush polymer is ideal for this purpose. Brush polymers are a unique type of macromolecules with a high density of side chains grafted to the backbone.[1-3] The compact structure leads to an extended backbone conformation, causing the polymer to adopt a cylindrical or wormlike structure.[4,5] Furthermore, cyclic brush polymers provide a versatile molecular platform to build up cyclic organic nanostructures, which are otherwise difficult to obtain.

However, facile and precise control over the architecture, size, and functionality of brush polymers remains a central challenge. Brush polymers are usually prepared by three grafting methods: “grafting from”, “grafting onto”, and “grafting through” (ca. the macromonomer (MM) approach).[2,3] The “grafting from” approach involves the growth of side chains from backbone polymers with pendent initiation sites (macroinitiators). This approach and has been the most widely explored route to brush polymers, and a variety of monomers has been used for both the backbone and the side chain.[6-11] Importantly, the initiation efficiency from the macroinitiators may be limited due to the high density of initiation sites.[12,13] The “grafting onto” method has the advantage that it allows for

individual preparation of backbone polymers and side chains.[14-17] The downside is that grafting becomes progressively more difficult as conversion increases, leading to limited grafting density, even when a large molar excess of side chains is used.[16] Additionally, due to the ultrahigh MW of cyclic functionalized polynorbornenes (often >1 MDa) we prepared using REMP, "grafting from" and "grafting onto" these polynorbornenes all resulted in gigantic polymers that cannot be dissolved for any measurements.

Therefore, we focused on the MM approach. Among the three methods for preparation of brush polymers, only the MM approach guarantees complete grafting (i.e., one side chain per repeating unit). Additionally, the MM approach can afford the most precise and easiest control of side chain length and main chain length, provided that the polymerization of MM is efficient and controlled. However, synthesis of polymacromonomers (polyMM) with a high degree of polymerization (DP) and low polydispersity index (PDI) remains synthetically challenging, largely because of the inherently low concentration of polymerizable groups and the demanding steric hindrance of side chains.

Conventional radical polymerization of highly concentrated MM solution[18-20] and metallocene-catalyzed polymerization of MM[21,22] have been shown to yield high molecular weight (MW) polyMM, but with limited conversion and high PDI. Controlled radical,[23] anionic,[24] and metathesis polymerizations[25-30] of MMs have shown limited success, and only low DPs for the backbone of graft polymers were obtained. In several examples, ring-opening metathesis polymerization (ROMP) of MMs using early transition metals, such as molybdenum, has been used to produce narrowly dispersed polyMMs. However, the DP of the backbone of these polyMMs remained low (typically

5-20).[25-30] Therefore, these graft polymers were believed to resemble star architectures instead of brushlike structures. In addition, the limited functional group tolerance and air and moisture sensitivity of these catalysts narrow their applications. More recently, Ru-based catalyst **1** was used in the ROMP of MMs. Although narrowly dispersed graft polymers were obtained, the relatively low reactivity of **1** limited the DP of these graft polymers.[31,32] To our knowledge, there exists only one example of a *narrowly dispersed* polyMM with high MW, which was prepared by the ROMP of a polylactide norbornenyl MM using catalyst **1**.[33] Ru catalyst **2** shows greatly increased reactivity compared to **1**, but the resulting polymers are generally polydisperse due to its slow initiation.[34] We have recently reported on a class of pyridine-containing catalysts, including catalyst **3**, that mediate living polymerization. These catalysts exhibit both fast initiation and high reactivity.[35-37] Catalyst **3** has been shown to polymerize sterically demanding monomers, as Fréchet and co-workers have recently demonstrated the block copolymerization of dendronized norbornenes.[38] The fast initiation, high reactivity, and high functional group tolerance of catalyst **3** make it ideal for the polymerization of MMs.

The synthesis of MMs presents another challenge. Most of the reported preparations of norbornenyl MMs involve anionic polymerization using either a functionalized norbornene as the initiator[25,26] or end capping of a "living" polymer chain to install the norbornenyl group.[27-30] However, these routes generally require stringent experimental conditions and limit functionality in the polymer. Over the last fifteen years, controlled radical polymerization (CRP) has emerged as a powerful and versatile technique for the preparation of a variety of functionalized polymers with controlled MW and end group functionality.[39-41] Wooley and co-workers[42] and Advincula and co-

workers[43] have recently studied the syntheses of norbornenyl MMs by atom transfer radical polymerization (ATRP) and reversible addition–fragmentation chain transfer (RAFT) polymerization, respectively, using functionalized norbornenes as the initiator or chain transfer agent. However, the norbornenyl functionality led to bimodal MW distributions with high MW components in both the ATRP and the RAFT polymerization of acrylates even in large excess of monomer. This was attributed to the copolymerization of the norbornene functionality with acrylate monomers. Therefore, we sought a more versatile approach to obtain well-defined norbornenyl MMs prepared via CRP.

The combination of ATRP and "click" functionalization has been demonstrated to be a highly efficient way to synthesize polymers with controlled MW and desired end group functionality for subsequent modifications.[44-48] Recently, Sumerlin and co-workers reported the synthesis of MMs through the "click" coupling of azido-terminated polymers with propargyl (meth)acrylate with a high degree of end group functionalization.[49] Considering the reported compatibility of ruthenium catalysts with the triazole group resulted from the "click" reaction,[50] we sought to extend this approach to the preparation of a variety of norbornenyl MMs by coupling azido-terminated polymers made by ATRP with alkyne-functionalized norbornene. Herein, we report the facile synthesis of various high MW brush polymers with controlled MW and narrow PDI in both the side chain and the backbone from norbornenyl MMs that were prepared efficiently by ATRP and "click" functionalization.

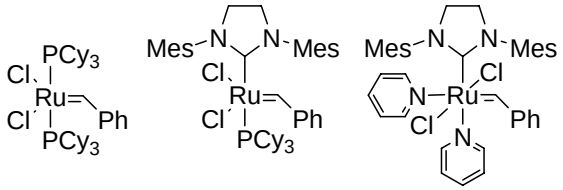

1 **2** **3**

Scheme 1. Ru-based metathesis catalysts.

Results and Discussion

Synthesis of Norbornenyl Macromonomers. Norbornene-based monomers (vs. cyclobutene or cyclooctene-based monomers) were chosen as the reactive group on the MMs due to their high ring strains, commercial availability, and the lack of chain transfer in ROMP. Particularly, *exo*-norbornenes were used in this study because they are known to exhibit significantly higher reactivity than their *endo*-norbornenyl analogs due to reduced steric hindrance at the olefin.[51-53]

To avoid the undesirable copolymerization of norbornene during the preparation of the side chains by ATRP, the norbornenyl functionality was attached to a pre-formed polymer chain end using copper catalyzed azide-alkyne "click" chemistry. *exo*-Norbornene monomer **4** bearing a terminal acetylene group was synthesized by condensation of *exo*-norbornene anhydride with 10-amino-1-decanol, followed by esterification with propargylacetic acid mediated by EDC/DMAP (Scheme 2). Both reactions gave clean products in good yields. The long alkyl spacer between norbornene and acetylene is designed to reduce the steric congestion during the ROMP of MMs.

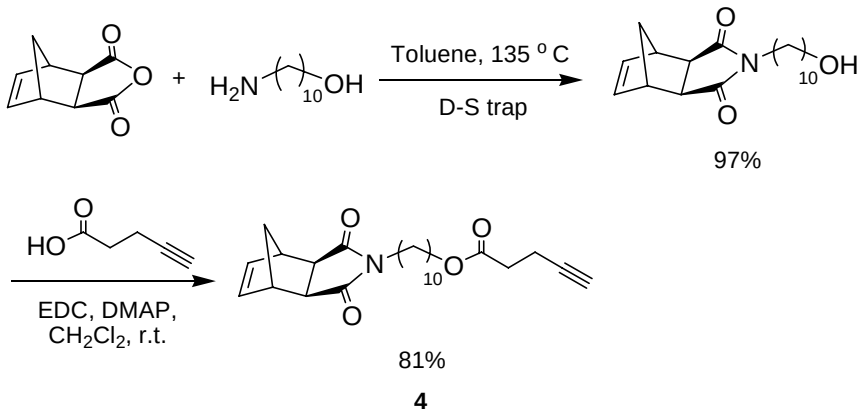

4

Scheme 2. Synthesis of monomer **4**.

ATRP of methyl acrylate (MA), *tert*-butyl acrylate (*t*BA) and styrene (St) were conducted using a CuBr/PMDETA catalytic system to produce a variety of side chain polymers with different MWs and functionalities. Polymerizations were stopped before 70% conversion was reached to retain the bromine chain-end functionality. Narrowly dispersed polymers were obtained in all cases, and their bromine end groups were subsequently transformed to azides quantitatively through nucleophilic substitution reaction with NaN_3 in DMF (Figure 1). Absolute polymer MWs were measured using GPC coupled with a multiangle laser light scattering (MALLS) detector (Table 1).

Next, the azido-terminated polymers were coupled with a stoichiometric amount of norbornene monomer **4** in THF at 50 ºC in the presence of a catalytic amount of CuBr with PMDETA as the ligand (Scheme 3). Regardless of the type of polymer or the MW, all ATRP polymers were furnished with norbornene end group quantitatively without the need for excess **4**. ^{1}H NMR spectroscopy clearly showed the end group transformation. When the terminal azide group was transformed to a triazole ring, the ω-terminal methine proton (H_a) resonance of the pre-polymer completely shifted from 3.9-4.0 ppm to 4.9-5.1 ppm for PS and from 3.7-3.8 ppm to 5.1-5.3 ppm for PMA and P*t*BA, respectively.

Concomitant appearance of signals from the norbornenyl moiety also confirmed that the desired reaction had taken place (Figure 1). The newly formed triazole proton was also observed to resonate at 7.4-7.5 ppm for PMA and P*t*BA, but was overlapped with broad aromatic proton signals in the case of PS. Integrations of norbornenyl olefin peak (H_e at 6.25 ppm) and the ω-terminal methine proton (H_a) peak gave a 2:1 ratio, indicating complete "click" coupling. Furthermore, the integrations of norbornenyl olefin and polymer backbone signals were compared to calculate the DP of the polymer. The DPs calculated by ^{1}H NMR spectroscopy (DP_{NMR}) were in good agreement with the DPs calculated by MALLS-GPC (DP_{GPC}), indicating an overall high degree of end group functionalization of these polymers (Table 1). Furthermore, the GPC peak shape of the pre-polymer and its corresponding MM remained unchanged. Interestingly, a difference in elution time of the GPC trace before and after "click" coupling could also be observed for smaller MMs (i.e., NB-PS, M_n = 2.2 kDa). The difference in their elution times may reflect the effect of the relatively large substituted norbornenyl end group (MW = 399.2 Da) on the size of the polymer coil.

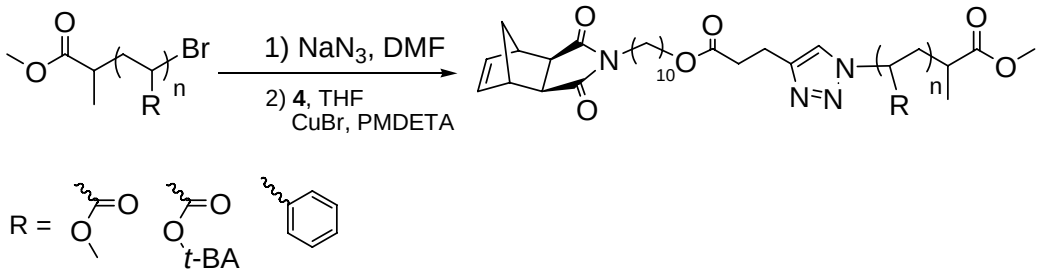

Scheme 3. Synthesis of macromonomers.

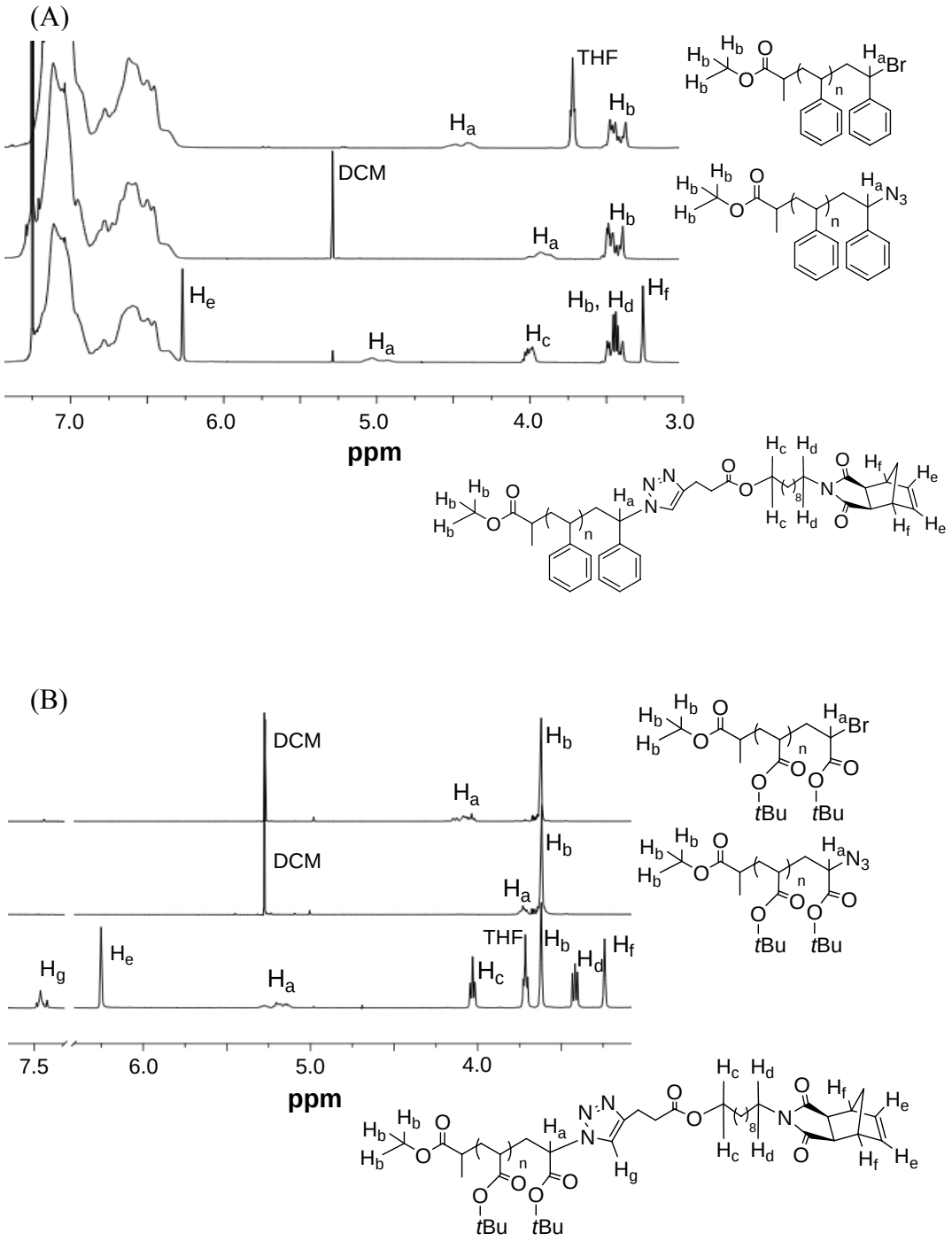

Figure 1. ^{1}H NMR spectra of end group transformations: (A) PS-Br (top), PS-N_3 (middle), NB(PS)2.2k (bottom); (B) P*t*BA-Br (top), PS-N_3 (middle), NB(P*t*BA)4.7k (bottom).

Table 1. Characteristics of ω-norbornenyl macromonomers

Sample name[a]	Polymer type	$M_{n,GPC}$[b] (kDa)	DP_{GPC}[c]	DP_{NMR}[d]	PDI[b]
NB(PMA)3.7k	PMA	3.7	38	36	1.03
NB(P*t*BA)4.7k	P*t*BA	4.7	33	33	1.03
NB(PS)2.2k	PS	2.2	17	19	1.03
NB(PS)6.6k	PS	6.6	60	66	1.02

[a]Macromonomers were named using a format of NB(X)Y, with X designating the type of pre-polymer and Y designating the M_n of macromonomer. [b]Determined by GPC in THF using RI and MALLS detectors. [c]Calculated by ($M_{n,GPC}$ − molar mass of **4** (399.2 Da)) / molar mass of monomer. [d]Calculated by comparing the integrations of norbornenyl olefin and polymer backbone proton signals from ^{1}H NMR spectra in $CDCl_3$.

ROMP of Macromonomers. We first investigated the ROMP of P*t*BA-macromonomer (P*t*BA-MM) as the *tert*-butyl group can be readily hydrolyzed to yield water soluble poly(acrylic acid) side chains, which can be used as polyelectrolytes and biomaterials, or further modified.[10] NB(P*t*BA)4.7k was dissolved in THF at 0.05 M, and catalyst **3** was injected from a stock solution at different MM to catalyst ratios ([M/C]) at room temperature. The solution became more viscous within a few minutes, and aliquots were withdrawn from the polymerization solutions at different time intervals and terminated immediately with excess vinyl ether. GPC analyses of the aliquots all showed narrow and monomodal peaks for the polyMM, and the MW increased linearly with conversion. The PDIs remained very low throughout the polymerization. Clean first-order kinetics were also observed from the linear logarithmic plots of conversion vs time ($\ln[M]_0/[M]_t$ vs time), indicating a constant concentration of propagating species (Figure 2). The polymerization rates measured by the slopes in the kinetic plot were also proportional to the catalyst loading (Figure 2C). The first-order kinetics and linear MW growth profile

both suggest that the living nature of ROMP was maintained even for MMs with large MWs. Moreover, very high conversions (>90%) were achieved within 5 min for [M/C] = 50 and within 20 min for [M/C] = 200 at room temperature, further revealing the extraordinary activity of catalyst **3**. Longer reaction times resulted in almost quantitative conversion (>97%) of MMs to brush polymers, while PDIs remained very low (≤1.02).

(A)

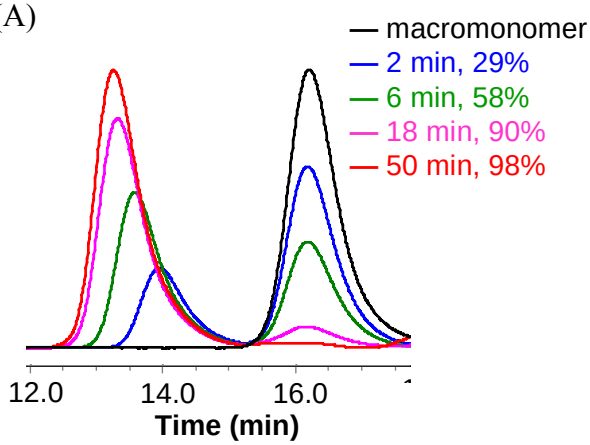

(B)

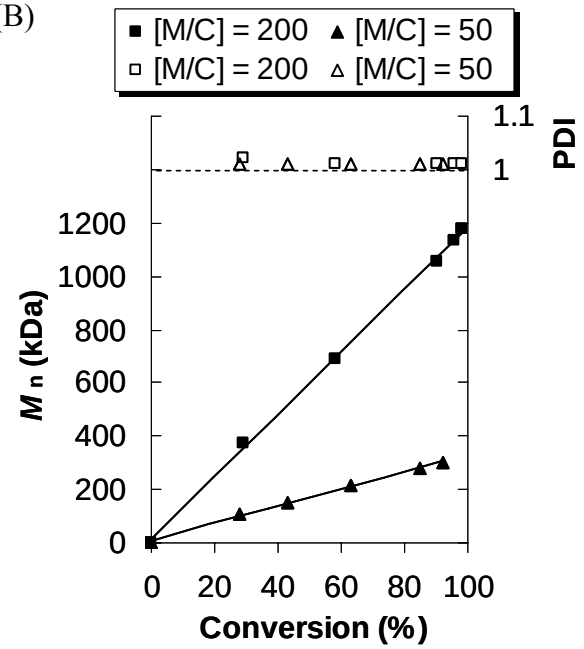

(C)

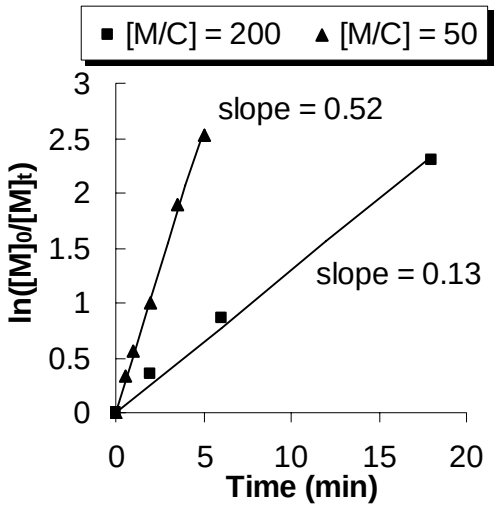

Figure 2. (A) Evolution of GPC traces during ROMP of NB(P*t*BA)4.7k; (B) Dependence of M_n and PDI on MM conversion, and (C) dependence of $\ln([M]_0/[M]_t)$ on time. Conditions: $[M]_0 = 0.05$ M in THF at room temperature.

The MW of the brush polymer, PNB-*g*-P*t*BA, could be controlled by the [M/C] ratio and was slightly higher than the theoretical values, especially when high [M/C] ratios were used. However, the MW was still proportional to the [M/C] ratio (Entry 1-4 in Table 2). GPC traces of the brush polymers obtained at different [M/C] ratios showed a consistent shift toward high MW as increasing the [M/C] ratio, while the peak remained as narrowly dispersed as the macromonomer (Figure 3).

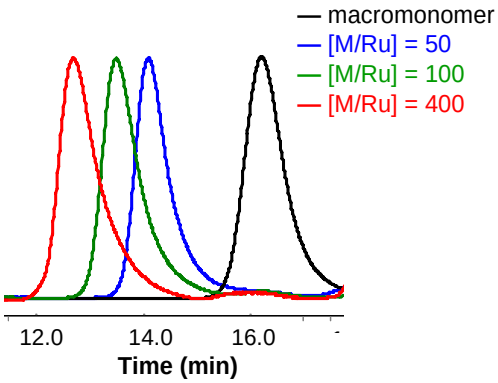

Figure 3. GPC traces of macromonomer NB(P*t*BA)4.7k (black) and crude brush polymers PNB-*g*-P*t*BA obtained at [M/C] = 50 (blue), 100 (green), and 400 (red). Conditions: $[M]_0 = 0.05$ M in THF at room temperature.

All other types of MMs were polymerized similarly using catalyst **3** at varying [M/C] ratios with olefin concentrations of 0.05 – 0.1 M in THF at room temperature (Scheme 4). As shown in Table 2, all of the brush polymers obtained had very narrow PDIs between 1.0 and 1.1 up to MWs of over 2000 kDa, regardless of the MW, functionality, and conversion of the MMs. The very low PDIs of these brush polymers are likely a result of the narrowly dispersed side chains and the highly efficient polymerization of MMs, leading to complete grafting coverage on the polymer backbone. Conversions of MMs to brush polymers were very high (i.e., >90%) in most cases and only weak residual MM peaks were noticeable by GPC. Conversions decreased slightly with increasing [M/C] ratios and increasing MWs of the MMs. However, the small amount of residual MMs can be easily removed simply through precipitation of the polymer solutions into selective solvents due to the large difference in MW between MMs and brush polymers.

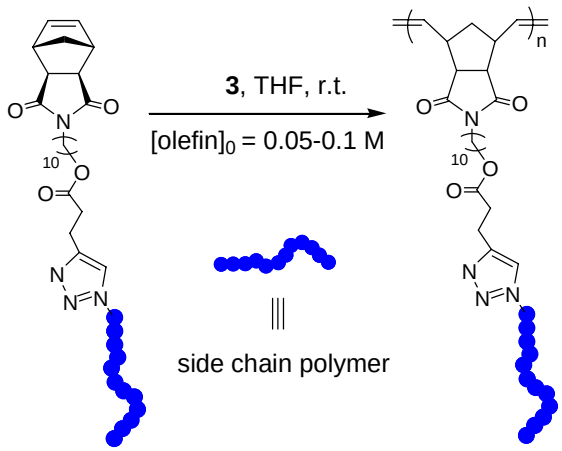

Scheme 4. Synthesis of polymacromonomer from ω-norbornenyl MM.

Table 2. ROMP of macromonomers using catalyst 3

Entry	Macromonomer	[M/C][a]	$M_{n,\ theo}$ (kDa)[b]	$M_{n,\ GPC}$ (kDa)[c]	PDI[c]	DP_{GPC}[d]	Conversion[e]
1	**NB(P*t*BA)4.7k**	50	230	267	1.02	57	98%
2	**NB(P*t*BA)4.7k**	100	461	647	1.01	137	98%
3	**NB(P*t*BA)4.7k**	200	921	1140	1.01	242	98%
4	**NB(P*t*BA)4.7k**	400	1 842	2 620	1.03	557	97%
5	**NB(PMA)3.7k**	50	176	202	1.02	55	95%
6	**NB(PMA)3.7k**	100	348	420	1.02	114	94%
7	**NB(PMA)3.7k**	200	703	891	1.03	241	95%
8	**NB(PMA)3.7k**	400	1 287	1 687	1.05	456	87%
9	**NB(PS)2.2k**	100	210	231	1.02	105	93%
10	**NB(PS)2.2k**	200	427	534	1.03	243	97%
11	**NB(PS)2.2k**	400	836	1271	1.07	578	95%
12	**NB(PS)6.6k**	50	330	348	1.01	53	93%
13	**NB(PS)6.6k**	100	607	701	1.01	106	92%
14	**NB(PS)6.6k**	200	1 162	1 478	1.02	224	88%

[a]MM to catalyst **3** ratio. [b]$M_{n,\ theo} = M_{n,\ GPC}$ (MM) x [M/C] x conversion. [c]Determined by GPC in THF using RI and MALLS detectors. [d]DP of brush polymer = $M_{n,\ GPC}$ (brush polymer)/$M_{n,\ GPC}$ (MM). [e]Conversion of MM to brush polymer is determined by comparing the peak areas of brush polymer and residual MM from GPC measurement of the crude product.

Some of the MMs were polymerized using cyclic catalysts. Due to the relatively low activity, catalysts with unsaturated NHC backbone (**UC-5** and **UC-6**) did not give measurable amount of brush polymer product by GPC. **SC-5** gave conversions of 43%

and 61% for NB(PS)6.6k and NB(PLA)4.7k, respectively, after 6 h at 55 °C in THF (Table 3). Prolonged heating did not further increase the conversions.

Table 3. REMP of macromonomers using SC-5.

Macromonomer	[M/**SC-5**][a]	$M_{n,\,GPC}$ (kDa)[b]	PDI[b]	Conversion[c]
NB(PS)6.6k	50	10 200	1.06[d]	43%
NB(PLA)4.7k	50	7 440	1.42	61%

[a]MM to catalyst **3** ratio, 55 °C in THF. [b]Determined by GPC in THF using RI and MALLS detectors. Only the brush polymer peak was selected to determine the PDI. [c]Conversion of MM to brush polymer is determined by comparing the peak areas of brush polymer and residual MM from GPC measurement of the crude product. [d]The artificially low PDI is because the extremely high MW has exceeded the separable MW range.

AFM of Brush Polymers. We used tapping-mode atomic force microscopy (AFM) to directly visualize individual brush polymers. Visualization of densely grafted brush polymers is facilitated by the large side chains, which prevent coiling of the brush polymer backbone due to the high steric congestion. But individual polymer imaging can be technically challenging: 1) Spin-casting a dilute polymer solution is necessary to disperse individual polymers on the surface for imaging. 2) Favorable polymer-surface interaction is another requirement to have stretched polymers on the surface, otherwise polymers would collapse and coil up to minimize their contact with the surface. 3) Atomically flat surfaces have to be used because as polymer side chains spread on the surface, their thickness is usually only ca. 1 nm. The common commercially available, atomically flat surfaces are highly oriented pyrolytic graphite (HOPG) (for hydrophobic polymers) and mica (for more hydrophilic polymers). The most successful imaging came from the PS grafted polynorbornene (PNB-*g*-PS) with the highest MW (Entry 14 in Table

2) that was spin-cast on HOPG (Figure 4). AFM revealed cylindrical shapes which were expected from the densely grafted nature of the polyMMs. These wormlike polymer brushes also had uniform length and width distributions as a result of their low PDI. Measuring multiple polymer brushes gave an average contour length of 140 nm, a width of 30 nm, and a height of 1 nm. With a backbone DP = 224, the length per monomeric unit, l_m, was calculated to be 0.62 nm. Considering each polynorbornene repeating unit has five backbone carbons, an average two-carbon distance in the polynorbornene brush polymer is 0.25 nm, corresponding to the value for a fully stretched all *trans* -CH_2-CH_2- bond conformation, l_{max}, of 0.25 nm.[5] Therefore, the dimensions of the brush polymers suggest an almost fully extended backbone conformation with side chains stretched and flattened on the surface, presumably as a result of significant steric repulsion of side chains that are grafted on every repeating unit of the backbone.

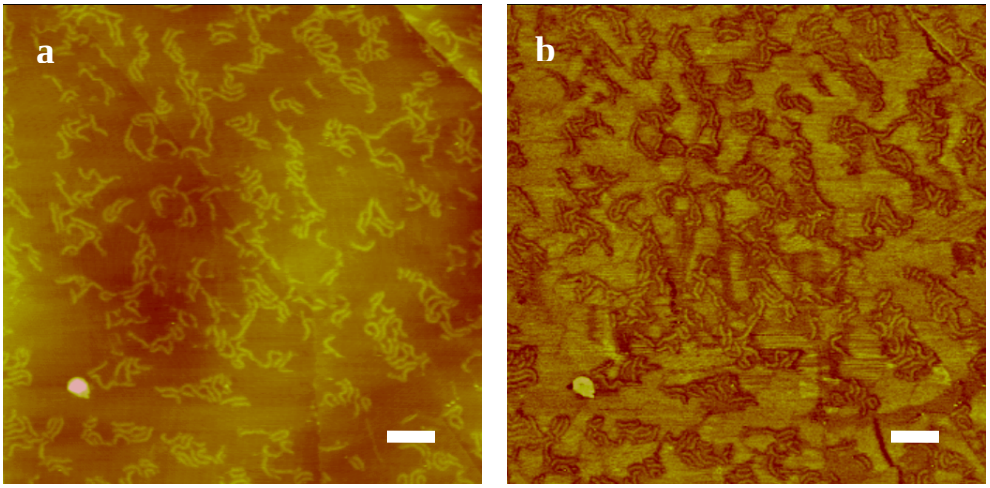

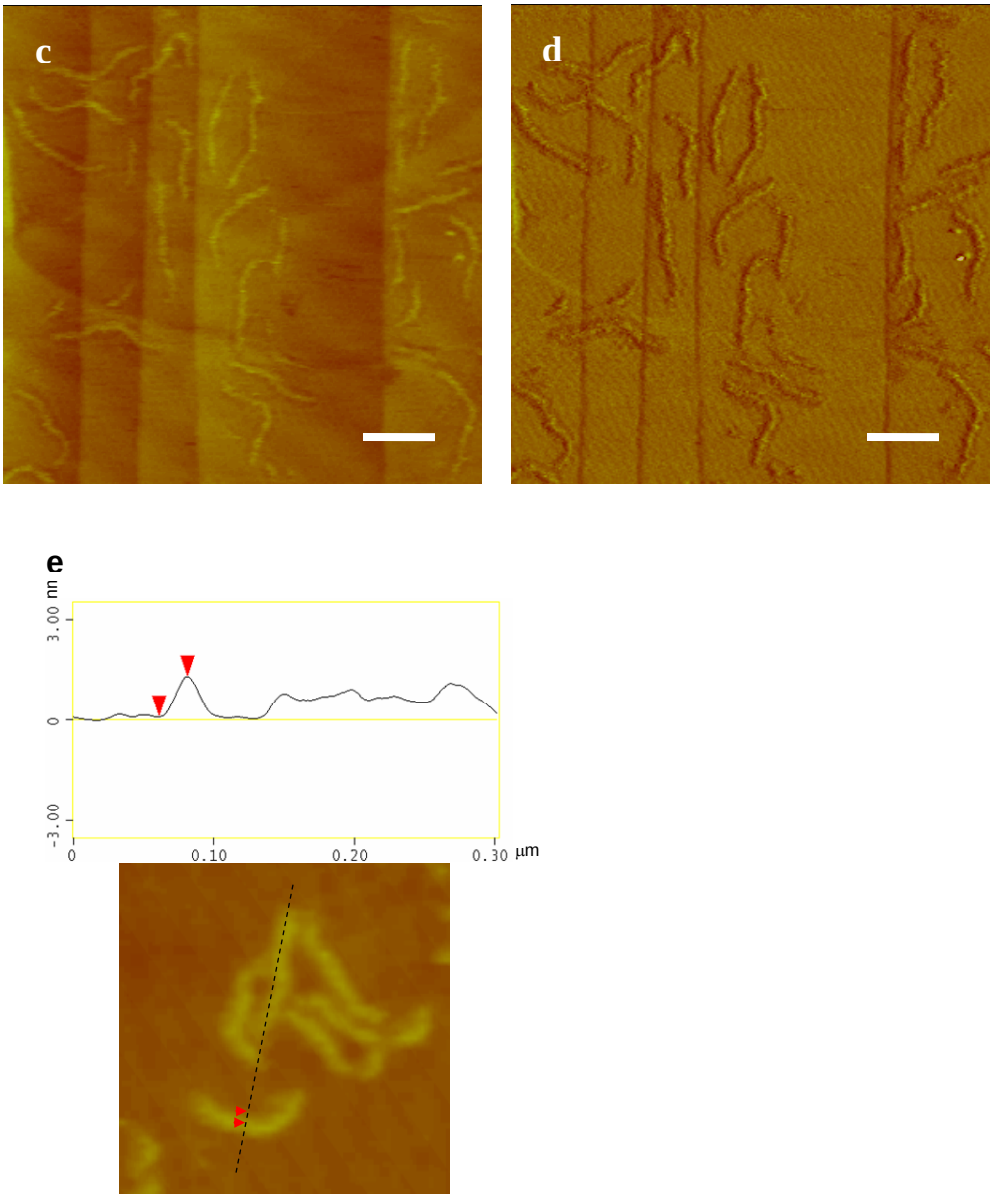

Figure 4. Tapping mode AFM images of brush polymer PNB-*g*-PS (Entry 14 in Table 2) spin-cast from chloroform solution onto HOPG. (a, b) Large scale height and phase images, bar = 300 nm; (c, d) enlarged height and phase images, bar = 100 nm; (e) cross-sectional analysis of an individual polymer brush.

Cyclic PNB-*g*-PS was imaged under the same conditions on HOPG. AFM clearly revealed cyclic structures for some of the brush polymers with open pores as a result of an extended backbone. The cyclic brush polymers had various diameters ranging from 100-300 nm, a reflection of the broad MW distribution of the samples. However, they all

poseesed a uniform width of ~30 nm and a thickness of 1 nm, the same as the linear brush polymers. Unfortunately, linear chain impurities were always observed together with the cyclic structures, and the length of the linear chains varied greatly from 100 nm to >1 μm (Figure 5A). We suspected that a small amount of linear olefin (such as residual monomer from ATRP) in the MM could potentially introduce the linear impurity during ROMP. To test this hypothesis, we synthesized MMs from non-olefinic monomers such as polylactide (PLA) (details on synthesis is in Chapter 5). Brush polymers prepared using NB-PLA and **SC-5** were imaged on freshly cleaved mica by AFM. The imaging quality for these PLA type polymers on mica was generally poor, but both very large cyclic and linear structures (>1 μm in contour length) were again observed (Figure 5B). Therefore, we reasoned that it was not the residual olefin monomer that introduced linear impurity.

There are other possible sources of linear polymer contamination: 1) catalyst decomposition during REMP of MMs; 2) metallocycle opening during REMP due to the highly strained brush polymer backbone; 3) opening of the cyclic polymers by carbon-carbon bond cleavage due to the shear force during spin coating or the surface tension on AFM substrates during imaging. Sheiko, Matyjaszewski, and co-workers reported surface tension-induced degradation of P*n*BA brush polymers, especially for those with long side chains ($DP_{side\ chain}$ = 140).[55,56] This bond cleavage was attributed to the attractive interaction between the spreading side chains and the substrate, which in turn induces tension along the polymer backbone. Any single chain rupture event on cyclic brush polymers will lead to the formation of linear chains. Whether the chain rupture

accounts, to some degree, for the linear contamination and what effect the side chain length has on the cyclic polymer purity warrant detailed investigation in the future.

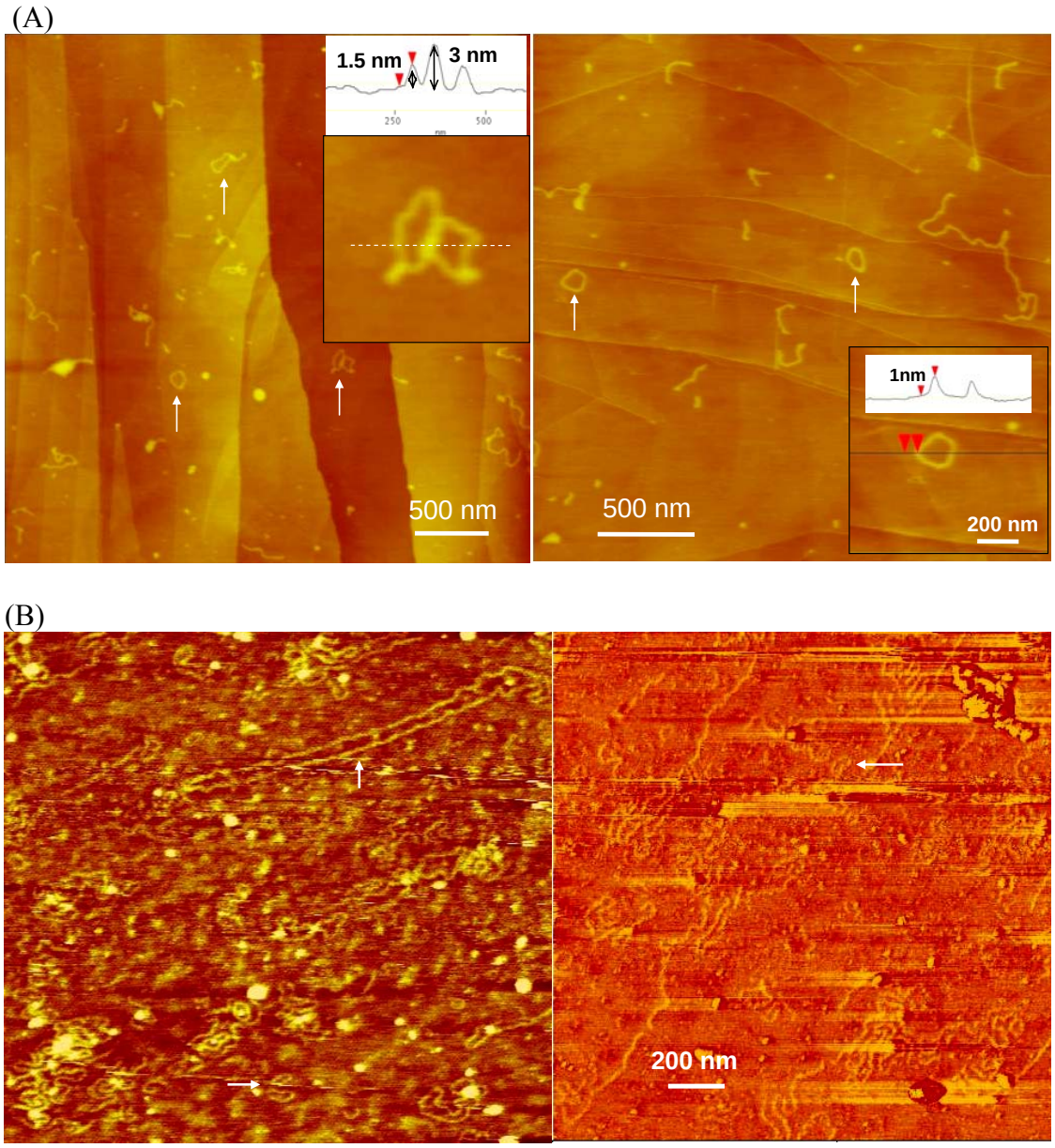

Figure 5. Tapping mode AFM images of cyclic brush polymers (A) PNB-*g*-PS (Entry 1 in Table 3) on HOPG and (B) PNB-*g*-PLA (Entry 2 in Table 3) on mica.

Conclusions

We have efficiently synthesized a series of MMs by "click" coupling of narrowly dispersed azido-terminated pre-polymers with propargyl norbornene. The ROMP of MMs using pyridine-containing ruthenium catalyst **3** has been found to be a general and highly efficient "grafting through" route for the synthesis of a variety of narrowly dispersed brush polymers. The ROMP of MMs exhibited first-order kinetics with respect to the MM concentration up to almost quantitative conversions (>95%) of MMs. MWs of brush polymers increased linearly with MM conversions and were approximately proportional to the ratios of MM to catalyst. Because of the high efficiency, easy experimental procedure, high functional group tolerance of the reported modular approach involving ROMP and "click" chemistry, it allows facile access to a variety of well-defined brush polymers with a broad range of functionalities and MWs.

Experimental Section

Materials. THF was purified by passing through solvent purification columns. $(H_2IMes)(pyr)_2(Cl)_2RuCHPh$ (**3**) was prepared according to a literature procedure.[54] *cis*-5-norbornene-*exo*-2,3-dicarboxylic anhydride was prepared as described previously.[37] St, MA, and *t*-BA were passed through a column of basic alumina immediately before use. All other materials were obtained from commercial sources and used as received. Azido-terminated pre-polymers, PMA (M_n = 3 270 g/mol and PDI = 1.03), P*t*BA (M_n = 4 100 g/mol and PDI = 1.03), and PS (M_n = 1 800 g/mol and PDI = 1.03; M_n = 6 200 g/mol and PDI = 1.03) were synthesized according to literature procedures.[16,49]

Characterizations. ^{1}H and ^{13}C NMR spectra were recorded in $CDCl_3$ using a Varian Mercury 300 or Varian Inova 500 spectrometer. Chemical shifts are reported in ppm relative to $CDCl_3$ ($\delta = 7.27$).

High-resolution mass spectra (FAB) were provided by California Institute of Technology Mass Spectrometry Facility.

Gel permeation chromatography (GPC) was carried out in THF on two PLgel 10 μm mixed-B LS columns (Polymer Laboratories) connected in series with a DAWN EOS multiangle laser light scattering (MALLS) detector and an Optilab DSP differential refractometer (both from Wyatt Technology). No calibration standards were used, and d*n*/d*c* values were obtained for each injection by assuming 100% mass elution from the columns.

Atomic Force Microscopy (AFM) images were taken using a Nanoscope IV Scanning Probe Microscope Controller (Digital Instruments, Veeco Metrology Group) in tapping mode in air at room temperature using silicon tips (spring constant = 40-50 N/m, resonance frequency = 170-190 kHz, and tip radius of curvature <10 nm). The samples were prepared by spin casting dilute solutions (0.01 wt%) in chloroform onto freshly cleaved highly oriented pyrolytic graphite.

***N*-(hydroxydecanyl)-*cis*-5-norbornene-*exo*-2,3-dicarboximide.**

A round-bottom flask was charged with *cis*-5-norbornene-exo-2,3-dicarboxylic anhydride (0.95 g, 5.8 mmol) and 10-amino-1-decanol (1.0 g, 5.8 mmol). To the flask was added 20 mL toluene, followed by triethylamine (80 μL, 0.58 mmol). A homogeneous solution was obtained upon heating. A Dean-Stark trap was attached to the flask, and the reaction mixture was heated at reflux (135 ºC) for 4 h. The reaction mixture was then cooled and

concentrated *in vacuo* to yield an off-white solid. This residue was dissolved in 20 mL CH_2Cl_2 and washed with 0.1 N HCl (10 mL) and brine (10 mL). The organic layer was dried over $MgSO_4$ and concentrated *in vacuo* to yield 1.8 g colorless, viscous oil (97% yield). ^{1}H NMR (500 MHz, $CDCl_3$): δ 1.20-1.28 (m, 13H), 1.49-1.56 (m, 5H), 2.65 (d, J = 1.5 Hz, 2H), 3.26 (t, J = 1.5 Hz, 2H), 3.44 (t, J = 7.5 Hz, 2H), 3.62 (t, J = 6.5 Hz, 2H), 6.27 (t, J = 2.0 Hz, 2H). ^{13}C NMR (125 MHz, $CDCl_3$): δ 25.9, 27.1, 27.9, 29.3, 29.5, 29.5, 29.6, 33.0, 39.0, 42.9, 45.4, 48.0, 63.3, 138.1, 178.4. HRMS (FAB+) *m/z* calcd for $C_{19}H_{30}O_3N$ $[M+H]^+$: 320.2226, found 320.2238.

***N*-(pentynoyl decanyl)-*cis*-5-norbornene-*exo*-2,3-dicarboximide 4.**

To a round-bottom flask was added N-(hydroxydecanyl)-*cis*-5-norbornene-exo-2,3-dicarboximide (0.80 g, 2.5 mmol), N-(3-dimethylaminopropyl)-N'-ethylcarbodiimide hydrochloride (EDC) (0.58 g, 3.0 mmol) and 4-dimethylaminopyridine (DMAP) (0.10 g, 0.82 mmol), followed by 10 mL CH_2Cl_2. Pentynoic acid (0.25 g, 2.5 mmol) was added as a solution in 5 mL CH_2Cl_2 via syringe. The reaction mixture was allowed to stir under argon at room temperature overnight. The reaction mixture was washed with water (2x20 mL) and brine (20 mL) and dried over $MgSO_4$. The solvent was evaporated and the remaining residual was purified by silica gel chromatography (ethyl acetate/hexanes, 3:7 v/v) to give 0.81 g **4** as a colorless oil (81% yield). ^{1}H NMR (500 MHz, $CDCl_3$): δ 1.22-1.33 (m, 13H), 1.50-1.55 (m, 3H), 1.62 (t, J = 7.5 Hz, 2H), 1.98 (t, J = 2.5 Hz, 1H), 2.17-2.56 (m, 4H), 2.67 (d, J = 1.5 Hz, 2H), 3.27 (t, J = 1.5 Hz, 2H), 3.45 (t, J = 7.5 Hz, 2H), 4.09 (t, J = 7 Hz, 2H), 6.28 (t, J = 2.0 Hz, 2H)1H). ^{13}C NMR (125 MHz, $CDCl_3$): δ 14.6, 26.1, 27.2, 28.0, 28.8, 29.3, 29.4, 29.5, 29.6, 33.6, 39.0, 42.9, 45.4, 48.0, 65.1, 69.2, 82.8,

138.1, 172.1, 178.4. HRMS (FAB+) *m/z* calcd for $C_{24}H_{34}O_4N$ $[M+H]^+$: 400.2488, found 400.2505.

General procedure for synthesis of macromonomers via "click" coupling of pre-polymer and 4. In a typical experiment, to a 20 mL scintillation vial was added 1 g azido-terminated pre-polymer, the desired amount of **4** (1 eq. to pre-polymer end group) and CuBr (0.1 eq to **4**), and a stir bar. The vial was then degassed and 10 mL degassed anhydrous THF was added via syringe under an argon atmosphere. PMDETA (1 eq to CuBr) was injected via a microsyringe. The reaction vial was stirred at 50 ºC under argon overnight. The reaction mixture was then passed through a short neutral alumina column to remove the catalyst. The resulting macromonomers were isolated by precipitation into MeOH for NB-PS or by removal of the solvent under high vacuum for NB-P*t*BA.

General procedure for ROMP of macromonomers. In a typical experiment, an oven-dried small vial was charged with 100 mg macromonomer and a stir bar. The vial was then degassed, and the desired amount of degassed, anhydrous THF ($[M]_0$ = 0.05-0.10 M) was added via syringe under an argon atmosphere to dissolve the macromonomer. A stock solution of catalyst **3** in degassed, anhydrous THF was prepared in a separate vial. The desired amount of catalyst was injected into the macromonomer solution to initiate the polymerization. The reaction vial was stirred at room temperature under argon. After the polymerization was complete, the reaction mixture was quenched with one drop of ethyl vinyl ether. A small sample was withdrawn for GPC measurement. The rest of the reaction mixture was then diluted and precipitated into 10 mL stirring MeOH for PNB-*g*-(PS) and PNB-*g*-(PMA) and MeOH/water (4:1) for PNB-*g*-(P*t*BA). Trace amount of residual macromonomer can be readily removed via precipitation into MeOH,

MeOH/water (4:1), and cyclohexane/heptane (1:2) for PNB-*g*-(PMA), PNB-*g*-(P*t*BA), and PNB-*g*-(PS) respectively. The resulting brush polymers were dried *in vacuo*.

References

(1) Percec, V.; Ahn, C. H.; Ungar, G.; Yeardley, D. J. P.; Moller, M.; Sheiko, S. S. *Nature* **1998**, *391*, 161-164.

(2) Hadjichristidis, N. P., M.; Pispas, S.; Iatrou, H. *Chem. Rev.* **2001**, *101*, 3747.

(3) Zhang, M.; Müller, A. H. E. *J. Polym. Sci., Part A: Polym. Chem.* **2005**, *43*, 3461-3481.

(4) Wintermantel, M.; Gerle, M.; Fischer, K.; Schmidt, M.; Wataoka, I.; Urakawa, H.; Kajiwara, K.; Tsukahara, Y. *Macromolecules* **1996**, *29*, 978-983.

(5) Sheiko, S. S.; Möller, M. *Chem. Rev.* **2001**, *101*, 4099-4124.

(6) Beers, K. L.; Gaynor, S. G.; Matyjaszewski, K.; Sheiko, S. S.; Möller, M. *Macromolecules* **1998**, *31*, 9413-9415.

(7) Börner, H. G.; Beers, K.; Matyjaszewski, K.; Sheiko, S. S.; Möller, M. *Macromolecules* **2001**, *34*, 4375-4383.

(8) Cheng, G.; Böker, A.; Zhang, M.; Krausch, G.; Müller, A. H. E. *Macromolecules* **2001**, *34*, 6883.

(9) Zhang, M.; Breiner, T.; Mori, H.; Müller, A. H. E. *Polymer* **2003**, *44*, 1449-1458.

(10) Kriegel, R. M.; Rees, W. S.; Weck, M. *Macromolecules* **2004**, *37*, 6644-6649.

(11) Runge, M. B.; Dutta, S.; Bowden, N. B. *Macromolecules* **2006**, *39*, 498-508.

(12) Neugebauer, D.; Sumerlin, B. S.; Matyjaszewski, K.; Goodhart, B.; Sheiko, S. S. *Polymer* **2004**, *45*, 8173-8179.

(13) Sumerlin, B. S.; Neugebauer, D.; Matyjaszewski, K. *Macromolecules* **2005**, *38*, 702-708.

(14) Deffieux, A.; Schappacher, M. *Macromolecules* **1999**, *32*, 1797-1802.

(15) Schappacher, M.; Deffieux, A. *Macromolecules* **2005**, *38*, 7209-7213.

(16) Gao, H.; Matyjaszewski, K. *J. Am. Chem. Soc.* **2007**, *129*, 6633-6639.

(17) Schappacher, M.; Deffieux, A. *Science* **2008**, *319*, 1512-1515.

(18) Tsukahara, Y. M., K.;Segawa, A.;Yamashita, Y. *Macromolecules* **1989**, *22*, 1546-1552.

(19) Tsukahara, Y. T., K.;Yamashita, Y.;Shimada, S. *Macromolecules* **1990**, *23*, 5201-5208.

(20) Dziezok, P.; Sheiko, S. S.; Fischer, K.; Schmidt, M.; Möller, M. *Angew. Chem. Int. Ed.* **1997**, *36*, 2812-2815.

(21) Neiser, M. W.; Okuda, J.; Schmidt, M. *Macromolecules* **2003**, *36*, 5437-5439.

(22) Neiser, M. W.; Muth, S.; Kolb, U.; Harris, J. R.; Okuda, J.; Schmidt, M. *Angew. Chem. Int. Ed.* **2004**, *43*, 3192-3195.

(23) Yamada, K.; Miyazaki, M.; Ohno, K.; Fukuda, T.; Minoda, M. *Macromolecules* **1999**, *32*, 290-293.

(24) Pantazis, D.; Chalari, I.; Hadjichristidis, N. *Macromolecules* **2003**, *36*, 3783-3785.

(25) Heroguez, V.; Breunig, S.; Gnanou, Y.; Fontanille, M. *Macromolecules* **1996**, *29*, 4459-4464.

(26) Heroguez, V.; Gnanou, Y.; Fontanille, M. *Macromolecules* **1997**, *30*, 4791-4798.

(27) Heroguez, V.; Amedro, E.; Grande, D.; Fontanille, M.; Gnanou, Y. *Macromolecules* **2000**, *33*, 7241-7248.

(28) Nomura, K.; Takahashi, S.; Imanishi, Y. *Polymer* **2000**, *41*, 4345-4350.

(29) Nomura, K.; Takahashi, S.; Imanishi, Y. *Macromolecules* **2001**, *34*, 4712-4723.

(30) Murphy, J. J.; Nomura, K. *Chem. Commun.* **2005**, 4080-4082.

(31) Liaw, D.-J.; Huang, C.-C.; Ju, J.-Y. *J. Polym. Sci., Part A: Polym. Chem.* **2006**, *44*, 3382-3392.

(32) Hilf, S.; Kilbinger, A. F. M. *Macromol. Rapid Comm.* **2007**, *28*, 1225-1230.

(33) Jha, S.; Dutta, S.; Bowden, N. B. *Macromolecules* **2004**, *37*, 4365-4374.

(34) Bielawski, C. W.; Grubbs, R. H. *Angew. Chem. Int. Ed.* **2000**, *39*, 2903-2906.

(35) Choi, T.-L.; Grubbs, R. H. *Angew. Chem. Int. Ed.* **2003**, *42*, 1743-1746.

(36) Camm, K. D.; Castro, N. M.; Liu, Y.; Czechura, P.; Snelgrove, J. L.; Fogg, D. E. *J. Am. Chem. Soc.* **2007**, *129*, 4168-4169.

(37) Matson, J. B.; Grubbs, R. H. *J. Am. Chem. Soc.* **2008**, *130*, 6731-6733.

(38) Rajaram, S.; Choi, T.-L.; Rolandi, M.; Fréchet, J. M. J. *J. Am. Chem. Soc.* **2007**, *129*, 9619-9621.

(39) Hawker, C. J.; Bosman, A. W.; Harth, E. *Chem. Rev.* **2001**, *101*, 3661-3688.

(40) Matyjaszewski, K.; Xia, J. *Chem. Rev.* **2001**, *101*, 2921-2990.

(41) Kamigaito, M.; Ando, T.; Sawamoto, M. *Chem. Rev.* **2001**, *101*, 3689-3746.

(42) Cheng, C.; Khoshdel, E.; Wooley, K. L. *Macromolecules* **2005**, *38*, 9455-9465.

(43) Patton, D. L.; Advincula, R. C. *Macromolecules* **2006**, *39*, 8674-8683.

(44) Gao, H.; Louche, G.; Sumerlin, B. S.; Jahed, N.; Golas, P.; Matyjaszewski, K. *Macromolecules* **2005**, *38*, 8979-8982.

(45) Lutz, J.-F.; Börner, H. G.; Weichenhan, K. *Macromol. Rapid Comm.* **2005**, *26*, 514-518.

(46) Golas, P. L.; Tsarevsky, N. V.; Sumerlin, B. S.; Matyjaszewski, K. *Macromolecules* **2006**, *39*, 6451-6457.

(47) Lutz, J.-F.; Börner, H. G.; Weichenhan, K. *Macromolecules* **2006**, *39*, 6376-6383.

(48) Whittaker, M. R.; Urbani, C. N.; Monteiro, M. J. *J. Am. Chem. Soc.* **2006**, *128*, 11360-11361.

(49) Vogt, A. P.; Sumerlin, B. S. *Macromolecules* **2006**, *39*, 5286-5292.

(50) Binder, W. H.; Kluger, C. *Macromolecules* **2004**, *37*, 9321-9330.

(51) Asrar, J. *Macromolecules* **1992**, *25*, 5150-5156.

(52) Rule, J. D.; Moore, J. S. *Macromolecules* **2002**, *35*, 7878-7882.

(53) Pollino, J. M.; Stubbs, L. P.; Weck, M. *Macromolecules* **2003**, *36*, 2230-2234.

(54) Love, J. A.; Morgan, J. P.; Trnka, T. M.; Grubbs, R. H. *Angew. Chem., Int. Ed.* **2002**, *41*, 4035–4037.

(55) Sheiko, S. S.; Sun, F. C.; Randall, A.; Shirvanyants, D.; Rubinstein, M.; Lee, H.; Matyjaszewski, K. *Nature* **2006**, *40*, 191–194.

(56) Lebedeva, N. V.; Sun, F. C.; Lee, H.; Matyjaszewski, K.; Sheiko, S. S. *J. Am. Chem. Soc.* **2008**, *130*, 4228–4229.

C h a p t e r 5

Efficient Synthesis of Narrowly Dispersed Brush Copolymers and Study of Their Assembly

Portions of this chapter have been published: Xia, Y.; Olsen, B. D.; Kornfield, J. A.; Grubbs, R. H. *J. Am. Chem. Soc.* **2009**, *131*, 18525.

Abstract

Efficient, one-pot preparation of synthetically challenging, high molecular weight (MW), narrowly dispersed brush block copolymers and random copolymers in high conversions was achieved by ring-opening metathesis (co)polymerization (ROMP) of various macromonomers (MMs) using the highly active, fast-initiating ruthenium olefin metathesis catalyst $(H_2IMes)(pyr)_2(Cl)_2RuCHPh$. A series of random and block copolymers were prepared from a pair of MMs containing polylactide (PLA) and poly(*n*-butyl acrylate) (P*n*BA) side chains at similar MWs. Their self-assembly in the melt state was studied by small angle X-ray scattering (SAXS) and atomic force microscopy (AFM). In brush random copolymers containing approximately equal volume fractions of PLA and P*n*BA, the side chains segregate into lamellae with domain spacing of 14 nm as measured by SAXS, which was in good agreement with the lamellar thickness measured by AFM. The domain spacings and order-disorder transition temperatures of brush random copolymers were insensitive to the backbone length. In contrast, brush block copolymers containing approximately equal volume fractions of these MMs self-assembled into highly-ordered lamellae with domain spacing over 100 nm, making the assembly structures photonic crystals.

Introduction

Brush polymers possess an interesting extended conformation due to the high steric crowding from high density sides chains, as discussed in Chapter 4.[1] Their nonspherical macromolecular geometries and lengths up to a few hundred nanometers afforded numerous potential applications in nanoscience, such as molecular actuators,[2] templates for inorganic particles,[3-5] and as precursors for nanocapsules[6], nanotubes[7], and other carbon nanostructures[8].

On the other hand, linear block copolymers have proven to be versatile, powerful tools in the "bottom-up" approach to create nanostructured materials with novel mechanical, optical, and electronic properties and with specific functionalities over the last few decades.[9] When two or more different types of side chains are attached to a linear polymer backbone to form brush copolymers, each side chain may behave like a block segment in a block copolymer: they can be long enough to drive segregation, due to selective solubility or enthalpically favored demixing, yet are constrained by covalent attachment onto a single molecule. The spatial arrangement of different types of side chains along the backbone and their relative ratio should dramatically affect the assembly of the copolymers. The assembly of brush copolymers may also be profoundly affected by the limited flexibility of the brush polymer backbone as a result of the high steric hindrance between densely grafted side chains. On the other hand, the densely grafted side chains and extended conformation of brush polymers give them reduced entanglement density compared to their linear analogs. The reduced entanglement is a favorable feature to overcome the kinetic barrier for self-assembly, especially for ultrahigh MW polymers. Bowden and co-workers and Rzayev have recently found that

brush-coil and brush-brush block copolymers can self-assemble into exceptionally large structures with domain spacing above 100 nm.[10-12] Large domain structures are scientifically attractive and technically important with the potential to create periodic dielectric media to manipulate and control light, but have been challenging to achieve with linear block copolymers.[13-16] However, self-assembly of brush copolymers has been much less explored relative to the vast number of reports on their linear copolymer analogs.[10-12,17-18]

Well-defined macromolecular characteristics, such as the lengths of the backbone and side chains as well as the grafting density, are prerequisites to obtain ordered self-assembled structures. However, due to the complex architectures and demanding steric congestion, brush copolymers with controlled and high MW, low polydispersity (PDI), and complete side chain grafting remain challenging targets for polymer chemists. Current synthetic strategies to approach these targets normally involve multi-step reactions and separations.

The most explored method to make brush polymers is "graft from": the majority of previously reported brush block copolymers were synthesized by polymerizing different monomers from a diblock copolymer backbone using orthogonal polymerization mechanisms (i.e., radical polymerization and ring-opening polymerization).[10-12,19-20] To grow distinct side chains from a given backbone requires orthogonal polymerization mechanisms and/or selective protection/deprotection and subsequent functionalization of the copolymer backbone. Furthermore, the initiation efficiency of the macroinitiators may be limited,[12,21-22] and the monomer conversions must be kept low to avoid crosslinking due to the high density of initiating sites.[2,6-

[8,10-12,19-22] Alternatively, pre-formed side chains can be "grafted onto" a polymer backbone to prepare brush polymers.[23-25] Lanson et al. recently prepared brush block copolymers[23,26] and random copolymers[18] by grafting anionically prepared side chains onto polymers with pendent functional groups and by a combination of "graft from" and "graft onto" methods. However, purification to remove the unreacted side chains was required in each grafting step and repetitive protection and deprotection of the backbone functional groups was required to synthesize brush block copolymers.

On the other hand, the macromonomer (MM) approach toward brush copolymers is highly desirable,[27] because 1) it does not require orthogonal, non-interfering chemistry for grafting different side chains; 2) the side chain and the graft polymer can be well characterized; and 3) it is the only approach that guarantees complete grafting on every repeating unit. However, the macromonomer (MM) approach toward brush block copolymers is exceedingly challenging due to steric hindrance at the propagating polyMM chain end. Brush-coil block copolymers and brush random copolymers have been reported using uncontrolled metallocene-catalyzed[17] or radical[28] polymerizations and polycondensation[29] of MMs. As a result, the final graft polymers were polydisperse, and the MM conversion was limited. Neugebauer et al. reported copolymerization of MMs containing poly(ethylene oxide) and poly(dimethylsiloxane) or octadecane side chains by atom transfer radical polymerization (ATRP) to produce random or gradient brush copolymers depending on the relative polymerization rates of MMs.[30-31] However, the MMs used in those reports were relatively small and less hindered (MW≤1100) and no brush block copolymers were reported.

Chapter 4 described the highly efficient syntheses we developed for a variety of ultrahigh MW brush polymers with controlled MW (up to 2600 kg/mol) and very low PDI (1.01-1.07) using the highly active, fast-initiating Ru olefin metathesis catalyst $(H_2IMes)(pyr)_2(Cl)_2RuCHPh$ (**1**). Atomic force microscopy (AFM) revealed their rigid, wormlike structure and narrow PDI.[34]

In this chapter, we utilized ROMP of MMs to efficiently prepare a library of high MW, narrowly dispersed brush copolymers with different side chains, including brush block copolymers and brush random copolymers, each in one pot. ROMP of MMs allowed for facile control of the side chain and backbone block lengths and virtually arbitrary selection of side chains. In contrast to prior reports of ROMP synthesis of short graft block copolymers using molybdenum-based catalyst that were limited to oligomers with 5-10 side chains per "block" (starlike rather than brushlike architectures),[32,33] the present polymers have DP up to 200 per block. To the best of our knowledge, this report contains the first examples of high MW, narrowly dispersed brush block copolymers prepared sequentially via living polymerization of MMs.[35] The well-defined molecular characteristics of these brush copolymers provided an excellent model system to study the effect of side chain arrangement on the backbone and the relative ratio of the MMs on the self-assembly of brush copolymers. Specifically, we compared brush block copolymers (Figure 1 top) to brush random copolymers (Figure 1 bottom), showing that they provide convenient routes to self-assembled nanostructures with the backbone either predominantly orthogonal to the "intermaterial dividing surface"[36] or localized to the "intermaterial dividing surface," respectively.

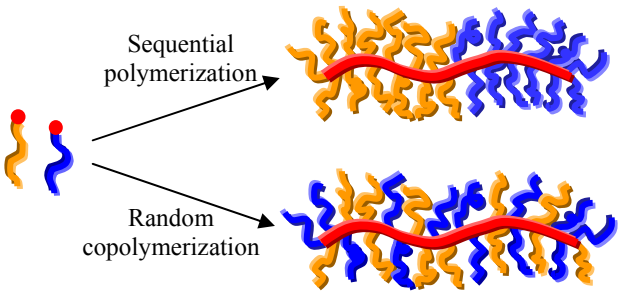

Figure 1. Schematic illustration of the synthesis of brush block copolymer through sequential addition (top) and brush random copolymer through random copolymerization (bottom) of MMs.

Results and Discussion

Syntheses of Brush Copolymers. We have synthesized ω-norbornenyl MMs containing poly(*n*-butyl acrylate) (P*n*BA), poly(*t*-butyl acrylate) (P*t*BA), and polystyrene (PS) side chains, as described in Chapter 4.[34] "Click" coupling of a norbornenyl group to the chain ends of polymers made by ATRP was used to prevent the unfavorable copolymerization of norbornene during ATRP.[37-38] ω-Norbornenyl MMs containing polylactide (PLA) side chains were also synthesized from ring-opening polymerization of D,L-lactide using a norbornenyl alcohol as the initiator and stannous octoate as the polymerization catalyst (Scheme 1). All MMs were narrowly dispersed. A high degree of norbornenyl end group functionalization was confirmed from good agreement between the degree of polymerization (DP) calculated by end group analysis using ^{1}H NMR spectroscopy (DP_{NMR}) and the DP calculated from the absolute MWs obtained from gel permeation chromatography (GPC) coupled with a multiangle laser light scattering (MALLS) detector (Table 1).

Scheme 1. Synthesis of macromonomers.[a]

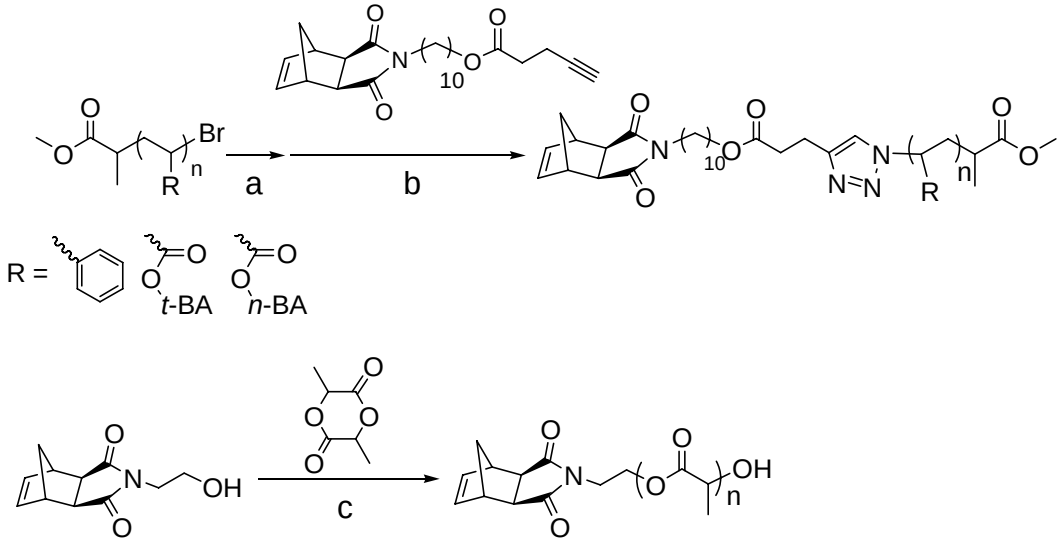

[a]Conditions: (a) NaN_3, DMF, 25 °C. (b) CuBr, PMDETA, THF, 50 °C. (c) $Sn[CH_3(CH_2)_3CH(C_2H_5)CO_2]_2$, 120 °C.

Table 1. Characteristics of *ω*-norbornenyl macromonomers and their polymerization rates

MM[a]	M_n[b] (kDa)	PDI[b]	DP_{NMR}[c]	DP_{GPC}[d]	k_p (min^{-1})[e]	$k_{p,rel}$[f]
NB(PS)6.6k	6.6	1.02	66	60	0.079	1
NB(PS)2.2k	2.2	1.03	19	17	0.092	1.2
NB(P*t*BA)4.7k	4.7	1.03	33	33	0.13	1.7
NB(PLA)7.0k	7.0	1.12	46	47	0.24	3.0
NB(PLA)4.7k	4.7	1.06	28	31	0.35	4.4
NB(P*n*BA)4.0k	4.0	1.06	29	28	0.33	4.2

[a]Macromonomers were named using a format of NB(X)Y, with X designating the type of prepolymer and Y designating the M_n of macromonomer. [b]Determined by GPC in THF using refractive index (RI) and MALLS detectors. [c]Calculated by comparing the integrations of the norbornenyl olefin and polymer backbone proton signals from ^1H NMR spectra in $CDCl_3$. [d]Calculated by (M_n – molar mass of norbornenyl end group) /

molar mass of monomer. [e]Conditions: $[MM]_0$ = 0.05M in THF at room temperature, $[MM/C]_0$ = 200. [f]$k_{p,\,rel}$ is the relative rate constant with respect to k_p of NB(PS)6.6k.

Polymerization of all these MMs using Ru catalyst **1** followed linear first-order kinetics (Figure 2A). GPC analyses of the polyMMs each showed narrow, monomodal peaks, and MWs increased linearly with conversion while the PDI remained less than 1.1 throughout the entire polymerization (Figure 2B). Furthermore, all MMs reached greater than 90% conversion within 1 h at room temperature. Although very weak signals that may correspond to MMs can be observed in the GPC traces of the crude polymer products, NMR spectroscopy of the reaction mixtures revealed the absence of the MM norbornene olefin signal. Therefore, the residual low MW peak may correspond to a small fraction of side chains with unfunctionalized chain ends in the MM. These observations collectively indicated the well-controlled character of ROMP of MMs and the extraordinary activity of catalyst **1**.

Due to the high activity of catalyst **1** and low critical monomer concentration of norbornene, the ROMP of MM can be performed at very low concentration ($[MM]_0$ = 0.05 M) to keep a relatively low viscosity of the solution throughout the polymerization. This is a distinct advantage over free radical polymerization of MMs.[39-42] Therefore, the polymerization is unlikely to be diffusion controlled (at least until the very late stage of the polymerization), in accord with the approximately linear first-order kinetics up to high conversions (>85%).

The polymerization rates, measured from the kinetic plot, depended weakly on both the MW and the structure of the MM (Table 1). In general, polyacrylate and polylactide MMs polymerized faster than polystyrene MMs. For example,

NB(PLA)7.0k polymerized about 3 times faster than NB(PS)6.6k despite their similar MW. The nature of the effects of side chain structure and MW on the polymerization rate of MMs warrants further investigation. It may be the local steric congestion around the propagating metallocycle or different solvent quality for various polymers that is causing the observed difference in the polymerization rate. Although the relative polymerization rates of different MMs varied less than an order of magnitude, they are significant when statistical copolymerization is attempted, since the relative polymerization rates can determine the distribution of side chains along the backbone (i.e., random vs. gradient).

(A)

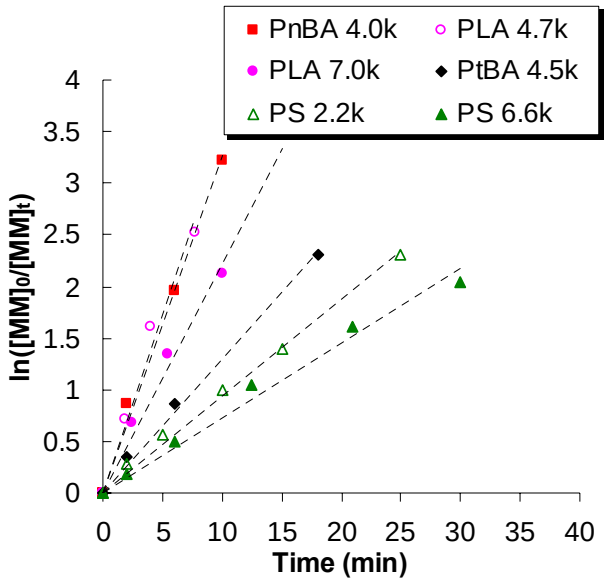

(B)

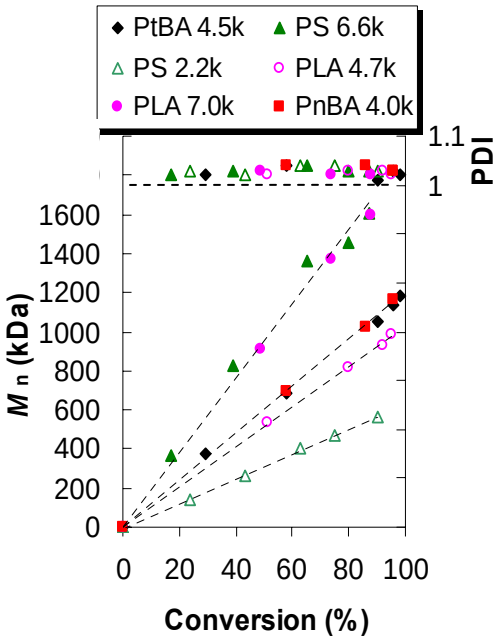

Figure 2. (A) Dependence of $\ln([MM]_0/[MM]_t)$ on time for ROMP of MMs. (B) Dependence of *M*n,GPC and PDI on conversion. Conditions: $[MM]_0$ = 0.05M in THF at room temperature, $[MM/C]_0$ = 200. The dashed lines are best-fit lines.

The controlled nature of the ROMP of MMs and the very high conversions motivated us to prepare brush block copolymers via simple sequential addition of MMs: Polymerization was initiated by injecting catalyst from a stock solution into a solution of the first type of MM at room temperature. As soon as the MM has been all consumed and only unfunctionalized side chains remained, a solution of a second type of MM was injected into the reaction mixture. GPC was used to analyze the reaction mixtures before the injection of the second MM and after completion of the second block polymerization. The GPC peak had shifted from the first block homopolymer to a shorter elution time corresponding to the brush diblock copolymer. The peak shape remained narrow without significant tailing, and the PDI remained low (≤1.10) (Figure 3). The low PDI was also indicated by the complete overlap of the light scattering trace and refractive index trace from GPC. Only very weak signal was

observed between 16 and 18 min in elution time, and this may correspond to unfunctionalized side chains in some of the MMs used. For example, in the brush PS and P*t*BA block copolymer, the intensity of the low MW peak remained similar in the first PS block and the diblock copolymer (Figure 3B), which may correspond to inert side chains in the PS MM. The order of addition of different MMs did not affect the MW or the PDI of the final block copolymers. Therefore, different MMs were arbitrarily polymerized sequentially to give various brush block copolymers, and the DP of each block was easily controlled by the ratio of MM to catalyst ([MM/C]). With narrow PDIs less than 1.1, regardless of the MW and combination of MMs, the MW of the copolymers measured by GPC-MALLS is close to or slightly higher than the theoretical MW. GPC analysis of the reaction mixture revealed the final conversions of MM to be greater than 90% in all the copolymerizations, while NMR spectroscopy showed no MM norbornene olefin signal.

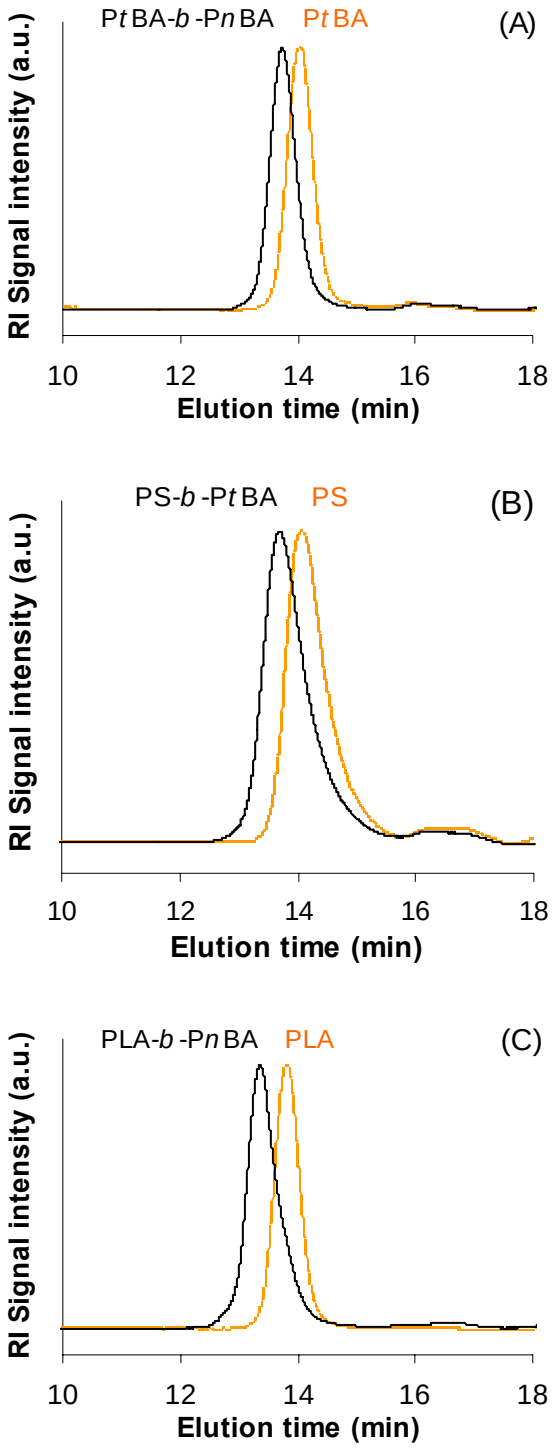

Figure 3. Representative GPC RI traces of the first block brush homopolymer (right) and the brush diblock copolymer (left) without any purification. (A) (PNB-*g*-P*t*BA)$_{100}$-*b*-(PNB-*g*-P*n*BA)$_{100}$; (B) (PNB-*g*-PS)$_{100}$-*b*-(PNB-*g*-P*t*BA)$_{50}$; (C) (PNB-*g*-PLA)$_{100}$-*b*-(PNB-*g*-P*n*BA)$_{100}$.

Table 2. Characteristics of brush copolymers

	MM_1	MM_2	Type	$[MM_1/C]$: $[MM_2/C]$[a]	Conv[b]	$M_{n,\,theo}$ (kDa)[c]	$M_{n,\,GPC}$ (kDa)[d]	PDI[d]
1	PS6.6k	P*n*BA4.0k	block	40:70	91%	540	730	1.04
2	PS6.6k	P*n*BA4.0k	block	40:200	91%	1060	1230	1.04
3	P*t*BA4.7k	P*n*BA4.0k	block	100:100	97%	870	890	1.05
4	P*t*BA4.7k	P*n*BA4.0k	block	100:200	98%	1270	1260	1.04
5	PS2.2k	P*t*BA4.7k	block	50:50	96%	345	340	1.03
6	PS2.2k	P*t*BA4.7k	block	100:50	94%	455	540	1.04
7	PLA4.7k	P*n*BA4.0k	block	20:180	98%	810	820	1.08
8	PLA4.7k	P*n*BA4.0k	block	40:160	97%	830	890	1.08
9	PLA4.7k	P*n*BA4.0k	block	100:100	97%	870	980	1.07
10	PLA4.7k	PnBA4.0k	block	200:200	96%	1740	1770	1.09
11	PLA4.7k	P*n*BA4.0k	random	50:50	98%	435	450	1.06
12	PLA4.7k	P*n*BA4.0k	random	100:100	97%	870	1050	1.05
13	PLA4.7k	P*n*BA4.0k	random	200:200	98%	1740	1880	1.10
14	PLA4.7k	P*n*BA4.0k	random	160:40	98%	910	1030	1.04
15	PLA4.7k	P*n*BA4.0k	random	130:70	98%	890	1030	1.05

[a] The ratio of each MM to Ru catalyst. [b] Conversion of MM to brush copolymer is determined by comparing the peak areas of brush copolymer and residual MM from GPC measurement of the final crude product without any purification. [c] $M_{n,\,theo} = M_{n,\,GPC}$ (MM_1) x $[MM_1/C]$ + $M_{n,\,GPC}$ (MM_2) x $[MM_2/C]$. [d] Determined by THF GPC using RI and MALLS detectors.

P*t*BA side chains in the brush block copolymers can be hydrolyzed into polyacrylic acid (PAA) using TFA in CH_2Cl_2, leaving the other block and the

backbone intact, as indicated by NMR spectroscopy. Thus, amphiphilic block brush copolymers were also easily obtained.

The side chain distribution along the brush copolymer backbone can dominantly affect the macromolecular packing in order to minimize the interfacial energy while retaining relatively extended backbone conformation. In this report, we focus on the study of the melt state self-assembly of copolymers containing PLA and P*n*BA side chains. We chose MMs NB(PLA)4.7k and NB(P*n*BA)4.0k as the side chains, because they possess very similar MWs and polymerization rates, and their copolymers can be thermally annealed relatively easily due to their low T_g's. These features allowed us to easily prepare a series of brush block and random copolymers with the same pair of side chains and matched backbone length, but varying the relative ratio of the two MMs (Table 2, entry 7-15). Brush block copolymers, *g*-[PLA_x-*b*-P*n*BA_y], with varied block lengths and ratios were synthesized via sequential addition of MMs. Brush random copolymers, *g*-[PLA_x-*ran*-P*n*BA_y], with varied total backbone length and side chain composition were synthesized via initiating a mixture of two MMs (Figure 3). Note that the subscripts x and y represent the number of side chains of each type—not the DP of the side chains, which was held fixed at approximately 30 for both the PLA and P*n*BA side chains (see the last two rows of Table 1). Since the ROMP of these MMs proceeded to very high conversions (>97%) and only a minute amount of catalyst was used (0.04-0.16 wt% to MMs used), no attempts to purify the polymer products were made. All polymer samples were simply dried under vacuum to remove solvent. These samples provided a model series to study how side chain distribution along the brush copolymer backbone affects brush

copolymer self-assembly in the melt state.

Thermal Analyses of Brush (Co)polymers. DSC analysis revealed the architectural effect of brush homopolymers and copolymers on the T_g of their side chains. For a PLA brush homopolymer (backbone DP=200) synthesized using NB(PLA)4.7k, a single thermal transition at 49 °C was observed in the temperature range of 0-200 °C scanned. This temperature corresponded to the T_g of amorphous PLA side chains and is close to the literature values. The T_g of the brush homopolymer was higher than that of the MM (42 °C), due to the increased MW and/or the increased molecular constraint resulting from linking the side chains along the formed polynorbornene backbone.[43] The T_g of PLA side chains in brush block copolymers was found to be about 49 °C, close to that of the PLA brush homopolymer, except for PLA_{20}-*b*-P*n*BA_{180} whose signal was too weak to enable accurate T_g determination (Table 3). This is consistent with phase separation in the block copolymers to form two distinct domains. In contrast, the T_g of PLA was found to be lower in the brush random copolymers, and increasing the P*n*BA content resulted in further suppression of the T_g of PLA. However, the T_g's of brush random copolymers were similar to that of the PLA MM, which indicated microphase separation of PLA and P*n*BA side chains. With equal amounts of PLA and P*n*BA in the brush random copolymers, the T_g was found to be 38 °C (Table 3). The lower T_g of PLA in random copolymers may be a result of smaller domain sizes than those in brush block copolymers.

Self-Assembly of Brush Copolymers in the Melt State. We investigated the self-assembly of brush copolymers in bulk using small angle X-ray scattering (SAXS) and in thin films using AFM. These two techniques provide complementary information

about the self-assembled morphology and domain spacing.

Brush random copolymers, *g*-[PLA-*ran*-P*n*BA], were thermally annealed at 100 °C for 12 h in order to achieve equilibrium, and prolonged annealing did not result in any further structural change. Brush random copolymers with an equal number of PLA and P*n*BA side chains (symmetric) exhibited a sharp principal SAXS peak at wavevector q^* along with peaks at integer multiples of q^* (Figure 4). This is indicative of a lamellar morphology, as expected due to the near symmetric volume fractions of the PLA and P*n*BA segments (f_{PLA} = 0.49). The domain spacing (d) calculated from q^* is very similar, 14.3 ± 0.3 nm, for all three symmetric random copolymers, independent of their backbone length. The independence of d-spacing on backbone length and the lamellar morphology suggest that the polynorbornene backbone is confined at the interface between PLA and P*n*BA layers, with the PLA and P*n*BA side chains segregated to opposite sides of the brush polymer backbone to minimize contact between dissimilar chains.

Furthermore, as the symmetric random copolymers were heated, they underwent a transition from an ordered lamellar phase into a microphase disordered regime. The order-disorder transition (ODT) temperature, T_{ODT}, can be evaluated using the discontinuity in the plot of inverse primary peak intensity vs inverse temperature (Figure 5), using SAXS patterns acquired in 5 °C step ramping with 5 min thermal equilibration at each temperature. This was accompanied by the disappearance of higher order peaks. The T_{ODT} was found to hardly change, giving 75-85 °C for *g*-[PLA_{50}-*ran*-P*n*BA_{50}], *g*-[PLA_{100}-*ran*-P*n*BA_{100}], and *g*-[PLA_{200}-*ran*-P*n*BA_{200}] as the MW increased from 450 to 1880 kDa. The broad scattering peak in

SAXS that remained above the ODT originated from intramolecular correlations of block copolymers.[44] For a wide range of block copolymers, T_{ODT} is controlled by the product of the Flory-Huggins interaction parameter χ and the total degree of polymerization N.[44] The similar T_{ODT}'s observed for the brush random copolymers over a wide range of the brush backbone length suggested that the degree of polymerization N of the side chains dictates the T_{ODT}. This is consistent with side chain microphase separation with the backbones localized at interfaces between PLA and P*n*BA domains (Figure 6 top).

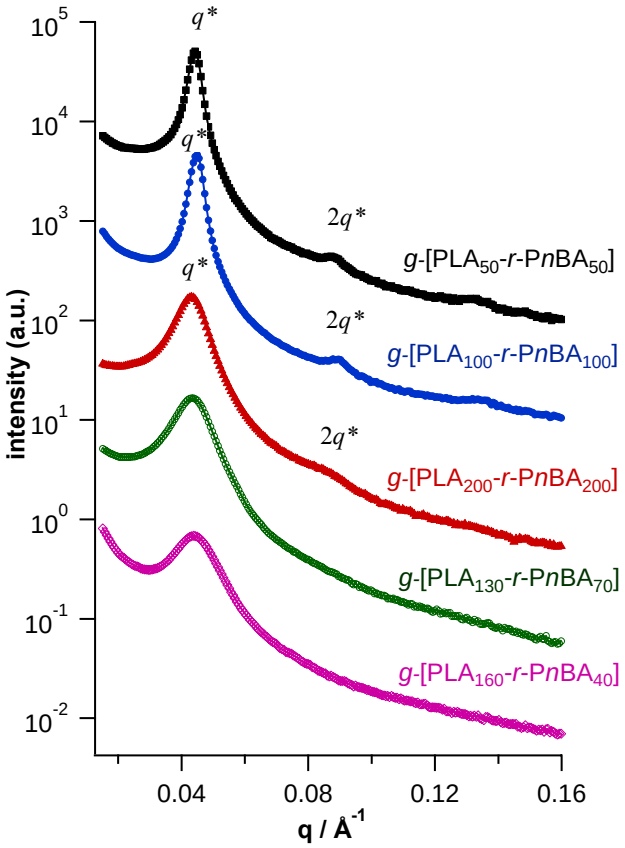

Figure 4. SAXS curves for brush random copolymers, *g*-[PLA-*ran*-P*n*BA].

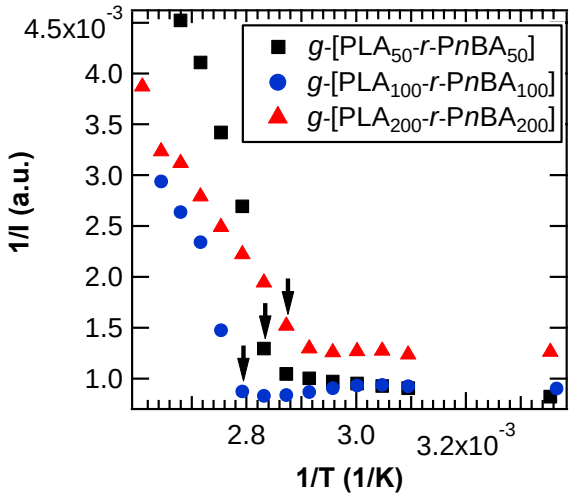

Figure 5. Inverse intensity of peak heights in the vicinity of the order-disorder transition for brush random copolymers, *g*-[PLA-*ran*-P*n*BA]. The arrows mark the T_{ODT}'s.

We studied the morphology of brush random copolymers in thin films using AFM. Based on the T_{ODT} determined using SAXS, these samples were annealed at 70 °C, which is below the T_{ODT} but still above the T_g of PLA. AFM showed that the films were featureless before annealing (Figure 7a). After annealing, a layer of islands with very uniform height was clearly observed for each of the symmetric random copolymers (Figure 7b-d). An island layer is formed if the natural repeat spacing of a parallel oriented block copolymer is incommensurate with the film thickness, and the film segregates excess material to the top surface to form an incomplete layer.[45-47] The height difference between the thicker and thinner regions of the film is equal to the natural period of the block copolymer. Here the island layers are remarkably uniform across areas of tens of micrometers, with thickness of 17-20 nm for all three samples. The height values are very close to the bulk *d*-spacings measured by SAXS, indicating that the domain spacing of parallel oriented lamellae in the film is similar to domain spacing in the bulk.

Table 3. Molecular and Morphological Characteristics of PLA-P*n*BA Brush Random and Block Copolymers

	f_{PLA}[a]	$T_{g,\ PLA}$/°C[b]	*d* (SAXS)/nm[c]	*d* (AFM)/nm[d]	T_{ODT}/°C[e]
g-[PLA_{50}-*ran*-$PnBA_{50}$]	0.49	38	14.2	18	80
g-[PLA_{100}-*ran*-$PnBA_{100}$]	0.49	38	14.0	21	85
g-[PLA_{200}-*ran*-$PnBA_{200}$]	0.49	38	14.6	17	75
g-[PLA_{130}-*ran*-$PnBA_{70}$]	0.63	39	-	-	-
g-[PLA_{160}-*ran*-$PnBA_{40}$]	0.79	42	-	-	-
g-[PLA_{100}-*b*-$PnBA_{100}$]	0.49	49	116	-	-
g-[PLA_{40}-*b*-$PnBA_{160}$]	0.19	49	-	-	-
g-[PLA_{20}-*b*-$PnBA_{180}$]	0.09	-	64	-	-

[a]volume fraction of PLA calculated using densities ρ_{PnBA} = 0.99 g/mL, ρ_{PLA} = 1.25 g/mL. [b]T_g of PLA side chain, measured by DSC with heating rate of 15 °C/min. [c]Domain spacing determined by SAXS. [d]Lamellar thickness determined by AFM cross-sectional analysis. [e]Order-disorder transition temperature determined by SAXS.

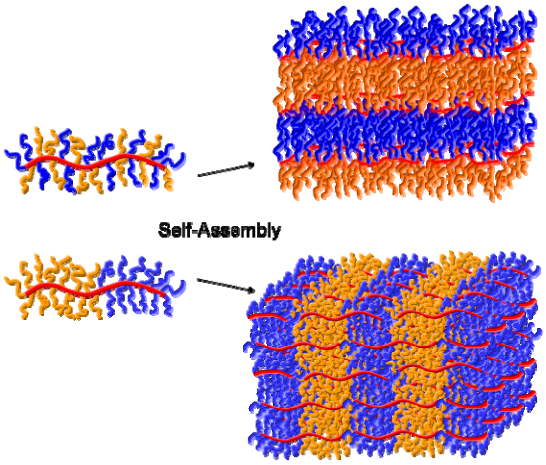

Figure 6. Proposed assembly of symmetric brush random copolymer and block copolymer.

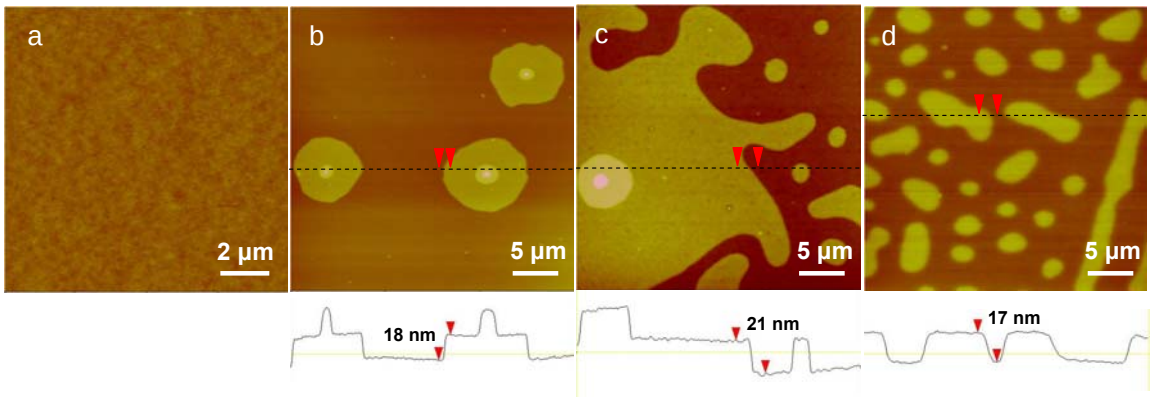

Figure 7. AFM height images of brush random copolymer thin films (120-150 nm) on silicon wafer and their cross-sectional analysis. (a) *g*-[PLA_{100}-*ran*-P*n*BA_{100}] as cast, and after annealing (b) *g*-[PLA_{50}-*ran*-P*n*BA_{50}], (c) *g*-[PLA_{100}-*ran*-P*n*BA_{100}], (d) *g*-[PLA_{200}-*ran*-P*n*BA_{200}]. The vertical scale is 30 nm for (a) and 100 nm for (b)-(d).

Due to the independence of lamellar thickness on brush polymer MW, we propose that uniform lamellar structures can be obtained using polydisperse brush copolymer samples. Indeed, an indistinguishable "islands and holes" morphology with 17-20 nm in height was obtained from blends of any two of the symmetric random copolymers at arbitrary ratios after annealing (Figure 8). This further supports the complete dominance of the side chains in governing the self-assembly of these brush random copolymers.

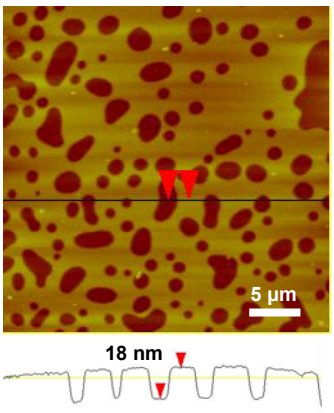

Figure 8. AFM height image of thin films of a mixture of two brush random copolymers, $(PNB\text{-}g\text{-}PLA)_{50}$-*ran*-$(PNB\text{-}g\text{-}PnBA)_{50}$ and $(PNB\text{-}g\text{-}PLA)_{100}$-*ran*-$(PNB\text{-}g\text{-}PnBA)_{100}$ (1:1), and its cross-sectional analysis. A hole layer was formed in this case.

In contrast to the symmetric random copolymers, when PLA and P*n*BA side chains were incorporated in uneven amounts (Table 2, entry 14 and 15), microphase separation of the side chains was not observed: No structural features were observed in thin films by AFM after extensive annealing at temperatures ranging from 75 to 140 °C. SAXS of *g*-[PLA_{160}-*ran*-P*n*BA_{40}] and *g*-[PLA_{130}-*ran*-P*n*BA_{70}] showed only one broad peak with no higher-order peaks; the single peak corresponds to intramolecular correlations between side chains of the block copolymers. Furthermore, the peak intensity continuously decreased upon heating, and no ODT was observed (Figure 9). As the side chains microphase separate to opposite sides of the backbone, the resulting asymmetric space filling on the backbone makes it impossible to assemble into lamellae. Meanwhile, the backbone of a brush polymer may be more difficult to coil than a linear polymer to adopt other morphologies, as a result of the high congestion of the segregated side chains.

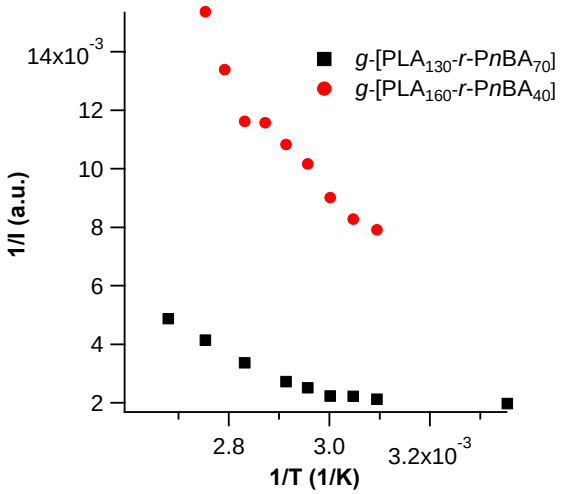

Figure 9. Inverse intensity of peak heights vs inverse temperature for asymmetric brush random copolymers.

We next investigated the self-assembly of brush block copolymers, *g*-[PLA-*b*-P*n*BA]. Due to the very large domain spacing in the assembled brush block

copolymers, principal q^* was out of the q range obtainable by SAXS in some samples (Figure 10). For the symmetric block copolymers, *g*-[PLA_{50}-*b*-P*n*BA_{50}] showed very sharp principal q^* and evenly spaced odd-order scattering peaks, and the even-order peaks were significantly suppressed. This scattering pattern strongly indicated symmetric lamellar morphology with a *d*-spacing of 50 nm. As the MW doubles, *g*-[PLA_{100}-*b*-P*n*BA_{100}] clearly showed multiple higher-order scattering peaks up to the 12th order. The even distribution of scattering peaks to $12q^*$ indicated remarkably well-ordered lamellar morphology with a *d*-spacing of 116 nm, consistent with the fact that principal q^* was out of the q range obtainable by SAXS. This length scale is close to the fully extended length of a polynorbornene brush homopolymer with backbone DP = 220 and PS side chains of 6.6 kDa, as previously observed by AFM.[34] Although clear AFM imaging of individual *g*-[PLA_{100}-*b*-P*n*BA_{100}] polymers has been difficult due to the aggregation of molecules, AFM revealed wormlike shapes with contour lengths of ca 110-130 nm for a PLA brush homopolymer with backbone DP = 200 prepared using the same MM as in the block copolymer (Figure 9a). Therefore, the large lamellar *d*-spacing of *g*-[PLA_{100}-*b*-P*n*BA_{100}] is dictated by the length of its highly extended polynorbornene backbone and suggests interdigitated packing of the molecules in the lamellae (Figure 6 bottom). This is further supported by the the almost linear increase of *d*-spacing from 50 to 116 nm, when the MW doubles from that of *g*-[PLA_{50}-*b*-P*n*BA_{50}] to that of *g*-[PLA_{100}-*b*-P*n*BA_{100}]. Notably, the largest symmetric block copolymer *g*-[PLA_{200}-*b*-P*n*BA_{200}] (Table 2, entry 10) appeared green spontaneously upon slowly evaporating the solvent (Figure 13). This indicates that the domain spacing in this ultrahigh MW sample is large enough to reflect green light.[48]

However, only some very low intensity SAXS peaks were observed for *g*-[PLA_{200}-*b*-P*n*BA_{200}] and *d*-spacing cannot be calculated. This is because the high-intensity lower-order scattering peaks were out of the range of the SAXS used due to the very large domain size in this sample. Ultrasmall angle X-ray scattering (USAXS) needs to be used in the future to study the brush polymer assembly pocessing large domain sizes (>100 nm).

On the other hand, highly asymmetric block copolymers, *g*-[PLA_{20}-*b*-P*n*BA_{180}] and *g*-[PLA_{40}-*b*-P*n*BA_{160}], formed non-lamellar morphologies. Both materials showed scattering peaks at very low *q*, a feature indicative of microphase separation, with *q** inaccessible for *g*-[PLA_{40}-*b*-P*n*BA_{160}] and *q** corresponding to a domain spacing of 64 nm for *g*-[PLA_{20}-*b*-P*n*BA_{180}] (Figure 11). Based on the domain spacing for *g*-[PLA_{20}-*b*-P*n*BA_{180}], it is clear that the backbone is not fully extended in its highly asymmetric polymer. In addition, both polymers show oscillations at higher *q* that originate from the form factor of the block copolymer aggregates.[49] Although the quality of fits is not sufficient to identify the specific shape of the aggregates, the period of the oscillations allows us to identify the characteristic size of the presumably spherical or cylindrical PLA domains with sizes of 38 and 67 nm in diameter, respectively, irregularly distributed in a matrix of P*n*BA. In addition, the PLA domain size is consistent with the calculated result using the domain spacing of 64 nm obtained from *q** and 9% PLA volume fraction in *g*-[PLA_{20}-*b*-P*n*BA_{180}]. The non-lamellar morphologies formed from these asymmetric brush block copolymers suggest that the backbone is not as fully extended as in the symmetric brush block copolymer, *g*-[PLA_{100}-*b*-P*n*BA_{100}]. On the other hand, the decreased ordering in

asymmetric block copolymers suggests frustrated packing when the backbone has to adopt non-lamellar morphologies due to its reduced flexibility. Similar packing frustration has also been suggested for asymmetric brush block copolymers with side chains of different MWs.[12]

Thin films of the block copolymer *g*-[PLA_{100}-*b*-P*n*BA_{100}] after spin-coating from toluene solution showed large cylindrical micellar structures of 200 nm wide and several micrometers long as imaged by AFM (Figure 12b), in sharp contrast to the featureless as-cast film from the random copolymer, *g*-[PLA_{100}-*ran*-P*n*BA_{100}], at the same MW and composition. After annealing, the surface topology became rough, but clear phase separation was observed from the sharp contrast in the phase image, which derives from mechanical property differences between the PLA and P*n*BA blocks in the copolymers. Microphase separation in thin films of the asymmetric brush block copolymers was also observed from the AFM phase images. However, the structural assignment for the thin film morphologies of these brush block copolymers was unclear. This is because the film thickness is similar to the polymer domain spacing in bulk and corresponds to one layer of molecular packing. Therefore, the surface effect on the thin film morphology makes it difficult to correlate to the bulk morphology for large brush block copolymers.

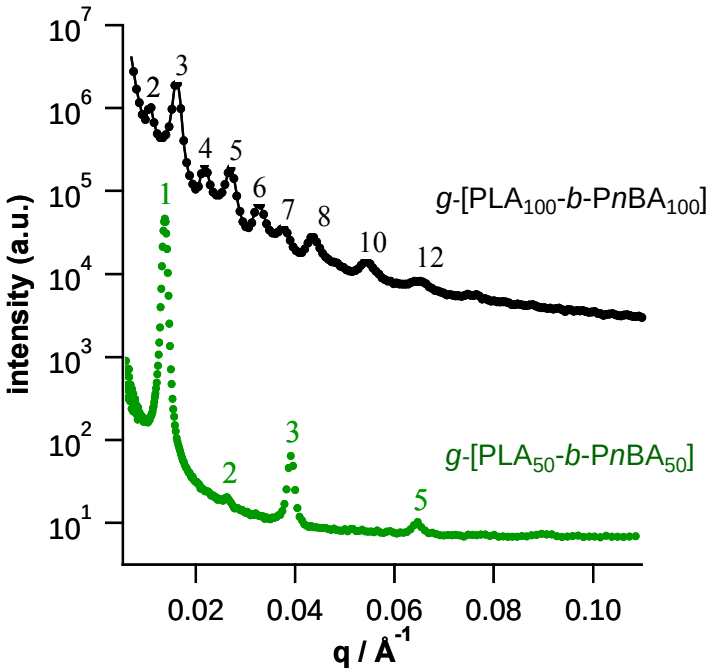

Figure 10. SAXS curves for symmetric brush block copolymers, *g*-[PLA-*b*-P*n*BA].

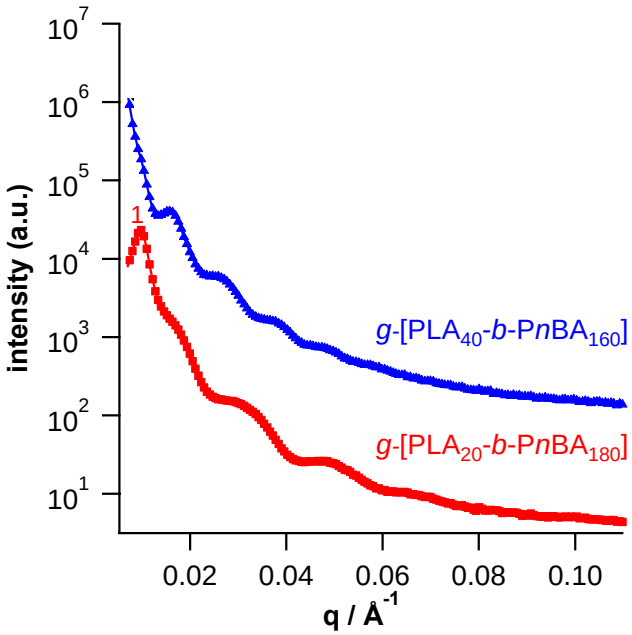

Figure 11. SAXS curves for asymmetric brush block copolymers, *g*-[PLA-*b*-P*n*BA].

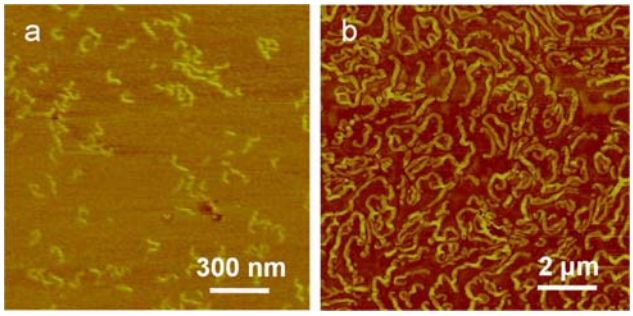

Figure 12. AFM phase images of (a) individual PLA brush homopolymers ($DP_{backbone}$ = 200, MM NB(PLA)4.7k was used) on mica; (b) brush block copolymer, *g*-[PLA_{100}-*b*-P*n*BA_{100}], morphology in thin film (ca 120 nm) as cast from 2.5% toluene solution onto silicon wafer.

Figure 13. Photograph of slowly dried *g*-[PLA_{200}-*b*-P*n*BA_{200}] (Table 2, entry 10) showing green color due to reflectance from the large self-assembled domains.

Conclusions

ROMP of various MMs bearing polyacrylate, polystyrene, and polylactide chains using highly active, fast initiating Ru catalyst has shown typical characteristics of a living polymerization, such as first-order kinetics and linear MW growth with increasing conversion. The living nature of ROMP and very high conversion (>90%) of MMs have allowed facile one-pot preparation of a variety of high MW narrowly dispersed brush block and random copolymers in high conversions, which otherwise involve multiple steps to synthesize using different grafting techniques. The length of each block and the overall backbone can be easily controlled by the ratio of MM to catalyst.

By choosing MMs with the similar polymerization rates, we prepared a series of brush block and random copolymers from a pair of MMs, NB(PLA)4.7k and NB(P*n*BA)4.0k, varying their relative ratios. In symmetric brush random copolymers (equal number of PLA and P*n*BA side chains), the side chains were found to microphase separate into lamellar morphology with domain spacing of about 14 nm as determined by SAXS. AFM studies of thin film samples also revealed lamellar structures with similar thickness of 17-21 nm. The domain spacing and T_{ODT} were insensitive to the brush copolymer backbone length, suggesting microphase separation of side chains to opposite sides of the brush polymer backbone and that the side chains played a dominant role in the self-assembly. On the other hand, the brush block copolymer with the same number of PLA and P*n*BA side chains self-assembled into highly ordered, large lamellar domains over 100 nm as revealed by SAXS. The domain size was dictated by the backbone length. The regular, spontaneous, large assembly of brush block copolymers makes them ideal polymer materials for single-component photonic crystals, which are important for advanced optical applications.

Asymmetric brush copolymers containing different numbers of two types of side chains did not form well-ordered morphologies. This may be attributed to the reduced backbone flexibility of brush polymers and their increased difficulty to adopt coiled conformations.

Controlled ROMP of MMs greatly simplifies the syntheses of brush copolymers. The combination of facile synthesis and good structural control of brush copolymers with the functional group tolerant Ru catalyst opens the door to further studies of the self-assembly of these macromolecular architectures. Brush copolymers provide a unique

macromolecular platform for bottom-up assembly to form nanostructures with large domain spacings and controlled intermaterial dividing surfaces.

Experimental Section

Materials. The synthesis and characterization of PMA, P*t*BA, and PS MMs have been described in Chapter 4 and the P*n*BA MM was synthesized in a similar manner. *n*-BA was passed through a column of basic alumina immediately before use. D, L-lactide was recrystallized from ethyl acetate three times. All other materials were obtained from commercial sources and used as received.

Synthesis of PLA macromonomers. A flame-dried Schlenk tube was charged with N-(hydroxyethyl)-*cis*-5-norbornene-exo-2,3-dicarboximide (54 mg, 0.26 mmol), D, L-lactide (1.5 g, 10.4 mmol), tin (II) 2-ethylhexanoate (2.1 mg, 5.2 μmol), and a stir bar. The tube was evacuated and backfilled with argon four times, and was then immersed in an oil bath at 120 °C. After 4 h, the contents were cooled to room temperature, diluted with dichloromethane, and precipitated into acidic methanol. The MM was isolated by decanting the supernatant and drying *in vacuo*. ^{1}H NMR (500 MHz, $CDCl_3$): δ 1.24 (br d, 1H), 1.40-1.70 (br, 253H), 2.72 (br, 2H), 3.28 (br, 2H), 3.70-3.85 (m, 2H), 4.22-4.40 (m, 3H), 5.00-5.30 (m, 84H), 6.30 (br t, 2H). GPC-MALLS: M_n = 7.0 kg/mol, M_w/M_n = 1.12.

General procedure for synthesis of brush block and random copolymers via ROMP of macromonomers. An oven-dried vial was charged with 100 mg MM for the first block and a stir bar. The vial was then degassed, and the desired amount of degassed anhydrous THF ($[M]_0$ = 0.05-0.10 M) was added via syringe under an argon atmosphere to dissolve the MM. A stock solution of Ru catalyst in degassed anhydrous THF was prepared in a separate vial. The desired amount of catalyst was injected into the MM

solution to initiate the polymerization. The reaction was allowed to proceed at room temperature for 20-30 min. After the first polymerization was complete, the desired amount of second MM was added as a solution in THF ($[M]_0$ = 0.05-0.10 M). After 1 h, the reaction mixture was quenched with one drop of ethyl vinyl ether. A sample was then withdrawn for GPC analysis without any purification. The block copolymer was isolated either by precipitating into cold methanol, or by simply drying *in vacuo.*

The random copolymers were synthesized using a similar procedure as the block copolymers, except that two types of MMs were added together in the reaction vial before catalyst injection.

Characterization. *^1H and ^{13}C NMR spectroscopy* was recorded in $CDCl_3$ or DMF-*d*7 using a Varian Mercury 300 or Varian Inova 500 spectrometer. Chemical shifts (δ) are expressed in ppm downfield from tetramethylsilane using the residual protiated solvent signal as an internal standard.

Gel permeation chromatography (GPC) was carried out in THF on two PLgel 10 μm mixed-B LS columns (Polymer Laboratories) connected in series with a DAWN EOS multiangle laser light scattering (MALLS) detector and an Optilab DSP differential refractometer (both from Wyatt Technology). No calibration standards were used, and d*n*/d*c* values were obtained for each injection by assuming 100% mass elution from the columns.

Atomic force microscopy (AFM) images were taken using a Nanoscope IV Scanning Probe Microscope Controller (Digital Instruments, Veeco Metrology Group) in tapping mode in air at room temperature using silicon tips (spring constant = 40-50 N/m, resonance frequency = 170-190 kHz, and tip radius of curvature <10 nm). The samples

for imaging individual polymers were prepared by spin casting very dilute solutions (<0.01 wt%) in chloroform onto freshly cleaved mica at 1500 rpm. Thin film samples were prepared by spin casting solutions (2.5 wt%) in toluene onto Si(100) with a native oxide layer at 1500 rpm. A Gartner L116-C ellipsometer was used to measure the film thickness.

Differential scanning calorimetry (DSC) was performed on a Perkin-Elmer DSC 7. Samples were heated to 180 °C at 20 °C/min to erase any thermal history, then cooled to 0 °C at 20 °C/min, and reheated to 150 °C at 15 °C/min. The second heating scan was used to determine the T_g of PLA.

Small angle X-ray scattering (SAXS). Samples for SAXS were prepared by annealing polymers in vacuum (10 mTorr) at 110 °C for 12 h to form 1 mm thick disks and then sealing the samples between Kapton windows. Experiments were performed on beamline 27X-C at Brookhaven National Lab. The beamline was configured with an X-ray wavelength of 1.371 Å. Samples were corrected for transmission, thickness, empty cell, and dark field scattering and radially averaged to produce 1 dimensional I vs. q plots. Temperature-dependent experiments were conducted by increasing temperature in 5 °C steps with 5 min of thermal equilibration after reaching each temperature before starting data acquisition.

References

(1) (a) Sheiko, S. S.; Möller, M. *Chem. Rev.* **2001**, *101*, 4099-4124. (b) Hadjichristidis, N. P., M.; Pispas, S.; Iatrou, H. *Chem. Rev.* **2001**, *101*, 3747-3792. (c) Zhang, M.; Müller, A. H. E. *J. Polym. Sci., Part A: Polym. Chem.* **2005**, *43*, 3461-3481.

(2) Li, C.; Gunari, N.; Fischer, K.; Janshoff, A.; Schmidt, M. *Angew. Chem. Int. Ed.* **2004**, *43*, 1101-1104.

(3) Djalali, R.; Li, S.-Y.; Schmidt, M. *Macromolecules* **2002**, *35*, 4282-4288.

(4) Zhang, M.; Drechsler, M.; Müller, A. H. E. *Chem. Mater.* **2004**, *16*, 537-543.

(5) Zhang, M.; Estournes, C.; Bietsch, W.; Müller, A. H. E. *Adv. Funct. Mater.* **2004**, *14*, 871-882.

(6) Cheng, C.; Qi, K.; Khoshdel, E.; Wooley, K. L. *J. Am. Chem. Soc.* **2006**, *128*, 6808-6809.

(7) Huang, K.; Rzayev, J. *J. Am. Chem. Soc.* **2009**, *131*, 6880-6885.

(8) Tang, C.; Dufour, B.; Kowalewski, T.; Matyjaszewski, K. *Macromolecules* **2007**, *40*, 6199-6205.

(9) (a) Bates, F. S.; Fredrickson, G. H. *Phys. Today* **1999**, *52*, 32-38. (b) Klok, H.-A.; Lecommandoux, S. *Adv. Mater.* **2001**, *13*, 1217-1229. (c) Discher, D. E.; Eisenberg, A. *Science* **2002**, *297*, 967-973. (d) Hamley, I. W. *Angew. Chem. Int. Ed.* **2003**, *42*, 1692-1712. (e) Hadjichristidis, N.; Iatrou, H.; Pitsikalis, M.; Pispas, S.; Avgeropoulos, A. *Prog. Polym. Sci.* **2005**, *30*, 725-782. (f) Ruzette, A.-V.; Leibler, L. *Nat. Mater.* **2005**, *4*, 19-31. (g) Cheng, J. Y.; Ross, C. A.; Smith, H. I.; Thomas, E. L. *Adv. Mater.* **2006**, *18*, 2505-2521. (h) Cui, H.; Chen, Z.; Zhong, S.; Wooley, K. L.; Pochan, D. J. *Science* **2007**, *317*, 647-650. (i) Tang, C.; Lennon, E. M.; Fredrickson, G. H.; Kramer, E. J.; Hawker, C. J. *Science* **2008**, *322*, 429-432.

(10) Runge, M. B.; Bowden, N. B. *J. Am. Chem. Soc.* **2007**, *129*, 10551-10560.

(11) Runge, M. B.; Lipscomb, C. E.; Ditzler, L. R.; Mahanthappa, M. K.; Tivanski, A. V.; Bowden, N. B. *Macromolecules* **2008**, *41*, 7687-7694.

(12) Rzayev, J. *Macromolecules* **2009**, *42*, 2135-2141.

(13) Joannopoulos, J. D.; Meade, R. D.; Winn, J. N. *Photonic Crystals*, Princeton University Press, 1995.

(14) Edrington, A. C.; Urbas, A. M.; DeRege, P.; Chen, C. X.; Swager, T. M.; Hadjichristidis, N.; Xenidou, M.; Fetters, L. J.; Joannopoulos, J. D.; Fink, Y.; Thomas, E. L. *Adv. Mater.* **2001**, *13*, 421-425.

(15) Park, C.; Yoon, J.; Thomas, E. L. *Polymer* **2003**, *44*, 6725-6760.

(16) Kang, Y.; Walish, J. J.; Gorishnyy, T.; Thomas, E. L. *Nat. Mater.* **2007**, *6*, 957-960.

(17) Neiser, M. W.; Muth, S.; Kolb, U.; Harris, J. R.; Okuda, J.; Schmidt, M. *Angew. Chem. Int. Ed.* **2004**, *43*, 3192-3195.

(18) Lanson, D.; Ariura, F.; Schappacher, M.; Borsali, R.; Deffieux, A. *Macromolecules* **2009**, *42*, 3942-3950.

(19) Runge, M. B.; Dutta, S.; Bowden, N. B. *Macromolecules* **2006**, *39*, 498-508.

(20) Lee, H.-I.; Matyjaszewski, K.; Yu-Su, S.; Sheiko, S. S. *Macromolecules* **2008**, *41*, 6073-6080.

(21) Neugebauer, D.; Sumerlin, B. S.; Matyjaszewski, K.; Goodhart, B.; Sheiko, S. S. *Polymer* **2004**, *45*, 8173-8179.

(22) Sumerlin, B. S.; Neugebauer, D.; Matyjaszewski, K. *Macromolecules* **2005**, *38*, 702-708.

(23) Lanson, D.; Schappacher, M.; Borsali, R.; Deffieux, A. *Macromolecules* **2007**, *40*, 5559-5565.

(24) Schappacher, M.; Deffieux, A. *Macromolecules* **2005**, *38*, 7209-7213.

(25) Gao, H.; Matyjaszewski, K. *J. Am. Chem. Soc.* **2007**, *129*, 6633-6639.

(26) Lanson, D.; Schappacher, M.; Borsali, R.; Deffieux, A. *Macromolecules* **2007**, *40*, 9503-9509.

(27) Hadjichristidis, N.; Pitsikalis, M.; Iatrou, H.; Pispas, S. *Macromol. Rapid Commun.* **2003**, *24*, 979-1013.

(28) Stephan, T.; Muth, S.; Schmidt, M. *Macromolecules* **2002**, *35*, 9857-9860.

(29) Deimede, V.; Kallitsis, J. K. *Chem.-Eur. J.* **2002**, *8*, 467-473.

(30) Neugebauer, D.; Zhang, Y.; Pakula, T.; Matyjaszewski, K. *Macromolecules* **2005**, *38*, 8687-8693.

(31) Neugebauer, D.; Theis, M.; Pakula, T.; Wegner, G.; Matyjaszewski, K. *Macromolecules* **2006**, *39*, 584-593.

(32) Heroguez, V.; Gnanou, Y.; Fontanille, M. *Macromolecules* **1997**, *30*, 4791-4798.

(33) Nomura, K.; Takahashi, S.; Imanishi, Y. *Macromolecules* **2001**, *34*, 4712-4723.

(34) Xia, Y.; Kornfield, J. A.; Grubbs, R. H. *Macromolecules* **2009**, *42*, 3761-3766.

(35) Karen L. Wooley and co-workers reported the synthesis of brush block copolymers using similar strategy soon after our initial report: Li, Z.; Ma, J.; Cheng, C.; Zhang, K.; Wooley, K. L. *Macromolecules* **2010**, *43*, 1182-1184.

(36) Winey, K. I.; Thomas, E. L.; Fetters, L. J. *J. Chem. Phys.* **1991**, *95*, 9367-9375.

(37) Cheng, C.; Khoshdel, E.; Wooley, K. L. *Macromolecules* **2005**, *38*, 9455-9465.

(38) Patton, D. L.; Advincula, R. C. *Macromolecules* **2006**, *39*, 8674-8683.

(39) Tsukahara, Y. T., K.;Yamashita, Y.;Shimada, S. *Macromolecules* **1990**, *23*, 5201-5208.

(40) Dziezok, P.; Sheiko, S. S.; Fischer, K.; Schmidt, M.; Möller, M. *Angew. Chem. Int. Ed.* **1997**, *36*, 2812-2815.

(41) Roos, S. G.; Müller, A. H. E.; Matyjaszewski, K. *Macromolecules* **1999**, *32*, 8331-8335.

(42) Shinoda, H.; Matyjaszewski, K. *Macromolecules* **2001**, *34*, 6243-6248.

(43) Fox, T. G.; Flory, P. J. *J. Polym. Sci.* **1954**, *14*, 315.

(44) Leibler, L. *Macromolecules* **1980**, *13*, 1602-1617.

(45) Coulon, G.; Collin, B.; Ausserre, D.; Chatenay, D.; Russell, T. P. *J. Phys. (Paris)* **1990**, *51*, 2801-2811.

(46) Mayes, A. M.; Russell, T. P.; Bassereau, P.; Baker, S. M.; Smith, G. S. *Macromolecules* **1994**, *27*, 749-755.

(47) Olsen, B. D.; Li, X.; Wang, J.; Segalman, R. A. *Macromolecules* **2007**, *40*, 3287-3295.

(48) The wavelength of the reflected light at the interfaces of multilayer lamellae is governed by: $\lambda = 2(n_1d_1 + n_2d_2)$, where n and d are the refractive index and the thickness of each layer. In a rough estimate, taking $n_1 = n_2 = 1.5$ for both polymer layers and $\lambda = 500$ nm for green light, the domain spacing is calculated to be about 170 nm for a symmetric lamellar morphology presumably formed in the symmetric block copolymer *g*-[PLA_{200}-*b*-P*n*BA_{200}].

(49) Kinning, D. J.; Thomas, E. L. *Macromolecules* **1984**, *17*, 1712-1718.

C h a p t e r 6

Well-Defined Liquid Crystal Gels from Telechelic Polymers via Ring-Opening Metathesis Polymerization and "Click" Chemistry

Portions of this chapter have been published: Xia, Y.; Verduzco, R.; Grubbs, R. H.; Kornfield, J. A. *J. Am. Chem. Soc.* **2008**, 130, 1735-1740.

Abstract

Well-defined liquid crystal networks with controlled molecular weight between crosslinks and crosslink functionality were prepared by “click” crosslinking of telechelic polymers produced by ring-opening metathesis polymerization (ROMP). The networks readily swell in a small molecule liquid crystal, 5CB, to form LC gels with high swelling ratios. These gels exhibit fast, reversible, and low-threshold optic switching under applied electric fields when they are unconstrained between electrodes. For a given electric field, the LC gels prepared from shorter telechelic polymers showed a reduced degree of switching than their counterparts made from longer polymer strands. The reported approach provides control over important parameters for LC networks, such as the length of the network strands between crosslinks, crosslinker functionality, and mesogen density. Therefore, it allows detailed study of relationships between molecular structure and macroscopic properties of these scientifically and technologically interesting networks.

Introduction

Liquid crystal (LC) elastomers and gels are composed of flexible, liquid crystal polymers crosslinked to form a network. The combination of LC order and rubber elasticity results in an anisotropic polymer network that is responsive to a variety of external influences, including heat, light, electric and magnetic fields. These materials display remarkable changes in shape and optical properties that make them of interest for technological applications.[1-3]

In the context of the theory of LC networks[4-7], key parameters are the rubbery modulus of the network and the strength of orientational coupling between pendant mesogens and the flexible polymer backbone. These are controlled by molecular attributes: the flexibility of the polymer backbone, backbone length between crosslinks, and the choice of mesogen and spacer. Experimental studies of LC elastomers[8-12] and, more recently, gels formed by swelling elastomers with small molecule LC[13-16] show that these molecular parameters strongly influence macroscopic properties. For example, it has been observed qualitatively that decreasing the crosslinker and/or monomer concentrations resulted in lower threshold fields and enhanced electro-optic and electro-mechanical responses of LC gels.[13-15]

Therefore, it is necessary to exert synthetic control of both overall crosslink density and its variability within the network. Widely studied LC elastomers and gels have been prepared either from functionalization and crosslinking of poly(methyl)hydrosiloxane,[10-12,17-19] or from uncontrolled radical polymerization in the presence of crosslinker.[9,13-15,20-23] The preparation methods in these studies all relied on random crosslinking of polysiloxane or on uncontrolled radical reactions, resulting in

poorly defined network structures that make the correlation between network structure and material property difficult. More recent studies have utilized the self-assembly of block copolymers to produce LC elastomers,[24-27] These materials show interesting new properties that arise both from the physical nature of the crosslinks and from the well-defined self-assembled structure; however, they lack the long-term stability that is achieved by covalent crosslinking. Here, we investigate the use of telechelic polymers to create covalent LC elastomers and gels. End-linking of telechelic polymers with polyfunctional crosslinkers is known to give well-defined polymer networks,[28-30] and to our knowledge this strategy has not been extended to the synthesis of LC networks.

We report the preparation of well-defined LC networks by controlled "click" crosslinking of telechelic LC polymers produced by ring-opening metathesis polymerization (ROMP). Copper(I)-catalyzed azide-alkyne "click" cycloaddition[31] has gained increasing attention in polymer and material research due to its extraordinary specificity, quantitative yield, and wide functional group tolerance.[32-34] Crosslinking of telechelic polymers by "click" chemistry has recently been utilized to produce well-defined hydrogels[35] and other networks.[36,37] Furthermore, recent developments in ROMP allow for the preparation of polyalkenamers with a variety of functional groups[38-40] and simultaneous facile control of the end groups can be achieved using a chain transfer agent (CTA).[41-43]

We combine ROMP and "click"-crosslinking to produce LC networks with a regular network architecture, including a controlled molecular weight between crosslinks and crosslink functionality. The resulting LC networks can be swollen in small molecule

LC to produce LC gels, which show fast, reversible, and low-threshold electro-optic switching.

Results and Discussion

Polycyclooctene was chosen for the side-group liquid crystalline polymer (SGLCP) backbone, anticipating that it would give a low T_g and fast segmental dynamics. In LC gels, the director reorientation is coupled to the segmental dynamics of the solvated polymers, so fast electro-optic response is favored by high mobility of the SGLCP. Additionally, control of chain end functionality for cyclooctene is readily achieved via a CTA. However, ROMP of functionalized cyclooctenes with large, pendant substituents have been rarely reported,[44,45] presumably due to the lower ring strain of cyclooctene compared to norbornene.

Synthesis of Telechelic LC Polymers. Cyclooctene monomers were functionalized with either one or two mesogenic groups as outlined in Scheme 1: cyano-biphenyl mesogens were coupled via a six-carbon spacer to either dihydroxy-cyclooctene to yield monomer **1** or hydroxy-cyclooctene to give monomer **2**. This monomer pair allows us to vary the mesogen density on the final polymer backbone. Both monomers were crystalline solids exhibiting a single phase transition to the isotropic state.

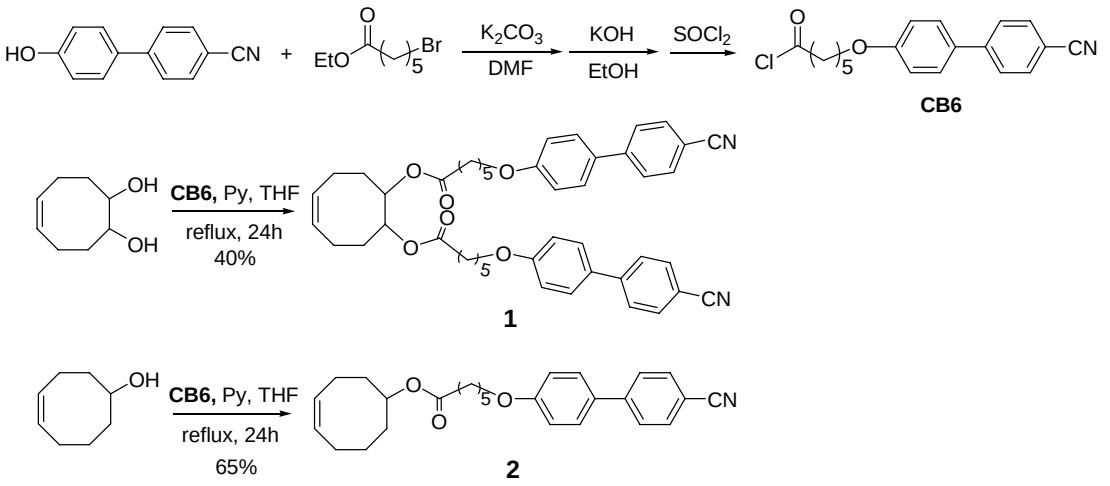

Scheme 1. Synthesis of monomers **1** and **2**.

To prepare telechelic SGLCPs, the monomers were polymerized by the highly active ruthenium catalyst, $(IMesH_2)(PCy_3)RuCl_2(CHPh)$, in dichloroethane at 55 °C for 24 h in the presence of a CTA (Scheme 2). Since the ruthenium catalyst is known to be incompatible with azide groups, 1,8-dibromo-4-octene was utilized as the CTA to give telechelic polymers with primary bromide end groups which can subsequently be converted to azide groups quantitatively. Monomer concentrations were chosen to be the maximum concentration possible while maintaining a low enough viscosity to permit efficient chain transfer: 1M for **1** and 1.5M for **2**. A monomer-to-catalyst ratio, [M]/[C], of 1000 was used for all polymerizations. Complete monomer conversion was achieved at this catalyst loading, as indicated by the complete shift of the monomer olefin resonance at 5.65 ppm to the polymer olefin resonance at 5.3 ppm in the ^{1}H-NMR spectrum. The polymer molecular weights were regulated by the ratio of monomer to CTA, [M]/[CTA] (Table 1). Good agreement between the absolute molecular weight obtained from GPC equipped with light scattering detector and the molecular weight determined by ^{1}H-NMR end group analysis indicates that the polymers are telechelic.

The bromide end groups of telechelic polymers **3** and **4** were transformed into azide groups by nucleophilic substitution with sodium azide in DMF. This substitution was carried out to quantitative yields as indicated by the complete shift of the terminal methylene signals from 3.4 to 3.2 ppm in the ^{1}H-NMR spectrum and the appearance of characteristic alkyl azide absorbance at 2099 cm^{-1} in the IR spectrum.

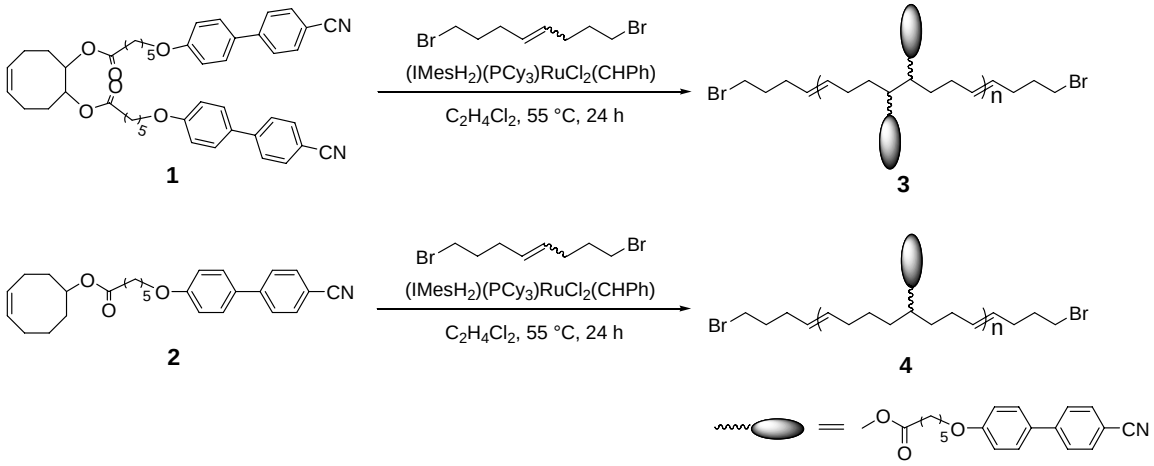

Scheme 2. ROMP of functionalized cyclooctene monomers.

Table 1. Synthesis and characterization of functionalized polycyclooctenes[a]

Polymer	$[M]_0/[CTA]_0$	% yield[b]	$M_{n,GPC}$[c]	$M_{n,NMR}$[d]	PDI	T_g / °C[e]	T_{NI} / °C[e]
3a	10	97	11 300	11 100	1.79	23.8	51.4
3b	20	99	24 800	26 200	1.84	27.1	58.5
4	20	95	13 700	16 600	1.43	8.5	N/A

[a]Polymerization conditions: $[M]_0$=1M for **1** and 1.5M for **2** in $C_2H_4Cl_2$; $[M]_0/[cat]$=1000; 55 °C, 24 h. [b]Isolated polymer yield. [c]Determined by THF GPC coupled with 18-way light scattering detector. [d]Determined by end group analysis from ^{1}H-NMR in $CDCl_3$ assuming F_n=2. [e]Measured by DSC, heating rate=10 °C/min.

Polymers **3a** and **3b** (Table 1) made from the disubstituted monomer **1** were nematic at room temperature, as confirmed by polarized optical microscopy (POM) and X-ray scattering. The polymer had a nematic to isotropic transition temperature (T_{NI}) between 50 and 60 °C, as measured by differential scanning calorimetry (DSC) and POM. On the other hand, polymer **4** prepared from the monosubstituted monomer **2** was not

liquid crystalline and did not show any phase transitions in the range of 20-100 °C under DSC or POM. Both polymers were soluble in a small molecule liquid crystal, 5CB, up to the highest concentration tested of 10 wt %.

Synthesis of LC Networks. Controlled "click" crosslinking of these telechelic polymers was achieved by reacting a triacetylene species, tripropargylamine, with the polymer azide end groups in the presence of CuBr as catalyst and PMDETA as a ligand in DMF at 50 °C (Scheme 3). The solution was allowed to react for 2 more days after gelation had occurred to ensure complete reaction. The resulting gels were extracted in DMF and THF repeatedly to remove copper catalyst and uncrosslinked fraction, and elastomers were obtained after drying under vacuum.

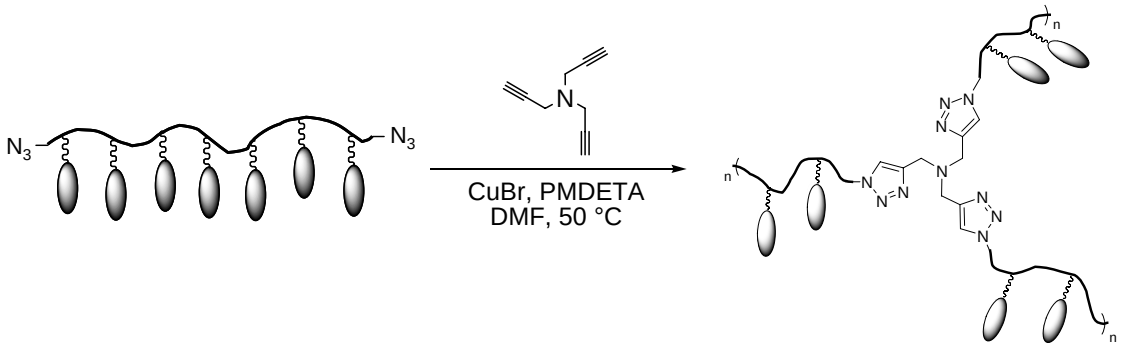

Scheme 3. Cross-linking of telechelic polymers by "click" chemistry.

Polymer **3a** was used to study the effect of crosslinking conditions on the gel fraction. Polymer concentration had minimal effect on the gel fraction (Table 2, entry 1-3). When high polymer concentrations (50 wt % and 33 wt %) were used, a gel was instantly formed as tripropargylamine was added, precluding preparation of thin films for electro-optic study. Therefore, 25 wt % polymer concentration was chosen to evaluate the effect of the ratio of acetylene (from crosslinker) and azide (from polymer end groups) groups (Table 2, entry 3-6). It was found that ratios deviating in either direction (more or

less acetylene groups) from a 1:1 ratio resulted in decreased gel fractions. The effect of acetylene:azide ratio is asymmetric: using less crosslinker than needed decreased gel fraction more strongly than using excess crosslinker. The effect of acetylene:azide ratio on gel fraction is consistent with the observed time for gelation to occur: only in the case of a 1:1 ratio did gelation occur instantaneously. In all other cases, an insoluble gel formed only after stirring for several hours up to 2 days.

Table 2. Effect of polymer precursor concentrations and stoichiometry of acetylene and azide groups on the gel fraction.

Polymer precursor	Polymer precursor concentration (wt %)	Acetylene:azide[a]	Gel fraction[b]
3a	50	1:1	92%
3a	33	1:1	91%
3a	25	1:1	89%
3a	25	0.75:1	71%
3a	25	1.25:1	85%
3a	25	1.5:1	78%
3b	25	1:1	93%
4	25	1:1	92%

[a]Molar ratio of acetylene functional groups (3 per crosslinker) to azide end group (2 per polymer chain); [b]gel fraction = (mass of polymer precursor-mass of extractable polymer) / mass of polymer precursor.

A polymer concentration of 25 wt% and a stoichiometric amount of crosslinker that allows the azide/acetylene ratio to be 1:1 were used to crosslink all the telechelic polymers for further characterization. Gelation typically occurred within 5 min and the gels were cured at 50 °C for 2 days to give high gel fractions. IR spectrometry of the

resulting crosslinked polymers showed complete disappearance of the azide absorbance, indicating that most of the azide end groups have reacted in the crosslinking. Films for electro-optic studies were made by crosslinking in glass cells with predetermined gaps.

All the elastomers readily swelled in 5CB to form LC gels with high swelling ratios, including the one derived from the non-LC polymer **4**. The swelling ratios exhibited the expected dependence on the molecular weight of the strands: larger network strands resulted in LC gels with higher swelling ratios (Table 3).

Table 3. T_{NI} and swelling ratio of liquid crystalline gels prepared from telechelic polymers

	Precursor polymer and its M_n	T_{NI} (gel)[a]	swelling ratio in 5CB[b]
LCG 1	Polymer **3a**, 11 k	37.5	10 ± 1
LCG 2	Polymer **3b**, 25 k	37.3	19 ± 2
LCG 3	Polymer **4**, 14 k	35.0	15 ± 1

[a]Measured by POM, heating rate=1 °C/min; [b]the ratio of absorbed 5CB and dried polymer network, W_{5CB}/W_p.

Electro-optic properties of LC gels. We are interested in understanding how the network structure affects the electro-optic switching of the LC gels between a scattering polydomain state and a transmissive monodomain state. We focused on the disubstituted gels LCG1 and LCG2 with the same polymer structure but different network strand lengths. The length of the network strands, the swelling ratio, and the degree of side-group substitution may all play a role in the electro-optic characteristics.

Previous studies of the electromechanical properties of LC gels have observed a significant difference for “constrained” LC gels that are physically pressed between electrodes and “unconstrained” LC gels that are freely floating in an LC solvent that fills

the gap between electrodes.[15,22,23,46] It was found that a mechanical constraint suppressed the electric field response of nematic gels. We investigated the electro-optic behavior of both constrained and unconstrained gels.

Constrained samples were prepared by pressing a LC gel sample between ITO-coated glass plates separated by spacers. The initial thickness of the LC gel was approximately twice the final gap. The threshold for the constrained gel was high, approximately 10 V/μm, and only partial alignment was achieved for fields as high as 19 V/μm (Figure 1). Notably, the constrained gel exhibited fast director oscillations that follow the AC signal. The director oscillates at twice the frequency of the applied field due to the uniaxial symmetry of the nematic director. The response time of the constrained gel was within 1 ms.

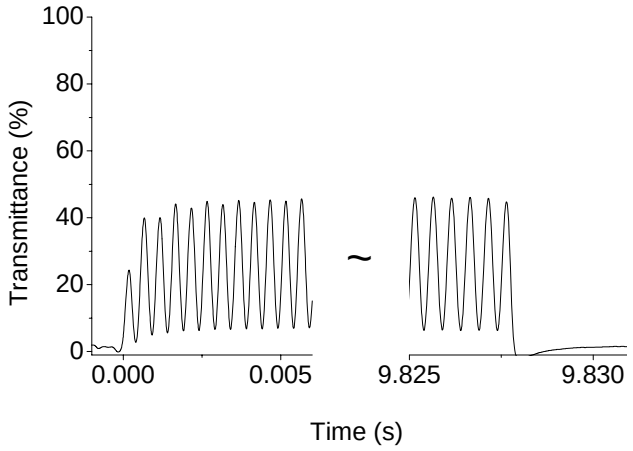

Figure 1. Dynamic electro-optic response of a constrained LC gel (LCG2, Table 3) under 19 V/μm, 1000 Hz AC signal. The signal is applied at 0 s and removed at 9.826 s approximately. Note that the transmitted intensity (recorded at 6000 Hz) quickly reaches its long-time value, and the oscillation of the optical intensity is 2000 Hz (2 cycles per 0.001 seconds). The data was smoothed using a spline interpolation.

Unconstrained samples were prepared by placing a thin (~40 μm) LC gel sample (LCG2, Table 3, same as for the constrained case described above) in a 100 μm thick gap between indium-tin-oxide (ITO) and lecithin coated glass plates filled with 5CB. The

lecithin layer aligns surrounding small molecule LC homeotropically at each substrate, so that it does not scatter light in orthoscopic imaging, ensuring that the observed change in transmission is due primarily to the response of the LC gel. In contrast to the constrained gel, the unconstrained LCG2 responds to the electric field at much lower fields (Figure 2). The transmission increases at fields as low as 0.1 V/μm; however, further experiments are required to exclude the possibility that this response may be due to the reorientation of the LC solvent at the gel interface. Nevertheless, a significant increase was observed below 1.0 V/μm, demonstrating the low threshold switching in these materials that has been confirmed for some LC gels.[13,22] Also, the transmitted intensities while ramping voltage up were almost superimposable with those recorded while ramping voltage down (Figure 3), demonstrating the excellent reversibility of the electro-optic response.

The dynamics of the electro-optic response for unconstrained LCG2 are fast and, in constrast to physically self-assmbled gels we have previously reported,[24] insensitive to the applied field. The transmittance reaches 90% of its maximum value after application of the AC field and drops down to 10% of its maximum after removal of the field in <50 ms (Figure 2). Interestingly, an oscillation in the transmitted intensity was also observed for unconstrained gels. The width of these oscillations strongly depends on the AC field frequency and amplitude. At the same electric field amplitude, the oscillation band is about 5 times wider at 100 Hz than at 1000 Hz. This reflects that the director oscillates fast enough to follow the AC field at 100 Hz, which roughly corresponds to a response time of 10 ms.

The electro-optic switching behavior of the LC gel was also captured by POM. An initially polydomain LCG2 gel shows strong birefringence in the absence of an

electric field (Figure 4A), but almost uniform alignment of the gel is obtained under an AC field of 2.0 V/μm (Figure 4B).

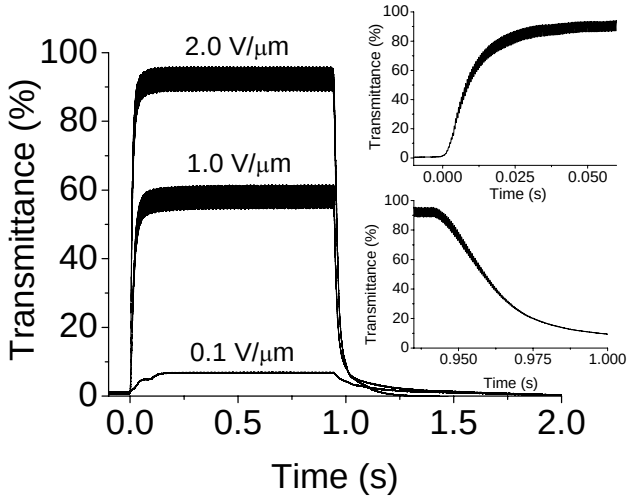

Figure 2. Transient electro-optic response of an unconstrained LC gel (LCG2) under various AC electric fields at 1000 Hz. The insets show the electro-optic response around the time the signal is applied (top inset) and removed (bottom inset).

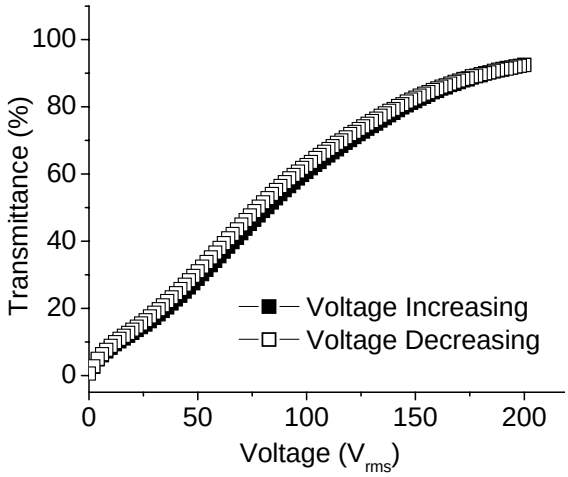

Figure 3. Transmittance as a function of voltage applied for an unconstrained LC gel (LCG2) in a 100 μm thick gap. The applied AC voltage (rms) sweeps from 0 to 200 V at 0.5 V interval and 1000 Hz. The measured intensity is the average of the oscillation; the software measures the intensity several times for each data point and averages them together. The transmittance when increasing the voltage (closed square) is almost superimposable with that when decreasing the voltage (open square).

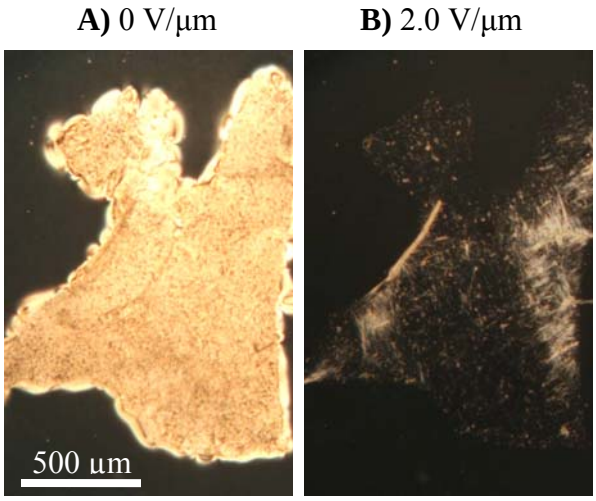

Figure 4. Polarized optical micrograph of unconstrained LC gel (LCG2) between ITO and lecithin coated glass plate under A) no AC field and B) an AC field of 2.0 V/μm.

The effects of molecular variables on electro-optic response are evident in comparisons between LCG2 (above), LCG1 (higher crosslink density, Figure 5), and LCG3 (greater space between mesogens, Figure 6), The main effects of increasing crosslink density are to reduce the transmittance at a given electric field but to speed switching: LCG1 reaches only ~50% transmittance at 2.0 V/μm (compared to ~90% for LCG2) but switches "on" and "off" in ~20 ms (compared to ~50 ms for LCG2). A gel having similar crosslink density to LCG2, but with only half the number of mesogens per repeat unit (LCG3), exhibits similar behavior to LCG2 with 75% transmittance at 2.0 V/μm, a fully reversible electro-optic response, low threshold switching, and fast dynamics.

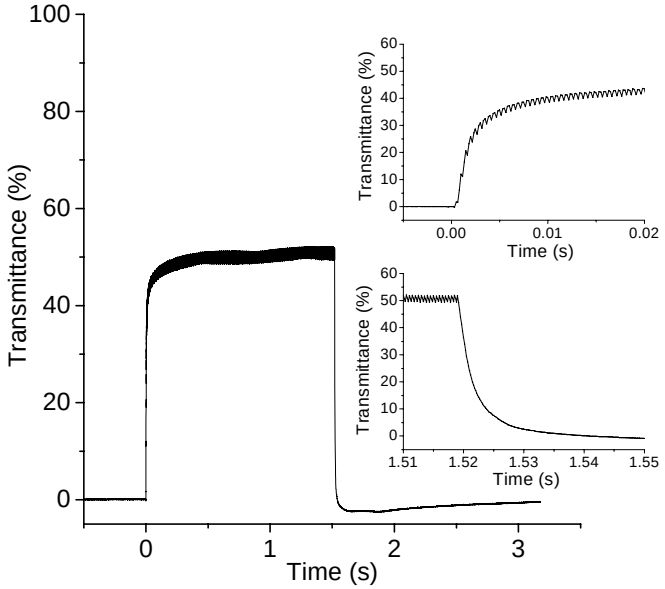

Figure 5. Transient electro-optic response of an unconstrained LC gel (LCG1) under an AC electric field of 2.0 V/μm at 1000 Hz. The insets show the electro-optic response near the time the signal is applied (top inset) and removed (bottom inset).

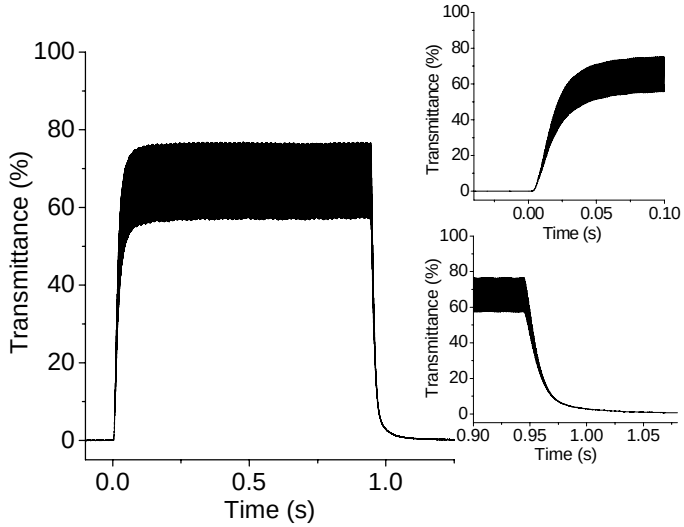

Figure 6. Transient electro-optic response of an unconstrained LC gel (monosubstituted LCG3) under an AC electric field of 2.0 V/μm at 1000 Hz. The insets show the electro-optic response near the time the signal is applied (top inset) and removed (bottom inset).

These electro-optic studies demonstrate important features of the electro-optic response of LC gels made by crosslinking telechelic polymers and of LC gels in general. First, mechanical constraints significantly affect the electro-optic response, even for low

concentration gels (5 wt% polymer). It is well known that mechanical deformation is strongly coupled to director orientation in LC elastomers,[1,47-49] and we found that this holds true for dilute gels as well. This can clearly be seen by comparing the response of constrained and unconstrained LCG2. Mechanically constrained gels have a greater threshold for a response and do not reach uniform alignment even for fields as high as 19 V/μm. Samples that were only slightly constrained had a significantly reduced electro-optic response, and much care had to be taken to prepare unconstrained samples. Mechanical constraints frustrate sample alignment, preventing the comparatively easy reorientation of the director observed for unconstrained gels. This hypothesis is supported by previous studies of monodomain LC gels that change shape in response to electric fields.[15,23]

Our gels with a controlled network strand length reveal how the network structure affects the electro-optic switching behavior. Unconstrained LCG2, which has longer network strands and a greater degree of swelling, has a stronger response to external fields. We expect that the electro-optic behavior depends on both the crosslink density and the degree of swelling, which are not independently varied in these experiments. The observed trends accord with previous studies of LC gels prepared by uncontrolled radical polymerization, which found that decreasing the crosslinker and/or monomer concentrations (expected to give the network longer strands overall), results in lower threshold fields and enhanced electro-optic and electro-mechanical responses of LC gels.[13-15]

The very low threshold observed here for LC gels prepared by end-linking telechelic polymers might be a result of a relatively uniform network structure. Regions

of high crosslink density are difficult to avoid in systems prepared by uncontrolled radical polymerizations. Trifunctional crosslinking of already formed polymers gives very few closely spaced crosslinks (random selection of three chains from the overall distribution gives a narrower distribution of the molar mass linked to a crosslink than that of the telechelic chains themselves). Therefore, the present strategy for making LC gels might find use in devices that require a low-threshold optical or mechanical response.

Finally, it is worth noting that the handling of the gels is rather delicate: the cell in which crosslinking is performed must be opened so that the copper catalyst may be fully extracted prior to introducing the small molecule LC. Ongoing attention is being given to making these procedures more robust. Significant sample-to-sample variability of the electro-optic response (maximum transmitted intensities varied from 95% to 75% for LCG2 and from 50% to 20% for LCG1) was observed, which is very likely due to variations in gel thickness (hence optical path length) and irregularities introduced when the gel is removed from the mold (partial adhesion to both glass plates) and when it is loaded in the electro-optic cell (as noted, the boundary conditions have strong effects and partial contact of the gel with the substrate may be responsible for some of the variability observed).

The demonstrated approach allows for the control of LC network structure, including the length of the network strands between crosslinks and crosslinker functionality. We believe that LC networks from telechelic prepolymers, like the ones described here, will enable quantitative tests of molecular theories of nematic elastomers and gels, an active area of current research. The first molecular description of LC nematic elasticity,[1] developed by Terentjev and Warner, described a variety of novel

effects, most notably “soft elasticity”, arising from the coupling of rubber elasticity and nematic order. This theory assumes an ideal, Gaussian network. More recent theoretical work has investigated the implications of this molecular theory to the dynamics[5] of LC networks and also extended the original theory to describe more realistic networks (i.e., with excluded volume interactions[50]). However, to experimentally validate predicted relationships between molecular structure and macroscopic properties, network details such as crosslink density and length between crosslinks must be known and systematically varied. Indeed, there is still controversy concerning the validity of the previous molecular theories proposed, and many scientists in the field[51,52] remain unconvinced that the molecular theories of Terentjev, Warner, and others are applicable to real LC networks. Synthetic routes to well-defined networks provide the molecular tools required to study these fundamental questions.

Conclusions

Azide-terminated telechelic side-group LC polymers were produced by ROMP and crosslinked with a triacetylene species to prepare covalent LC networks in high yields. These well-defined networks were highly swollen in 5CB, resulting in nematic gels with low polymer content. In accord with Urayama’s findings,[15,23] these LC gels are sensitive to mechanical constraint, which suppressed the electro-optic response of the gels. Unconstrained LC gels exhibited fast and completely reversible switching at low electric fields. For a given electric field, the LC gels prepared from longer telechelic polymers (hence, lower polymer concentration at equilibrium swelling) showed a higher degree of switching than their counterparts made from shorter polymer strands. Thus, the present approach for preparing LC elastomers and gel materials with well-defined

structures will be valuable in establishing the relationship between the LC network structure and material properties, which may guide rational design of LC materials in the future. We are currently investigating methods for making monodomain LC gels through crosslinking in the nematic state[15,23] and producing telechelic LC polymers with a higher degree of anisotropy.[25]

Experimental Section

General procedures. NMR spectra were recorded on a Varian Mercury 300 MHz spectrometer. All NMR spectra were recorded in $CDCl_3$ or DMSO-d_6, and referenced to residual proteo species. For end group analysis, a Varian Mercury 500 MHz ^{1}H NMR was used. FT-IR spectra were recorded on a Perkin-Elmer Paragon 1000 spectrometer. Gel permeation chromatography (GPC) was carried out in THF on two PLgel 5 μm mixed-C columns (Polymer Labs) connected in series with a DAWN EOS multiangle laser light scattering (MALLS) detector and an Optilab DSP differential refractometer (both from Wyatt Technology). No calibration standards were used, and d*n*/d*c* values were obtained for each injection by assuming 100% mass elution from the columns.

Materials. Dichloroethane (DCE) was dried over CaH_2 and distilled prior to use. *trans*-5,6-dihydroxy-cyclooctene[53] and 5-hydroxy-cyclooctene[38] were synthesized according to literature procedures. All other materials were used as received.

Synthesis of functionalized cyclooctene-based monomers. Ethyl 6-bromohexanoate (19.8 mL, 111 mmol) was attached to 4-cyano-4′-hydroxybiphenyl (15.4g, 78.9 mmol) in anhydrous DMF (100 mL) with anhydrous K_2CO_3 (10.8 g, 78.1 mmol) at 90 °C for 6 h. The product was recrystallized in ethanol (89% yield), and was then deprotected by reacting with KOH (6 g, 150 mmol) in anhydrous ethanol (200 mL) at 90 °C for 6 h. 1 M

HCl (50 mL) was added to precipitate the acid product which was collected by filtration, washed with water and cold acetone, and dried in vacuo at 60 °C (95% yield).

The acid (5.2 g, 16.2 mmol) was reacted in $SOCl_2$ (60 mL, 766 mmol) at 70 °C for five hours to convert into the acid chloride. Excess $SOCl_2$ was removed under reduced pressure. The acid chloride was then dissolved in 20 mL anhydrous THF and was added dropwise to a solution of *trans*-5,6-dihydroxy-cyclooctene (0.77 g, 5.4 mmol) in anhydrous pyridine (5 mL, 63.2 mmol) and anhydrous THF (50 mL). The mixture was refluxed for 24 h and the product was purified by extraction with 1 N HCl (20 mL, 3 times), followed by extraction with a saturated solution of aqueous $NaHCO_3$ (50 mL) and with a saturated aqueous solution of KCl (50 mL). The product was dried over MgSO4 and purified on a silica gel column (ethyl acetate/hexanes, 3:7 v/v) to give 1.6 g disubstituted cyclooctene **1** as a white crystal (40% yield). ^{1}H NMR (300 MHz, $CDCl_3$) δ 7.69-7.60 (m, 8H), 7.52-7.49 (m, 4H), 6.97-6.94 (m, 4H), 5.64 (t, J = 4.2 Hz, 2H), 5.18 (t, J = 3.3 Hz, 2H), 3.98 (t, J = 6.3 Hz, 4H), 2.52-2.00 (m, 12H), 1.85-1.45 (m, 12H); ^{13}C NMR (75 MHz, $CDCl_3$) δ 172.6, 159.6, 145.2, 132.6, 131.4, 128.7, 128.3, 127.0, 119.5, 115.0, 109.5, 73.7, 67.7, 34.3, 29.9, 28.9, 25.7, 24.7, 23.0. HRMS (FAB) *m/z* calc. for $C_{46}H_{48}O_6N_2$: 724.3522, found 724.3512.

Monosubstituted cyclooctene **2** was synthesized in analogy to **1** by coupling the acid chloride with 5-hydroxy-cyclooctene (65% yield). ^{1}H NMR (300 MHz, $CDCl_3$) δ 7.71-7.62 (m, 4H), 7.55-7.50 (m, 2H), 7.00-6.95 (m, 2H), 5.73-5.57 (m, 2H), 4.88-4.80 (m, 1H), 4.00 (t, J = 8.1 Hz, 2H), 2.38-2.07 (m, 6H), 1.92-1.50 (m, 12H); ^{13}C NMR (75 MHz, $CDCl_3$) δ 172.9, 159.7, 145.3, 132.6, 131.3, 129.8, 129.6, 128.3, 127.1, 119.1,

115.0, 110.0, 75.5, 67.8, 34.6, 33.8, 33.7, 28.9, 25.6, 25.5, 24.8, 24.7, 22.3. HRMS (FAB) *m/z* calc. for $C_{27}H_{31}O_3N$: 417.2304, found 417.2294.

Synthesis of 1,8-dibromo-4-octene. 5-Bromo-1-pentene (1.0 g, 6.7 mmol) was added to a solution of Grubbs 1st generation catalyst (30 mg, 0.036 mmol) in 5 mL degassed CH_2Cl_2, and the reaction stirred at room temperature overnight. The solvent was evaporated and the remaining residual was purified on a silica gel column (ethyl ether/hexanes, 1:20 v/v) to give 0.80 g 1,8-dibromo-4-octene (89% yield). ^{1}H NMR (300 MHz, $CDCl_3$) δ 5.45-5.37 (m, 2H), 3.43-3.38 (m, 4H), 2.24-2.12 (m, 4H), 1.96-1.86 (m, 4H); ^{13}C NMR (75 MHz, $CDCl_3$) δ 129.8, 129.3, 33.3, 32.5, 32.2, 30.8, 25.7. HRMS (FAB) *m/z* calc. for $C_8H_{14}Br_2$: 269.9442, found 269.9455.

General procedure for polymerization and end group functionalization. In a typical experiment, an oven-dried small vial was charged with 0.725 g (1.0 mmol) of monomer **1** and a stir bar. Under an argon atmosphere, 1.0 mL of degassed DCE was added via syringe. The vial was then degassed through three freeze-pump-thaw cycles. Next, the desired amount of CTA was injected from its stock solution in degassed DCE. 84 μL of a 10.0 mg/mL Grubbs 2nd generation catalyst solution in degassed DCE was injected to initiate the polymerization. The reaction vial was stirred at 55 °C under argon for 24 h. The reaction mixture was quenched with 0.1 ml of ethyl vinyl ether and then dissolved in 2 ml CH_2Cl_2 and precipitated into 200 ml stirring MeOH. The pale yellow precipitate was washed with fresh MeOH and dried in vacuo overnight to yield 0.70 g of white polymer (97% yield).

0.7 g (0.1 mmol -Br) dibromo-terminated polymer and 13 mg (0.2 mmol) NaN_3 were dissolved in 15 ml DMF. The resulting solution was stirred at 25 °C overnight and

then concentrated and precipitated into 200 ml MeOH three times and dried in vacuo overnight to yield 0.65 g light yellow polymer (93% yield). ^{1}H NMR (500 MHz, $CDCl_3$) δ 7.7-7.6 (m, 8H), 7.6-7.5 (m, 4H), 7.0-6.9 (m, 4H), 5.4-5.3 (br, 2H), 5.1-5.0 (br, 2H), 4.05-3.9 (br, 4H), 3.3-3.2 (m, end group -C*H*$_2$-N_3), 2.4-2.3 (m, 4H), 2.2-1.45 (br m, 20H).

Diazido-terminated polymer **4** was synthesized from monomer **2** using a similar procedure. ^{1}H NMR (500 MHz, $CDCl_3$) δ 7.7-7.6 (m, 4H), 7.6-7.5 (m, 2H), 7.0-6.9 (m, 2H), 5.4-5.3 (br, 2H), 4.95-4.8 (br, 1H), 4.05-3.95 (br, 2H), 3.3-3.2 (m, end group -C*H*$_2$-N_3), 2.4-2.3 (m, 2H), 2.2-1.2 (br m, 16H).

General procedure for crosslinking. The desired diazido-terminated polymer and CuBr (2 eq. to alkyne) were added to a small vial with a Teflon-lined cap. The vial was evacuated and backfilled with argon three times. The desired amount of degassed, anhydrous DMF (resulting in a 25 wt% polymer solution) and pentamethyl diethylene triamine (PMDETA) (1 eq. to CuBr) were injected and the vial was stirred for 5 min. The correct amount of tripropargylamine (1/3 eq. to polymer azide end group) was then injected from its stock solution. The mixture was stirred at room temperature for 20 seconds. The vial was then placed in an oven preset to 50 °C and allowed to react for 2 days. The resulting gels were repeatedly extracted with DMF and then THF (2 h for each extraction and for 1-2 days until the solution was visually colorless) to remove copper catalyst and soluble polymer fraction. Upon drying in vacuo, the material returns to the light yellow color of the prepolymer. The elastomer films for electro-optic studies were prepared by injecting the reaction mixture into rectangular glass cells with predetermined gaps. This was required for preparing samples of a uniform thickness. A cell was sealed in a degassed vial with a Teflon-lined cap. After injecting the reaction mixture into the

rectangular cell, the vial was placed in a heating oven at 50 ^{o}C. After 2 days at 50 °C, the glass cell was soaked in DMF for several hours and opened carefully to remove the gel. The catalyst and soluble polymer fraction was extracted as described above. The gel was then dried in vacuo and the resulting film was reswelled with 5CB for 24 h to give the LC gel film.

Electro-optic measurements of the gels. The electro-optic properties of the gels were measured under oscillating applied voltage using a polarized He-Ne laser, a beam splitter, and a CCD detector as previously described.[24] Constrained samples were prepared by pressing a LC gel sample between indium-tin-oxide (ITO)-coated quartz plates separated by 10 μm spacers. Unconstrained samples were prepared by placing a thin (ca. 40 μm, measured using an outside micrometer by gently placing the gel between the anvil and the spindle) piece of the LC gel in a 100 μm thick gap between ITO and lecithin coated glass plates filled with 5CB, and the samples were allowed to stand overnight to allow full alignment of 5CB before measurements.

References

(1) Warner, M.; Terentjev, E. M. *Liquid Crystal Elastomers*; Oxford University Press: Oxford, 2003.

(2) Yu, Y.; Ikeda, T. *Angew. Chem., Int. Ed.* **2006**, *45*, 5416-5418.

(3) Ikeda, T.; Mamiya, J.; Yu, Y. *Angew. Chem., Int. Ed.* **2007**, *46*, 506-528.

(4) Olmsted, P. D. *J. Phys II France* **1994**, *4*, 2215-2230.

(5) Stenull, O.; Lubensky, T. C. *Phys. Rev. E* **2004**, *69*, 051801.

(6) Warner, M.; Terentjev, E. M. *Prog. Polym. Sci.* **1996**, *21*, 853-891.

(7) Terentjev, E. M.; Warner, M. *Euro. Phys. J. E* **2001**, *4*, 343-353.

(8) Clarke, S. M.; Hotta, A.; Tajbakhsh, A. R.; Terentjev, E. M. *Phys. Rev E* **2001**, *6406*.

(9) Hirschmann, H.; Roberts, P. M. S.; Davis, F. J.; Guo, W.; Hasson, C. D.; Mitchell, G. R. *Polymer* **2001**, *42*, 7063-7071.

(10) Zanna, J. J.; Stein, P.; Marty, J. D.; Mauzac, M.; Martinoty, P. *Macromolecules* **2002**, *35*, 5459-5465.

(11) Cho, D. U.; Yusuf, Y.; Cladis, P. E.; Brand, H. R.; Finkelmann, H.; Kai, S. *Chem. Phys. Lett.* **2006**, *418*, 217-222.

(12) Cho, D. U.; Yusuf, Y.; Cladis, P. E.; Brand, H. R.; Finkelmann, H.; Kai, S. *Jpn. J. Appl. Phys.* **2007**, *46*, 1106-1113.

(13) Ren, H.; Wu, S.-T. *Appl. Phys. Lett.* **2002**, *81*, 1432-1434.

(14) Urayama, K.; Kondo, H.; Arai, Y. O.; Takigawa, T. *Phys. Rev. E* **2005**, *71*, 051713.

(15) Urayama, K.; Honda, S.; Takigawa, T. *Macromolecules* **2006**, *39*, 1943-1949.

(16) Urayama, K.; Honda, S.; Takigawa, T. *Phys. Rev. E* **2006**, *74*, 041709.

(17) Finkelmann, H.; Kock, H.-J.; Rehage, G. *Makromole. Chem. Rapid Commun.* **1981**, *2*, 317-322.

(18) Küpfer, J.; Finkelmann, H. *Makromole. Chem. Rapid Commun.* **1991**, *12*, 717-726.

(19) Lacey, D.; Beattie, H. N.; Mitchell, G. R.; Pople, J. A. *J. Mater. Chem.* **1998**, *8*, 53-60.

(20) Chang, C.-C.; Chien, L.-C.; Meyer, R. B. *Phys. Rev. E* **1997**, *56*, 595-599.

(21) Thomsen, D. L.; Keller, P.; Naciri, J.; Pink, R.; Jeon, H.; Shenoy, D.; Ratna, B. R. *Macromolecules* **2001**, *34*, 5868-5875.

(22) Yusuf, Y.; Huh, J. H.; Cladis, P. E.; Brand, H. R.; Finkelmann, H.; Kai, S. *Phys. Rev. E* **2005**, *71*, 061702.

(23) Urayama, K.; Honda, S.; Takigawa, T. *Macromolecules* **2005**, *38*, 3574-3576.

(24) Kempe, M. D.; Scruggs, N. R.; Verduzco, R.; Lal, J.; Kornfield, J. A. *Nature Mater.* **2004**, *3*, 177-182.

(25) Li, M.-H.; Keller, P.; Yang, J.; Albuoy, P.-A. *Adv. Mater.* **2004**, *16*, 1922-1925.

(26) Gabert, A. J.; Verploegen, E.; Hammond, P. T.; Schrock, R. R. *Macromolecules* **2006**, *39*, 3993-4000.

(27) Ahir, S. V.; Tajbakhsh, A. R.; Terentjev, E. M. *Adv. Func. Mater.***2006**, *16*, 556-560.

(28) Hild, G. *Prog. Polym. Sci.* **1998**, *23*, 1019-1149.

(29) Patel, S. K.; Malone, S.; Cohen, C.; Gillmor, J. R.; Colby, R. H. *Macromolecules* **1992**, *25*, 5241-5251.

(30) Hedden, R. C.; Saxena, H.; Cohen, C. *Macromolecules* **2000**, *33*, 8676-8684.

(31) Rostovtsev, V. V.; Green, L. G.; Fokin, V. V.; Sharpless, K. B. *Angew. Chem., Int. Ed.* **2002**, *41*, 2596–2599.

(32) Helms, B.; Mynar, J. L.; Hawker, C. J.; Frechet, J. M. J. *J. Am. Chem. Soc.* **2004**, *126*, 15020-15021.

(33) Hawker, C. J.; Wooley, K. L. *Science* **2005**, *309*, 1200-1205.

(34) Malkoch, M.; Thibault, R. J.; Drockenmuller, E.; Messerschmidt, M.; Voit, B.; Russell, T. P.; Hawker, C. J. *J. Am. Chem. Soc.* **2005**, *127*, 14942-14949.

(35) Malkoch, M. V., R.; Gupta, N.; Mespouille, L.; Dubois, P.; Mason, A. F.; Hedrick, J. L.; Liao, Q.; Frank, C. W.; Kingsbury, K.; Hawker, C. J. *Chem. Commun.* **2006**, 2774-2776.

(36) Johnson, J. A.; Lewis, D. R.; Diaz, D. D.; Finn, M. G.; Koberstein, J. T.; Turro, N. J. *J. Am. Chem. Soc.* **2006**, *128*, 6564-6565.

(37) Johnson, J. A.; Finn, M. G.; Koberstein, J. T.; Turro, N. J. *Macromolecules* **2007**, *40*, 3589-3598.

(38) Hillmyer, M. A.; Laredo, W. R.; Grubbs, R. H. *Macromolecules* **1995**, *28*, 6311-6316.

(39) Maughon, B. R.; Weck, M.; Mohr, B.; Grubbs, R. H. *Macromolecules* **1997**, *30*, 257-265.

(40) Bielawski, C. W.; Grubbs, R. H. *Angew. Chem., Int. Ed.* **2000**, *39*, 2903-2906.

(41) Bielawski, C. W.; Morita, T.; Grubbs, R. H. *Macromolecules* **2000**, *33*, 678-680.

(42) Morita, T.; Maughon, B. R.; Bielawski, C. W.; Grubbs, R. H. *Macromolecules* **2000**, *33*, 6621-6623.

(43) Scherman, O. A.; Ligthart, G. B. W. L.; Ohkawa, H.; Sijbesma, R. P.; Meijer, E. W. *Proc. Natl. Acad. Sci. USA* **2006**, *103*, 11850-11855.

(44) Winkler, B.; Rehab, A.; Ungerank, M.; Stelzer, F. *Macromol. Chem. Phys.* **1997**, *198*, 1417-1425.

(45) Breitenkamp, K.; Simeone, J.; Jin, E.; Emrick, T. *Macromolecules* **2002**, *35*, 9249-9252.

(46) Zentel, R. *Liquid Crystals* **1986**, *1*, 589-592.

(47) Camacho-Lopez, M.; Finkelmann, H.; Palffy-Muhoray, P.; Shelley, M. *Nature Mater.* **2004**, *3*, 307-310.

(48) Kundler, I.; Finkelmann, H. *Macromole. Rapid Commun.* **1995**, *16*, 679-686.

(49) Yu, Y. L.; Nakano, M.; Ikeda, T. *Nature* **2003**, *425*, 145.

(50) Oyerokun, F. T.; Schweizer, K. S. *J. Phys. Chem. B* **2005**, *109*, 6595-6603.

(51) Fried, E.; Sellers, S. *J. Mech. Phys. Solids* **2004**, *52*, 1671-1689.

(52) Brand, H. R.; Pleiner, H. M., P. *Soft Matter* **2006**, *2*, 182-289.

(53) Jernow, J. L.; Gray, D.; Closson, W. D. *J. Org. Chem.* **1971**, *36*, 3511-3515.

Appendix 1

GPC Characterization of Cyclic Polymers

Cyclic metathesis catalysts described in Chapters 2 and 3 also exhibit functional group tolerance, and can be used to readily polymerize functionalized monomers, such as 5-acetoxy-, 5-bromo-, and 5-hydroxycyclooctene with complete monomer conversion as detected by ^{1}H-NMR spectroscopy.

The dilute solution properties, such as intrinsic viscosity ([η]), of the resulting cyclic polymers were routinely examined using GPC coupled with a triple detecting (light scattering/differential viscometer/differential refractometer) system to obtain the Mark-Houwink-Sukurada plot and the elution volume vs time. As shown in Table 1, MW was not proportional to the catalyst loading ($[M/Ru]_0$) as a result of poor initiation.

Interestingly, all types of cyclic polymers tested were found to have lower dn/dc values than their linear analogues, but dn/dc decreased as $[M/Ru]_0$ decreased (Table 1). On the other hand, linear polymers prepared using different $[M/Ru]_0$ had very similar dn/dc values. In order to confirm the difference in dn/dc between linear and cyclic samples, we mixed different amounts of linear polymer into the cyclic one with similar MW and used the RI detector and viscometer on the GPC to check the dn/dc and [η] values and of these mixtures. The addition of linear into cyclic polymer was found to indeed increase the dn/dc and [η] values (Table 2 and Figure 1).

Table 1. Linear and cyclic polymers prepared using **(H_2IMes)(PCy_3)$(Cl)_2$RuCHPh** and **UC-6**, respectively[a]

Polymer	$[M/Ru]_0$	dn/dc[b]	M_w[c]	PDI
LPCOAc	1500	0.083	103 k	1.39
LPCOAc	200	0.086	40 k	1.43
CPCOAc	1000	0.088	134 k	1.37
CPCOAc	500	0.077	131 k	1.32
CPCOAc	200	0.074	109 k	1.28
CPCOAc	100	0.061	95 k	1.40
LPCOBr	1000	0.117	98 k	1.50
CPCOBr	500	0.105	142 k	1.54
CPCOBr	200	0.081	167 k	1.30
LPCDT	200	0.128	92 k	1.45
CPCDT	200	0.103	150 k	1.40

[a]Polymerization conditions: $[M]_0$ = 1.5 M (PCOAc), 1.5 M (PCOBr), and 2.5 M (PCDT) in CH_2Cl_2; 40 °C, 12 h. [b]Measured by an "Optilab" DSP differential refractometer attached to GPC in THF by assuming 100% mass elution from the columns. [c]Measured by THF GPC coupled with 18-way light scattering detector.

Table 2. Mixture of linear and cyclic PCDT at various ratios[a]

Polymer	M_w[b]	dn/dc[c]
CPCDT (C)	150k	**0.103**
L:C=2:8	157k	**0.103**
L:C=5:5	137k	**0.108**
L:C=8:2	110k	**0.118**
LPCDT (L)	92k	**0.128**

[a]Polymerization conditions: $[M]_0$ = 2.5 M in CH_2Cl_2; 40 °C, 12 h. [b]Measured by THF GPC coupled with 18-way light scattering detector. [c]Measured by an "Optilab" DSP differential refractometer attached to GPC in THF by assuming 100% mass elution from the columns.

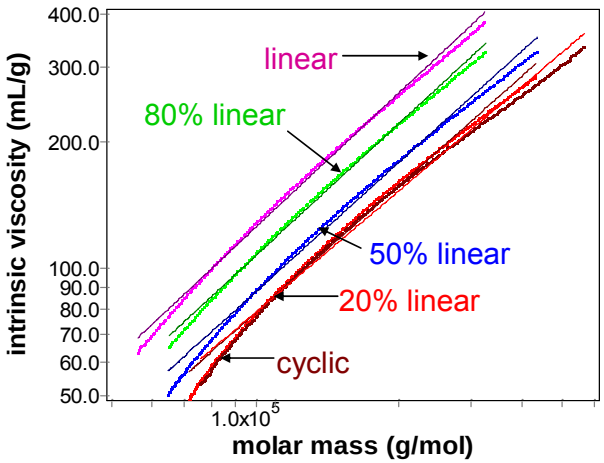

Figure 1. Intrinsic viscosities of cyclic and linear PCDT and their mixtures from GPC.

In order to investigate the effect of linear olefin on the fidelity of the cyclic polymerization and correlate the observed variance of dn/dc to the purity of cyclic polymer, we doped the monomer with a small amount of cis-3-hexene as the chain transfer agent (CTA). Linear olefin impurity is known to either react with cyclic catalyst or break up the cyclic organometallic complex through chain transfer, thus leading to linear chains. COAc was chosen as the monomer as it always gave polymers with symmetric, unimodal MW distributions, making the determination of dn/dc more accurate. The least active catalyst, **UC-5**, was used in this study.

In the absence of deliberately added CTA, consistently low dn/dc was obtained when [M/Ru] = 300 was used. However, with a ratio of monomer to CTA ([M/CTA]) at 3000, the dn/dc already started to increase (increased by 30% of the dn/dc difference between cyclic and linear polymers) and the MW dropped to 64% of the original MW. As the amount of CTA was increased, the dn/dc systematically increased to that of linear

polymers and the MW dropped to 5% of the original MW, when [M/CTA] = 30 was used (Table 2). When compared at the same MW, the addition of CTA caused the dn/dc, [η], and hydrodynamic radius (R_h) of the resulting polymers to steadily increase with increasing the amount of CTA from entry 2 to 4. This observation indicated that even a small amount of linear olefin can result in linear chain impurity during REMP.

Table 2. REMP of 5-acetoxy-cyclooctene using **UC-5** in the absence and presence of chain transfer agent (CTA)[a]

	$[M/CTA]_0$	$[CTA/Ru]_0$	dn/dc	$M_{w,GPC}$
1	-	0	**0.059**	214k
2	3000	0.1	**0.068**	137k
3	300	1	**0.080**	63k
4	30	10	**0.088**	10k

[a]Polymerization conditions: $[M]/[cat]_0 = 300$, $[M]_0$=1.5 M in CH_2Cl_2; 40 °C, 12 h.

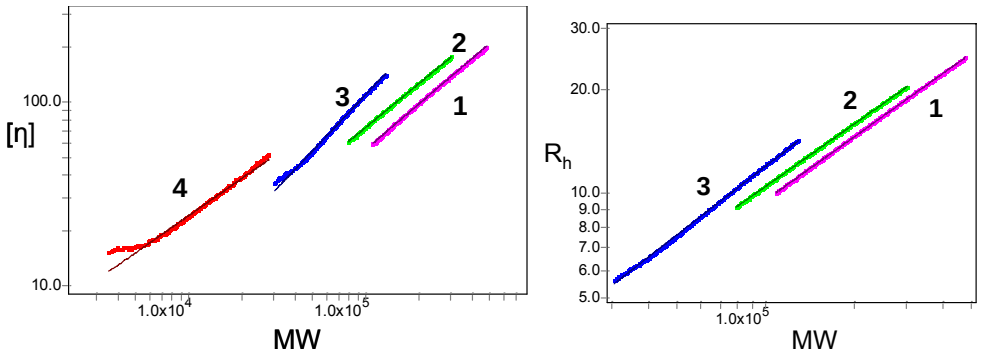

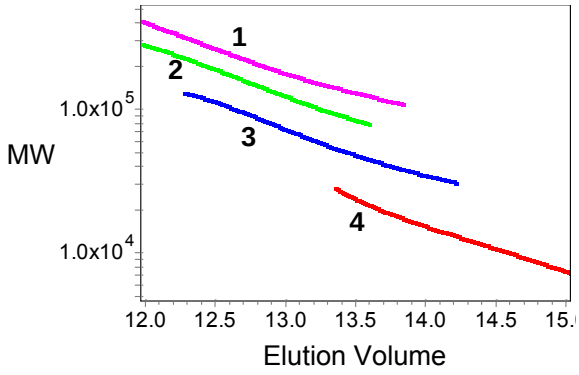

Figure 2. Comparison of (a) intrinsic viscosity, (b) hydrodynamic radius, and (c) elution time of PCOAc prepared without (1) and with (2-4) different amount of CTA.

The dn/dc value is an important parameter in the GPC characterization, because it is used to calculate the absolute MW and to derive [η], using the light scattering equation: $I(\theta)_{scatter} = cM_w(dn/dc)^2P(\theta)$, where c is the polymer concentration and P(θ) is the angular dependence of the scattering intensity, $I(\theta)_{scatter}$. In theory, dn/dc value is only related to the chemical composition of a polymer, but not the topology. There have been very few reports on dn/dc values of polymers with different architectures. Our *observed* lower dn/dc values from on-line mode GPC for cyclic polymers are very surprising. Therefore, we sought to measure dn/dc manually to verify their values. Polymer solutions with five concentrations in the range of 0.1 – 2.5 mg/mL were prepared and injected directly into the refractometer via a syringe pump to get the differential refractive index (n) for each concentration. The slope of the n value vs the concentration gave the dn/dc (Figure 3). The dn/dc values of cyclic and linear polymers turned out to be the same using manual measurement (Table 3), as theory predicts. Surprisingly, although the dn/dc values measured manually and using on-line mode GPC were very close for linear polymers, the dn/dc values were artificially smaller for cyclic polymers when measured assuming 100% mass recovery from the GPC column. Therefore, this result indicated that, for

cyclic polymers, certain mass retained on the column during normal elution time. The reason for this and whether this is universal or unique to our column system are unknown. However, using the correct dn/dc values (the same for linear and cyclic polymers) should still give the correct M_w and [η] for the population of cyclic polymer that elutes normally.

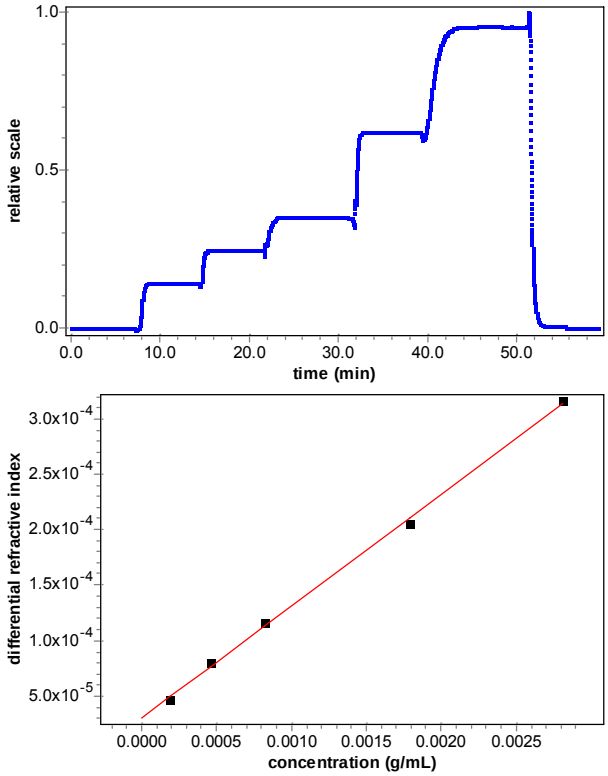

Figure 3. Exemplary manual measurement of dn/dc.

Table 3. Comparison of dn/dc obtained via manual measurement and via on-line mode GPC assuming 100% mass recovery

Polymer	Manual dn/dc	On-line dn/dc
LPCOAc	0.0866	0.084
CPCOAc	0.0852	0.06
LPCOE	0.1008	0.10
CPCOE	0.1016	0.08

If the lower dn/dc value, although not correct, is an indication of the cyclic topology, the fact that dn/dc values were lower when high catalyst loading was used may suggest that short polymerization times gave cyclic polymers with higher purity. This may be rationalized if catalyst decomposition before the completion of polymerization is the major source of linear impurity and catalyst re-incorporation to the polymer is not favored (decomposition of released catalyst does not generate linear chains).

Appendix 2

Hydrogenation of Polyalkenamers

Hydrogenation of polyalkenamers can lead to linear polyethylene (PE) with desired mechanical properties and greater stability against thermal and oxidative degradation. Hydrogenation of the polybutadiene or polyisoprene blocks in thermoplastic elastomers is often used to improve the stability and resistance of the elastomers.

Hydrogenation of unsaturated polymers can be performed either in a noncatalytic or a catalytic fashion.

Noncatalytic hydrogenation using hydrazine (N_2H_4) can be performed under nitrogen gas at an atmospheric pressure and is easily set up with simple glassware. Thermal decomposition of *p*-toluenesulfonylhydrazide (TSH) is commonly used to produce hydrazine *in situ*.[1]

Catalytic hydrogenation normally requires very high pressure H_2 gas and special high pressure vessel. Catalysts include heterogeneous Pd/C and $Pd/CaCO_3$ and homogeneous catalysts, such as the Wilkinson's catalyst.

Catalytic hydrogenation is known to retain the macromolecular structure through hydrogenation, although it requires more expensive catalyst and special high pressure apparatus. On the other hand, hydrazine hydrogenation may alter the macromolecular structure.[2] Therefore, we evaluated the efficiency and fidelity of hydrogenation of PCOE using TSH and $Pd/CaCO_3$ as outlined in Scheme 1.

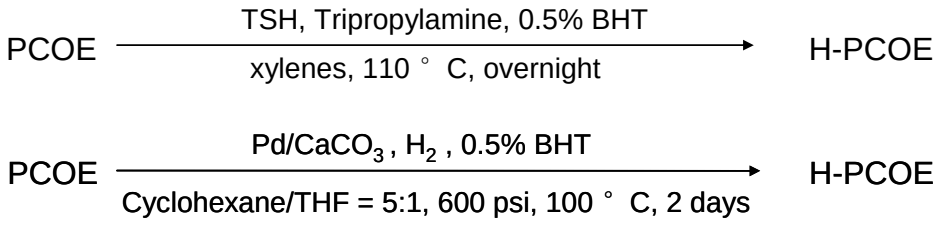

Scheme 1. Noncatalytic (top) and catalytic (bottom) hydrogenation of PCOE.

Both hydrogenation methods gave complete hydrogenation as indicated by the disappearance of the =C-H signal at 965 cm^{-1} in their IR spectra. However, the hydrogenated PCOE (H-PCOE) by TSH showed broad absorption around 1100 cm^{-1}, which has been attributed to residual TSH that is covalently bound to the polymer by Graessley.[2]

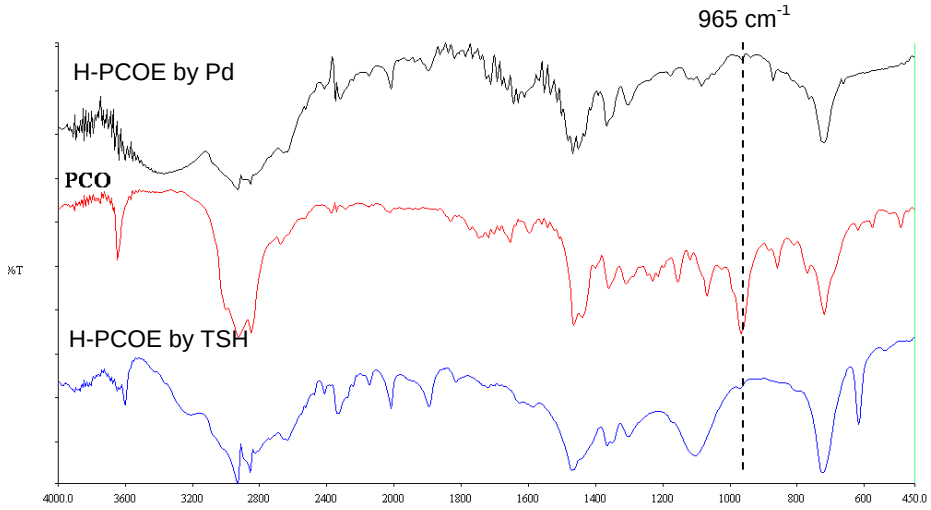

Figure 1. IR spectra of PCOE (middle) and hydrogenated PCOE using $Pd/CaCO_3$ (top) and TSH (bottom).

Comparison of the dynamic rheological spectra of the polymers before and after hydrogenation revealed a large difference between the two hydrogenation methods. After hydrogenation using TSH, the shape of the dynamic spectrum has significantly changed: the storage modulus (G') was larger than the loss modulus (G'') in the full frequency range tested (0.01−100 s^{-1}), and the difference was enlarged especially at low frequencies (Figure 2). This result indicated that the large-scale polymer structure has been changed during TSH hydrogenation. On the other hand, Pd catalyzed hydrogenation using H_2 gave H-PCOE similar dynamic spectrum with the precursor PCOE (Figure 3), indicating good preservation of the macromolecular structure.

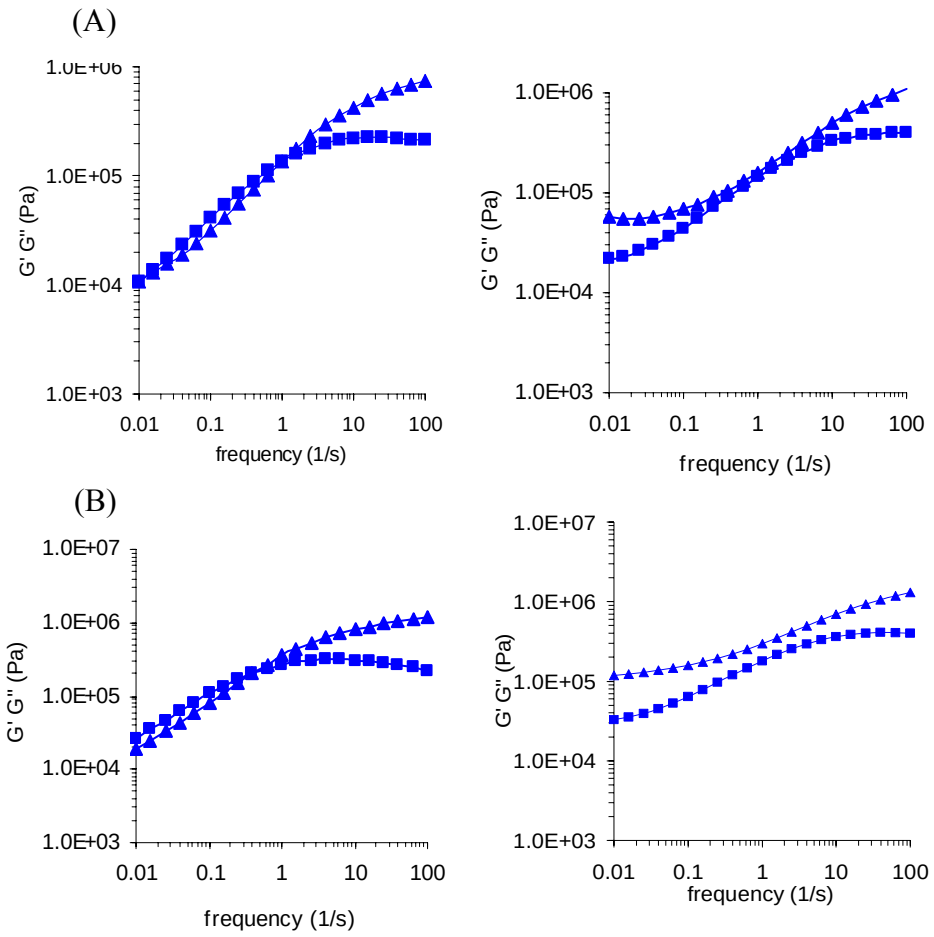

Figure 2. Comparison of dynamic rheological spectra of PCOE precursor polymers (left) and H-PCOE by TSH (right). (A) PCOE M_w = 200 k, PDI = 1.5; (B) PCOE M_w = 320 k, PDI = 1.2.

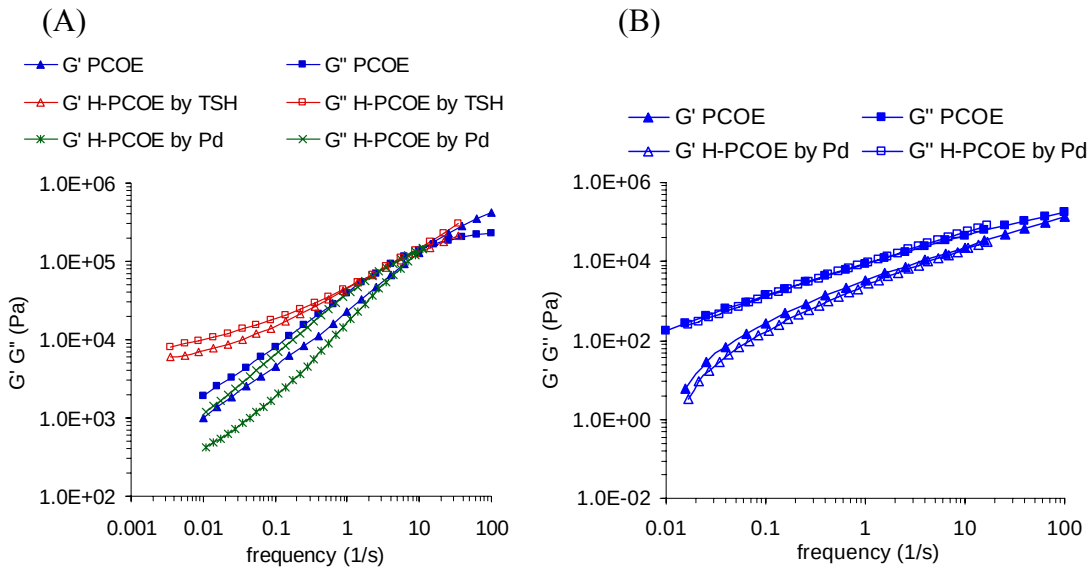

Figure 3. Comparison of dynamic rheological spectra of PCOE precursor polymers and H-PCOE. (A) PCOE M_w = 140 k, PDI = 1.5; (B) Commercial PCOE "vestenamer" M_w = 90 k, PDI = 2.0.

Therefore, catalyzed hydrogenation using H_2 as the hydrogen source should be used to preserve the macromolecular structure. In practice, heterogeneous Pd catalyzed hydrogenation was reliable for PCOE with MW < 200 k. However, for very high MW PCOEs, this method usually gave incomplete hydrogenation, which is partially due to the poor solubility of high MW H-PCOEs and the high viscosity of the solution. Catalyst powder was often found coagulating and was wrapped with insoluble polymer, which isolated the catalyst surface from the reaction media, although low precursor polymer concentration is preferred and can alleviate the problem to some extend. In addition, hot filtration (130 ºC in xylene) was needed to remove the catalyst and this process often resulted in some loss of the final polymer product.

On the other hand, homogeneous Wilkinson's catalyst, $RhCl(PPh_3)_3$, can overcome the dispersion problem in heterogeneous Pd system. It has been found very effective to fully hydrogenate functionalized PCOE.[3]

References

[1] Phinyocheep, P.; Pasiri, S.; Tavichai, O. *J. Appl. Polym. Sci.* **2003**, *87*, 76.
[2] (a) Graessley, W. W. et al *J. Polym. Sci. Polym. Phys. Ed.,* **1979**, 17, 1211. (b) Graessley, W. W. et al *J. Polym. Sci. Polym. Phys. Ed.,* **1979**, 17, 1224
[3] Ongoing work: Boydston, A. J.; Xia, Y.; Grubbs, R. H.; a typical condition is 10% polymer in THF, 1 % catalyst loading (to olefin), 50 ºC, 700 psi H_2, 12 h.